UCLouvain

AGRO LOUVAIN BIOINGÉNIEURS

Faculty of bioscience engineering

Mapping vegetation and open water in Palo Verde National Park, and impact of Fangueo technique : a descriptive study

Author : François Toussaint

Supervisors : Pr. Mathieu Javaux
Dr. Alice Alonso

Readers : Pr. Rafael Muñoz-Carpena
Pr. Pierre Defourny

Academic Year : 2020 - 2021

End of studies/Master thesis presented to obtain the diploma of Bioengineer : Environmental Sciences and Technologies

Acknowledgments

I would first like to thank my co-supervisors Pr. Mathieu Javaux and Dr. Alice Alonso for their support throughout the year, their expert advice, and for giving me the chance to conduct an exploratory thesis with great freedom.

I also want to thank the readers of this thesis, Pr. Rafael Muñoz-Carpena and Pr. Pierre Defourny for their expertise, their interest in my work and for taking the time to advise me during this academic year.

Thank you to Rasmus Lørup Arildsen and Christian Josef Köppl from the Danmarks Tekniske Universitet who worked on the classification of vegetation in the Palo Verde wetland. Thank you for sharing your results and allowing me to develop my Master thesis based on your excellent work.

I would like to thank the Organization for Tropical Studies for awarding me a grant to financially support the fieldwork I had planned to do in Palo Verde National Park. Unfortunately, I was unable to use it due to the inability to travel to Costa Rica because of the Covid-19 pandemic.

Finally, I would like to thank my parents, family and friends for their support during this past year.

Contents

List of Abbreviations

Term	Definition
EVI	Enhanced vegetation index
GEE	Google Earth Engine
MNDMI	Modified normalized difference water index
NDVI	Normalized difference vegetation index
NDWI	Normalized difference water index
NIR	Near infrared
PVNP	Palo Verde National Park
RF	Random Forest
SWIR	Shortwave infrared

List of Figures

List of Tables

1 Introduction

The Palo Verde National Park (PVNP), located in the Tempisque-Bebedero watershed in the North-West of Costa Rica, is recognized internationally as an ecologically important wetland in Central America. Thousands of migratory and resident birds visit the area and make it a true haven of biodiversity. In the late 1970's, major anthropogenic transformations in the watershed led to ecological disturbances in the whole area. After 1980, the wetland landscape changed from diverse vegetation and large open water areas to a monotypic stand of Typha domingensis, also called cattail. The reduction in plant heterogeneity and open water areas resulted in a decrease in biodiversity, wildlife habitat and bird visits.

Therefore, programs to reduce Typha invasion were implemented, and a particular vegetation management technique called Fangueo was applied. It consists in underwater crushing of Typha with a tractor. Previous studies found Fangueo to be effective in reducing Typha spread and opening water areas after the intervention. However, long-term impact of Fangueo on vegetation cover and open water has not been studied so far.

Despite the strong interest and the numerous studies investigating various impacts of this plant in the wetland eco-hydrology, the spatial distribution of Typha is not well-documented. In addition, the dynamic and total area of open water in the PVNP wetlands have not been investigated so far.

Studying Typha spatial distribution in the area, quantifying and mapping open water areas, and evaluating the long-term impact of the Fangueo technique on open water and vegetation cover is desirable to improve our knowledge of the eco-hydrology of PVNP.

The current study aims at developing a map of the spatial distribution of Typha, by taking advantage of differences in evolution of a vegetation index for different land covers using satellite imagery. We also aim at quantifying and mapping open water areas by thresholding a near-infrared spectral band. Finally, we aim at assessing the long-term impact of the Fangueo technique on open water and vegetation cover in PVNP.

1.1 Palo Verde National Park

The Palo Verde National Park (PVNP) is located in the North-West of Costa Rica (N: 10°20'35"−W: 85°20'26"), between the Tempisque and Bebedero rivers. It covers an area of 18,500 hectares, just upstream of the mouth of the Tempisque River where the waters flow in the Gulf of Nicoya (Guzmán Álvarez, 2007), as shown on figure 1.

The wetlands of PVNP host a rich biodiversity and provide vital shelter to more than 60 species of migratory and resident birds (Trama et al., 2017). It is therefore one of the most ecologically important tropical wetlands in Central America. In 1991, PVNP and surrounding wetlands in the lower Tempisque were registered as a Ramsar Site (figure 1. The Ramsar convention is an international treaty for the conservation and wise use of wetlands and that recognizes their important ecological value. In 1993, PVNP was included in the Montreux list of Ramsar sites that have or could undergone ecological change due to human activities and require management activities (Trama, 2009).

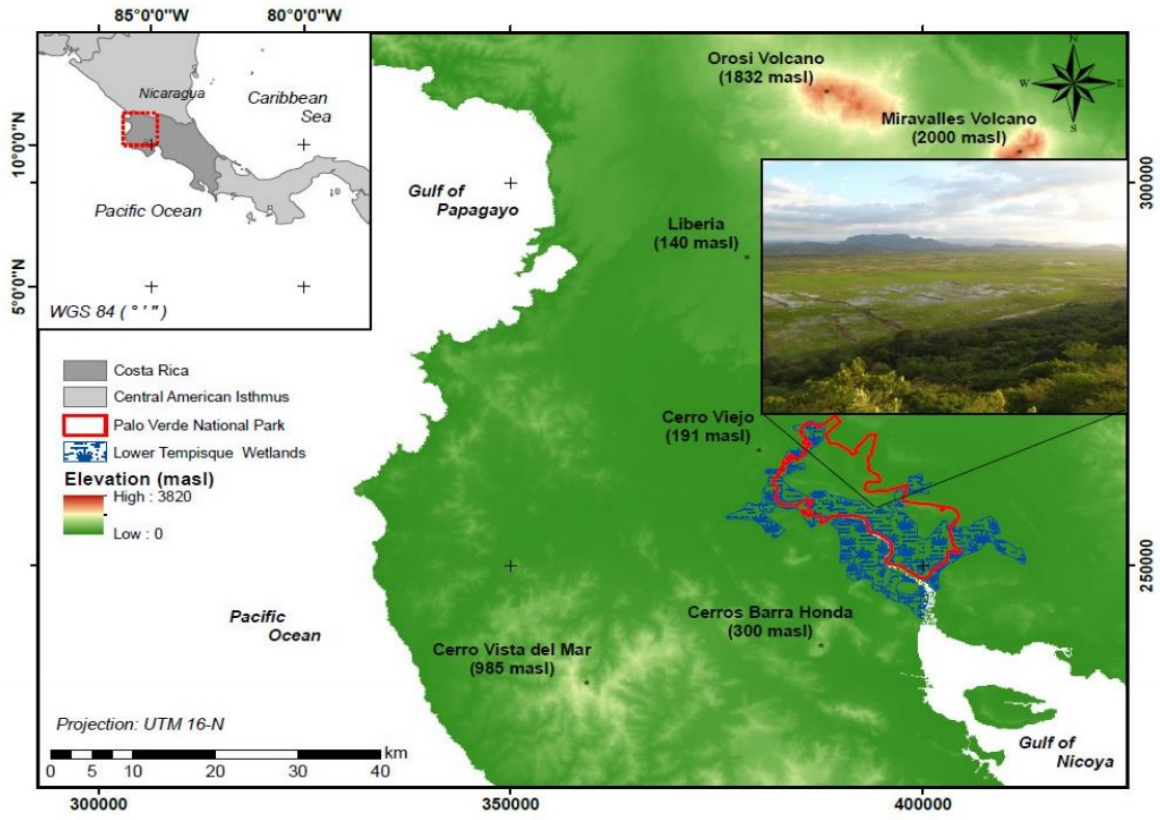

Figure 1: Palo Verde National Park location in the North-West of Costa Rica. Reprinted from Jiménez-Rodríguez et al. (2019).

The Park contains two different landscapes, a hilly and tropical dry forest and

seasonally flooded plains which are usually divided into 6 sub-wetlands (La Bocana, Nicaragua, Palo Verde, Piedra Blanca, Poza Verde and Varillal). Together with 4 other sub-wetlands outside the park (Cipanci, Corral de Piedra, El Viejo and Mata Redonda), see figure 2, they are classified as Ramsar wetlands of international importance. The elevation ranges from 8 meters at the southernmost point of PVNP up to 271 meters.

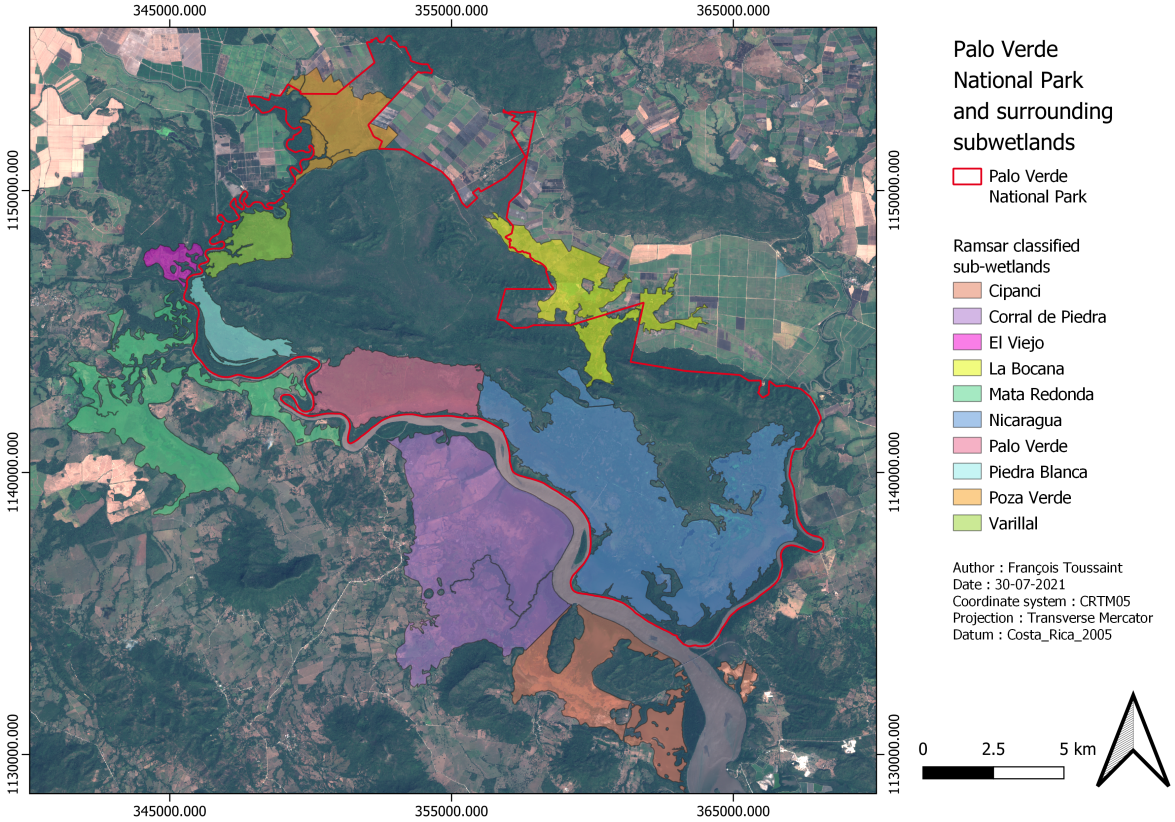

Figure 2: Palo Verde National Park and surrounding wetlands

The soils of the wetland are mainly Vertisols, typically found in the tropics and in wetlands (Guzmán Álvarez, 2007). This type of soil has the characteristic of swelling in wet conditions and shrinking in dry conditions. The soils are completely saturated at the end of the wet season and present cracks during the dry season. The wetlands have poor drainage, except for intermittent streams that appear during the rainy season.

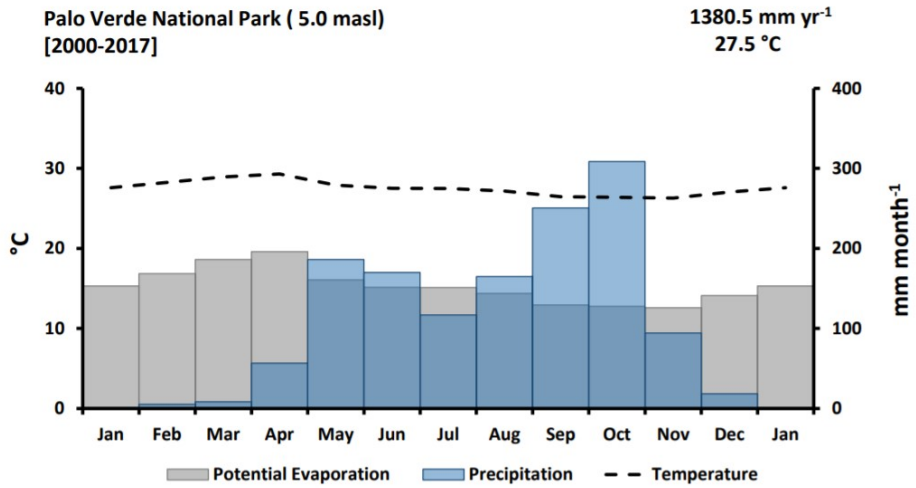

Figure 3: Average monthly temperature and precipitation at PVNP from 2000 to 2017. Reprinted from Jiménez-Rodríguez et al. (2019).

The mean annual temperature at the park is 27.5 °C and the annual precipitations averaged 1380.5 mm per year between 2000 and 2017 (Jiménez-Rodríguez et al., 2019). As shown on figure 3, the region experiences a wet season from May to November with a dryer period around the month of July and peak precipitations during the months of September and October. The dry season extends from December to April. The mean temperatures, contrary to precipitations, do not vary much during the year. Climatic events in the region have a high inter-annual variability due to the El Niño-Southern Oscillation. Hot years tend to experience prolonged droughts and cold years increased precipitation (Waylen and Laporte, 1999). The mean annual potential evapotranspiration was 1834.3 mm between 2000 and 2017 (Jiménez-Rodríguez et al., 2019). In terms of actual evapotranspiration, Crombé (2019) showed that there is some variability between the PVNP sub-wetlands. During the wet season, cumulative actual evapotranspiration ranges from 629 to 826 mm, and during the dry season from 308 to 446 mm. This spatial variability could be explained by differences in resilience to water stress between sub-wetlands. This would be due to different soil conditions, soil salinity and presence of cattle in some sub-wetlands. It could also be explained by differences in vegetation and land cover.

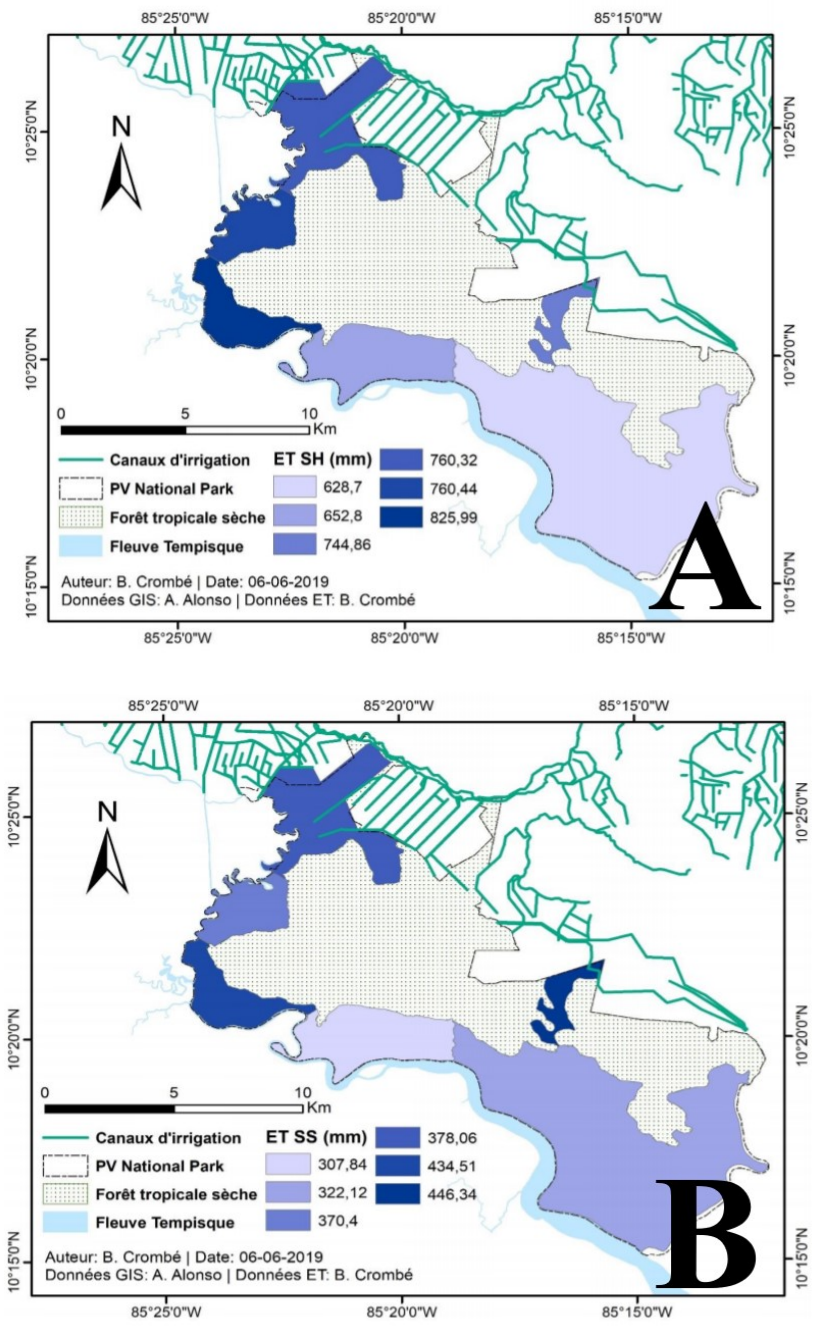

Figure 4: Mean cumulative actual evapotranspiration during the wet (**A**) and dry (**B**) season, calculated between 2001 and 2018 based on MODIS data. Reprinted from Crombé (2019).

Most of the water inflow to the park sub-wetlands occurs during the wet season, primarily from rainfall, but also from regular flooding of the Tempisque River due to high water levels and high tides in the Gulf of Nicoya, and from the groundwater table. Water level in the wetlands shows great interannual variability as well as important spatial variability, as illustrated in figure 5. This figure also clearly shows that water levels do not follow clean seasonal cycles. The level of the Tempisque and Bebedero

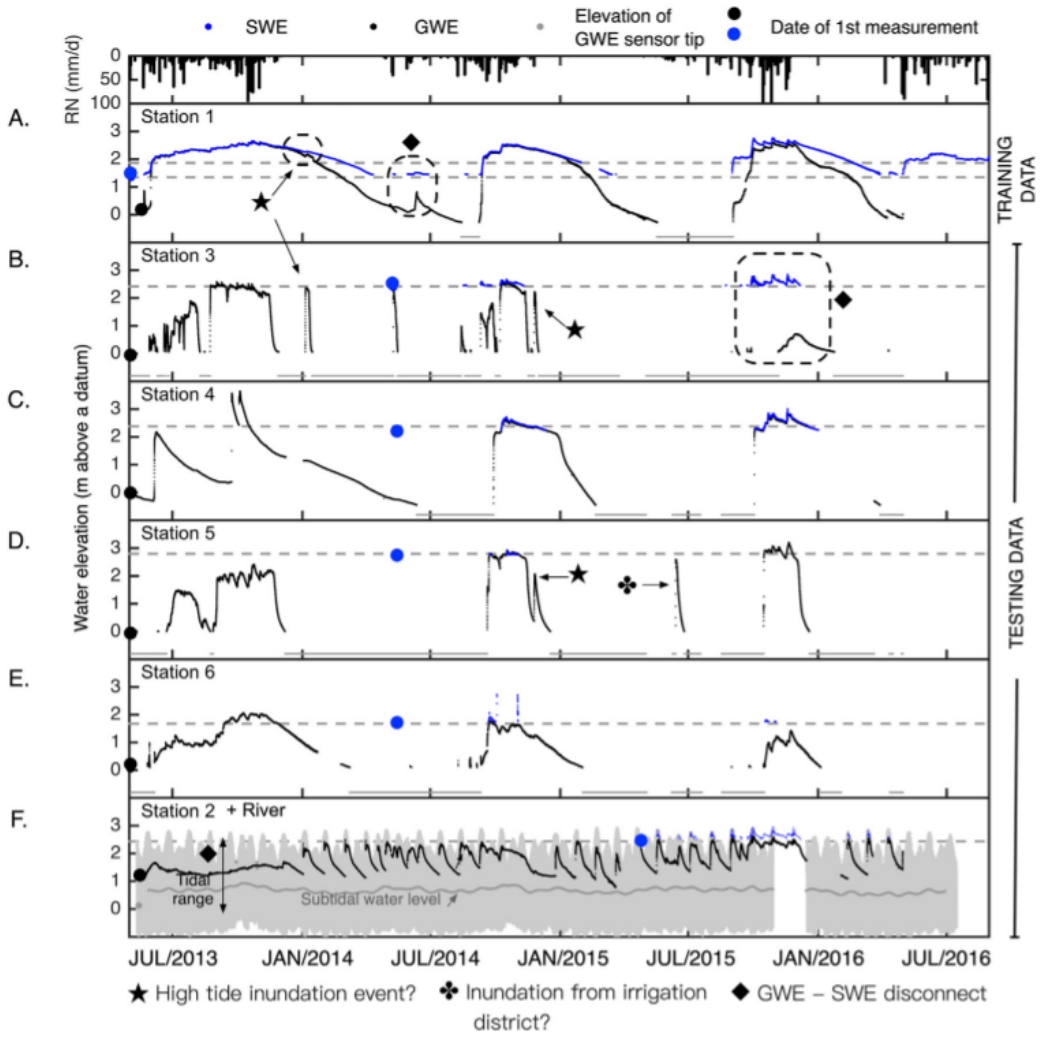

Figure 5: Rainfall (RN) at the PVNP weather station and 15-minute groundwater elevation (GWE) and surface water elevation (SWE) at the field monitoring stations. Dashed lines indicate ground level for all the stations. Data gaps are due to sensor malfunction. Reprinted from Alonso et al. (2020)

rivers is influenced by the ocean tides from the Gulf of Nicoya. During high tides, salt water flows up the river. Measurements of cation concentration at groundwater monitoring stations in PVNP have shown that salt water is entering the water table in the two most downstream sub-wetlands, Palo Verde and Nicaragua (Ledeganck, 2019).

According to Jiménez-Rodríguez et al. (2019), the PVNP wetland vegetation is dominated by *Thalia geniculata*, *Canna glauca L.* and *Typha domingensis*, also called "Cattail stands", which are emergent plants. This means that they are rooted in soil and emerging above the water surface when the wetland in flooded. Floating species such as *Neptunia plana* and *Eichornia crassipes* can also be found in the park, during the rainy season where water is deeper than 80 cm (Guzmán Álvarez, 2007). Palo Verde trees, *Parkinsiona aculata*, and other species of shrubs are abundant in areas

with shallow water during the wet season. There are also large areas of bare soil. Trees and mangrove can be found along the Tempisque and Bebedero rivers. Figure 7 shows that the most predominant plant species during the wet and the dry seasons vary greatly. The measurements were made in the Palo Verde sub-wetland and vegetation cover was measured in three 1-m^2 squares in each of 30 20-m^2 plots in the area (Osland and Richardson, 2011).

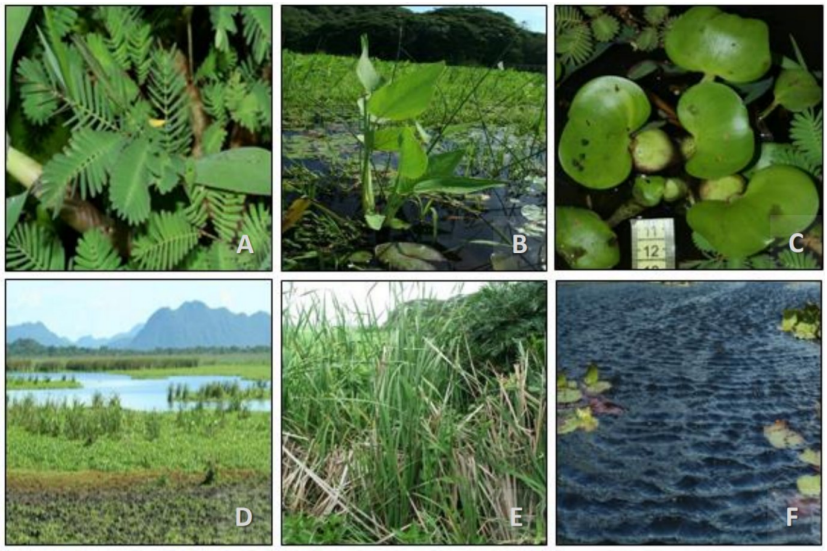

Figure 6: Pictures of PVNP land cover. (A): *Neptunia Natans*; (B): *Thalia geniculata*; (c): *Eichlornia craspies*; (D): Species mix; (E): *Typha domingensis*; (F): Open water. Reprinted from Jiménez-Rodríguez et al. (2019).

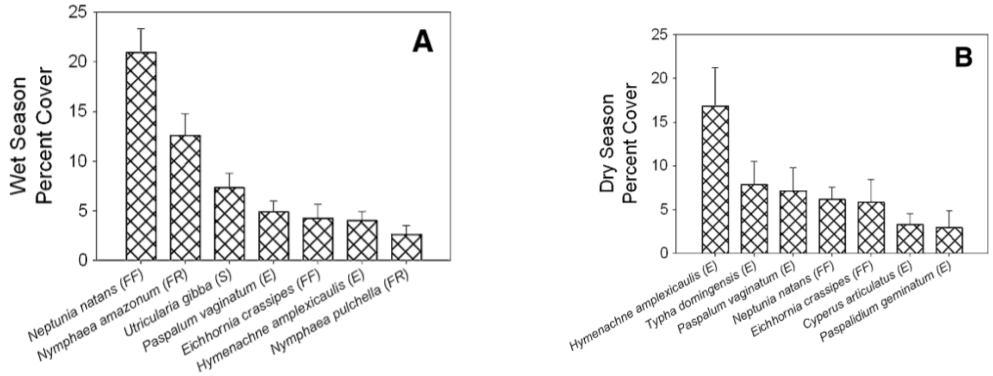

Figure 7: Plant species with the highest percent cover measurements in PVNP during the **A)** wet season and **B)** dry season. The letters indicate the vegetation species' predominant life form : E = emergent; FF = free-floating; FR = floating-rooted and S = submerged. Reprinted from Osland and Richardson (2011).

1.2 PVNP ecosystem disturbances in the 1980's

Until the national park was created at the end of the 1970's, the wetland of PVNP was used for cattle grazing (Jiménez-Rodríguez et al., 2019). Up to 15,000 heads of cattle were brought each year to the park between November and March or April (McCoy, 1996). After 1980, cattail plants proliferated rapidly, reducing overall habitat value for waterfowl, waterbirds, fish, amphibians and invertebrates (Trama, 2009). According to Trama (2009), the wetland landscape changed from "open water areas, low grasses, and floating and low emergent vegetation with some tall emergent patches of cattail to a monotypic stand of cattail", as illustrated in figure 8.

To understand how a single plant species can cause such ecological damage, it is necessary to better comprehend the biological and physiological characteristics of Typha. *Typha domingensis*, also called "Cattail stands", is a common invasive wetland plant found around the world. It has wind-dispersed seeds that allow it to colonize wetland areas across great distances. It can also reproduce asexually by means of rhizomes, which ensures rapid propagation (Bansal, 2019). Its growth rates are relatively high, around 10 to 30 tonnes ha^{-1} yr^{-1} (Andrews and Pratt, 1978). Typha is an obligate wetland plant, it is flood-tolerant but periodic low or prolonged high water levels can hinder it. It is hydrologic variability that keeps the plant under control. Hydrologic alterations, which can induce a lack of variability via water level control, are ideal conditions for Typha to thrive because it is no longer stressed. The plant then has a tendency to form dense nearmonotypic stands (Bansal, 2019). These nearmonotypic stands eliminate open water areas and replace other emergent, floating or submerged species, altering the vegetative structure wildlife species depend on for feeding, nesting or hiding. These replaced plants produce large quantities of seeds that are eaten by many species of birds, whereas the seeds of Typha are quite small and are not usually eaten. Other emergent plants form less dense canopies, allowing movement through the canopy, ideal for birds (Bansal, 2019). Typha stays present in the PVNP wetland all year long, because the soil under the plant retains moisture during the dry season(Trama, 2009).

The drastic change in land cover in PVNP has most generally been attributed to the end of cattle grazing in the area, which would have had the benefit of controlling the wetland vegetation dominated by indigenous and highly competitive cattail plants, leaving open large areas of water. This has, however, never rigorously been tested. Some argue that the vegetation shift in PVNP could (also) be explained by changes in abiotic conditions in that period, i.e. droughts and wildfires as well as water diversion for

agriculture in the upstream watershed (Trama, 2009; Osland et al., 2011) and resulting change in the wetland hydroperiod (Alonso et al., 2020). Water was brought into the Tempisque watershed from the artificial Arenal lake, to feed irrigation water to the more than 44,000 ha of agricultural lands via a network of irrigation canals. It is estimated that this inter-basin transfer of water resulted in a doubling of the amount of water entering the Tempisque watershed, completely changing its water dynamics. (Alonso et al., 2016).

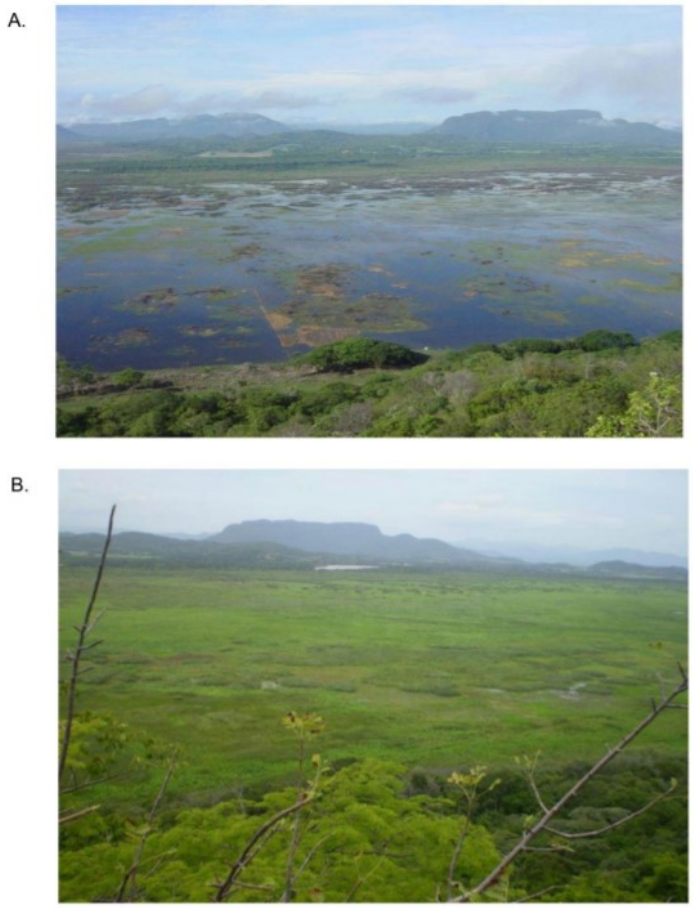

Figure 8: Pictures illustrating the change in land cover in PVNP, with *Typha domingensis* proliferating and closing up open water areas. **A)** Picture from 1986 (Photo credit: OTS archive) **B)** Picture from 2012 (Photo credit: Dr. Carolina Murcia). Reprinted from Alonso (2017).

By 1988, it was estimated that Typha was covering 95% of the Palo Verde subwetland (McCoy, 1996). The same year, a peak of 3000 black-bellied whistling ducks and 500 blue-winged teals was counted. Those numbers compared to the 35,000 black bellied whistling ducks and 25,000 blue-winged teals that could regularly be counted in 1979 show the massive decrease in bird diversity (McCoy, 1996).

1.3 Vegetation restoration strategies

In 1986, a five-year contract was signed with a local rancher to reintroduce 1,000 cattle heads into the wetland to prevent Typha invasion. Some argue that it was not successful due to the small number of animals used and the fact that the cattle were not accustomed to wetland conditions (Trama, 2009). At the end of the 1980's, research initiatives were put in place to restore the wetland. It was found that a particular technique, called Fangueo, helped reduce the cattail plants population. It consists in crushing the cattail plants underwater with a tractor equipped with angle-iron paddle wheels (McCoy, 1996), as shown on figure 9. Fangueo is usually implemented at the beginning of the dry season, when the water level is less than 75 cm high (Osland et al., 2011).

Figure 9: Fangueo tractor crushing cattail plants. Reprinted from Society for ecological restoration (2014).

In 2001, a plan was developed by the Organization for Tropical Studies and the Ministry of Environment and Energy to manage a 50 hectare area of the wetland with the Fangueo technique. A year later, an additional area of 250 hectares was included in this management plan.

Trama (2009) and Osland et al. (2011) show that the Fangueo technique results in a significant decrease in Typha population in the first year after it was implemented. They also show an increase in plant diversity in managed plots. A reduction in total live vegetation area was witnessed suggesting that Fangueo caused an increase in open water areas or exposed ground in the dry season. The two studies also found an increase in the amount of bird species and numbers recorded in managed plots. Open water and exposed ground were the two preferred land covers for waterbirds. It should be noted that Typha did not completely disappear after Fangueo events and that is also not desirable. In fact, they provide a resting or hiding place for several species of birds,

reptiles and invertebrates (Trama, 2009).

Both abovementioned studies only lasted a year and could not evaluate the long-term impact of Fangueo on vegetation, open water areas and bird population and species diversity. Osland et al. (2011) suggests that "once the (Typha) seedlings produce new ramets and become clonally integrated, Typha will dominate these plots again without additional management (i.e., within 2-4 years)". This has, however, not been studied so far.

2 State of the art

2.1 Introduction to wetlands

Wetlands are one of the most important ecosystems in the world even though they only cover between 5 to 8 percent of the Earth's land surface. These are ecosystems that are characterized by their hydrology: they are either permanently or periodically flooded. They are unique habitats for many species and very rich ecosystems, considered as havens of biodiversity. Wetlands have an important ecological and hydrological function. They function as downstream receivers of water and waste from both human and natural sources. They can potentially clean polluted waters, protect shorelines, recharge groundwater aquifers and mitigate floods and droughts. They are also considered important carbon sinks and climate stabilizers (Mitsch and Gosselink, 2015).

According to Mitsch and Gosselink (2015), wetlands are difficult to precisely define because of the variety of hydrological conditions in which they are found. They are generally located at the boundary between terrestrial and aquatic ecosystems but vary in size, in location - coastal or inland wetlands for example, in depth and duration of flooding. Biota also varies greatly among wetland types, but with one common trait, they are all flood tolerant species.

All over the world, wetlands are under threat or being lost. Many wetlands have been drained, converted to agricultural land or used for residential or commercial development. Some wetlands suffer under the consequences of off-site development, like excessive upstream water use or water pollution. Experts estimate that more than half of the world's wetland have been lost since 1900. As suggested by Davis and Hirji (2005), the most common causes of wetland deterioration are "agricultural impacts, water flow regulation, pollution, and habitat destruction or deterioration". Invasive vegetation is also an issue in some wetlands to which they seem to be particularly vulnerable. In fact, a quarter of the world's most invasive plants are wetland species (Zedler and Kercher, 2004). Hydrologic disturbances of the ecosystem can be a cause of plant invasion. Zedler and Kercher (2004) found that "hydrological disturbances facilitate wetland invasion and that the result is a decline in both the quantity and quality of native plant species", primarily because they affect nutrient availability. Not all invasive plants are exotic, some, such as *Typha domingensis*, commonly referred to as 'cattail', are native to the ecosystem they invade. Species that significantly modify

the physical structure of a site have a strong potential to alter hydrologic conditions and animal use. Invasive plants also reduce plant and animal diversity (Zedler and Kercher, 2004).

According to Mitsch and Gosselink (2015), "hydrology is probably the single most important determinant of the establishment and maintenance of specific types of wetlands and wetland processes". Indeed, hydrological inputs and outputs, water depth, flow patterns, duration and frequency of flooding all influence the biophysical state of a wetland, from its soil biochemistry, levels of nutrients, plant and animal species and vegetation cycles, as shown in figure 10. Small changes in hydrology can therefore lead to large biotic changes affecting species composition and richness or ecosystem productivity. In turn, the biota influences the hydrology and chemistry of the system. Microbes, for example, control nutrient availability to plants by catalyzing almost all changes in wetland soils. Plants influence sediment and nutrient flows, reduce erosion and can interrupt or divert water flows (Mitsch and Gosselink, 2015).

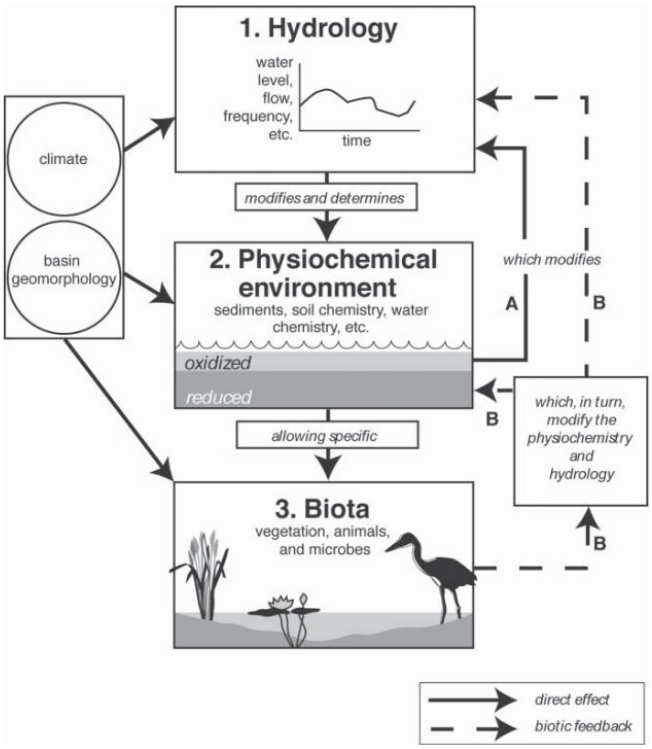

Figure 10: Conceptual diagram depicting the effects of hydrology on the wetland's physiochemical environment and biota and the biotic feedbacks that take place. Reprinted from Mitsch and Gosselink (2015).

One of the most important concepts of wetland hydrology is the hydroperiod, corresponding to the seasonal pattern of water level fluctuation within a wetland. The hydroperiod is defined by the flood duration, the amount of time the wetland is under

water, and by the flood frequency which is the number of times the wetland is flooded over a given period. The hydroperiod of a particular wetland can vary on a annual basis. This is especially true for riparian wetlands that are adjacent to and flooded by rivers. The intensity, duration, and frequency of floods in these wetlands vary from year to year.

A second essential concept of wetland hydrology is water budget. It consists in the balance of water inflows, outflows and storage, as calculated by equation (2.1). Water storage refers to the volume of water above the soil surface, in the soil vadose zone and in the underlying aquifer. The water budget is used to determine the hydrological state of a wetland at a given time.

$$\frac{\Delta V}{\Delta t} = P_n + S_i + G_i - ET - S_0 - G_0 \pm T \tag{2.1}$$

where

V = Volume of water storage in wetland;
$\Delta V/\Delta t$ = change in volume of water storage in wetland per unit time;
P_n = net precipitation;
S_i = surface inflows;
G_i = groundwater inflows;
ET = evapotranspiration;
S_0 = surface outflows;
G_0 = groundwater outflows;
T = tidal inflow or outflow (Mitsch and Gosselink, 2015).

Each term of eq. 2.1 can be expressed in terms of depth per unit time or volume per unit time.

2.2 Introduction to remote sensing

Remote sensing has been defined by the American Society of Photogrammetry as "the measurement or acquisition of information of some property of an object or phenomenon, by a recording device that is not in physical or intimate contact with the object or phenomenon under study" (Colwell, 1983). This acquisition of information is usually done via the measurement of electromagnetic wave radiations reflected or emitted by the studied object or phenomenon. Remote sensing is done using either handheld sensors or sensors fixed on aerial platforms such as drones, aeroplanes, or satellites. For many applications, remote sensing now represents a practical and economical opportunity to collect data.

Sensors used in remote sensing can either be categorized as active or passive sensors. Passive sensors, also called optical sensors, rely on light from the sun. They measure radiations between 400 to 2500 nm, in the visible, near-infrared and shortwave, mid- and long-infrared regions of the electromagnetic spectrum. Active sensors emit energy and measure the return time or the energy level reflected back. These are particularly useful since they do not need sunlight to operate and they can obtain data through cloud cover (Coops and Tooke, 2017).

Sensors measure light energy levels in different fractions of the electromagnetic spectrum. The reflectance curve, which correlates radiant energy levels and wavelength, is used for distinguishing or interpreting objects, as shown in figure 11. Multispectral sensors have a small number of bands, while hyperspectral sensors measure reflectance in many narrow spectral bands, up to a few hundred.

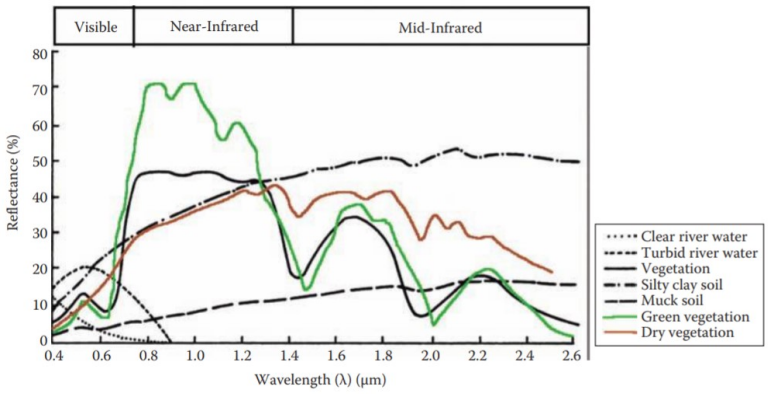

Figure 11: Typical reflectance curves of different land covers. Reprinted from Thenkabail (2016).

The resolution of the image must be taken into account depending on the remote sensing application. According to Thenkabail (2016), the concept of image resolution refers to four characteristics:

- the spatial resolution is the size of the minimum area that can be resolved by the sensor;
- the temporal resolution indicates the frequency of measurement by the sensor at the same location;
- the spectral resolution is the number, width and location of the spectral wavelength measured by the sensor;
- the radiometric resolution is the number of intensity levels that a sensor is able to quantify when detecting reflectance.

2.3 Satellite missions and sensors characteristics

As stated above, satellites carry sensors that collect many types of data. In this thesis, only optical satellite sensors are considered, mounted aboard the Landsat constellations and Sentinel 2A and 2B satellites. These are the platforms of the respective American NASA/USGS and European Copernicus space programs for Earth observations. General information about the satellites and sensors used in this thesis and their bands characteristics are shown in table 1.

Table 1: Landsat and Sentinel-2 satellites general information (European Space Agency; NASA; United States Geological Survey).

Resolution	**Landsat 4, 5 : Multi spectral Scanner (MSS) and Thematic Mapper (TM)**	**Landsat 7 : Enhanced Thematic Mapper Plus (ETM+)**	**Landsat 8 : Operational Land Imager (OLI)**	**Sentinel 2 : Multi Spectral Instrument (MSI)**
Launch and termination year	Landsat 4: 1982 - 1993 Landsat 5: 1984 - 2011	1999 - still active	2013 - still active	2015 - still active
Resolution				
Temporal (days)	16	16	16	5 (10 for each satellite)
Spatial	30 m (B6: 120 m)	30 m (B6: 60 m; B8: 15 m)	30 m (B8: 15 m)	10 m (B1: 60 m; B5-6-7-8A-11-12: 20 m)
Radiometric (bits)	8	8	8	12
Spectral (µm)				
Band 1	0.45-0.52 (Blue)	0.45-0.52 (Blue)	0.43-0.45 (Coastal aerosols)	0.43-0.45 (Aerosols)
Band 2	0.52-0.60 (Green)	0.52-0.60 (Green)	0.45-0.51 (Blue)	0.46-0.53 (Blue)
Band 3	0.63-0.69 (Red)	0.63-0.69 (Red)	0.53-0.59 (Green)	0.53-0.59 (Green)
Band 4	0.76-0.90 (Near infrared)	0.76-0.90 (Near infrared)	0.64-0.67 (Red)	0.64-0.67 (Red)
Band 5	1.55-1.75 (Shortwave infrared 1)	1.55-1.75 (Shortwave infrared 1)	0.85-0.88 (Near infrared)	0.70-0.71 (Red edge 1)
Band 6	10.40-12.5 (Brightness temperature)	10.40-12.5 (Brightness temperature)	1.57-1.65 (Shortwave infrared 1)	0.73-0.75 (Red edge 2)
Band 7	2.08-2.35 (Shortwave infrared 2)	2.08-2.35 (Shortwave infrared 2)	2.11-2.29 (Shortwave infrared 2)	0.77-0.79 (Red edge 3)
Band 8		0.52-0.90 (Panchromatic)	0.50-0.68 (Panchromatic)	0.78-0.89 (Near infrared)
Band 8A				0.85-0.88 (Red edge 4)
Band 9			1.36-1.38 (Cirrus)	0.94-0.96 (Water vapor)
Band 10			10.60-11.19 m (Brightness temperature)	1.36-1.39 (Cirrus)
Band 11			11.50-12.51 m (Brightness temperature)	1.57-1.66 (Shortwave infrared 1)
Band 12				2.11-2.29 (Shortwave 2)

2.4 Remote sensing of wetland vegetation

Mapping and monitoring the distribution, quality and quantity of plant species or the spatial distribution of water are just some of the critical tasks needed for sustainable wetland management. While these tasks used to be quite labour-intensive, remote sensing has opened a wide range of opportunities for wetland management. This section focuses on the use of remote sensing for wetland vegetation classification.

Most techniques of classification rely on different spectral responses of wetland veg-

etation types for classification. Classification methods are of three types: unsupervised, supervised and hybrid, which combines unsupervised and supervised methods. With unsupervised classification, also called clustering, pixels with similar spectral values are grouped together. Based on additional data acquired by other means, the analyst will label the groups by classes. Unsupervised classification doesn't require training data and is therefore less time-consuming. On the other hand, the clusters created by the algorithm do not always correspond to desired classes. Supervised classification does require a training data set and trains an algorithm to recognize the various classes previously defined (Ozesmi and Bauer, 2002).

The first step of any supervised classification method is defining the classes into which the data will be classified. The variance between classes must be greater than the variance within classes to facilitate a proper classification by the algorithm. The class separability is typically positively correlated to the dimensionality of the training data set, i.e. the number of discriminating variables used (Foody and Arora, 1997). A training data set is then sampled.

Different supervised classification algorithms exist. The most common ones are *K Nearest Neighbours*, *Maximum Likelihood*, *Support Vector Machine*, *Decision Trees* and *Random Forest*. No algorithm is optimal for all applications, but *Random Forest* has recently received a lot of attention in the field of wetland vegetation mapping (Mahdavi et al., 2018). The *Random Forest* (RF) algorithm is an "ensemble of decision trees, in which each tree is constructed using a subset of training samples with replacements"(Mahdavi et al., 2018). RF is an non-parametric classifier meaning it does not require any assumption over the distribution of the training data set.

Wetlands are very dynamic ecosystems. Water spatial distribution or vegetation growth and lushness can change in just a few days or weeks. The use of multi-temporal images takes advantage of this dynamic and has been found to improve the classification accuracy.

Validation is the last step to vegetation classification. It is crucial to assess the accuracy of the map created and its limitations. A subset of the sampled data should be used exclusively for validation. Training and validation data should be statistically independent (Millard and Richardson, 2015). By comparing the ground truth with the classification, one can assess its accuracy. This is usually done using a confusion matrix, as illustrated on figure 12. A confusion matrix compares the actual class of each validation point to the class it was assigned to on the map. The classification error can be described by the commission and the omission errors. Congalton and

Green (2009) define them as follows : "a commission error occurs when an area is included in an incorrect category; an omission error occurs when an area is excluded from the category to which it belongs. Every error on the map is an omission error from the correct category and a commission error to an incorrect category.". Observed accuracy can be calculated by dividing the sum of all sample units correctly classified by the total number of validation sample units. Producer's and user's accuracy are used to assess individual category accuracies. The producer's accuracy compares a category's number of correctly classified sampled units and the total number of reference sample units from this category. The user's accuracy compares a category's number of correctly classified sampled units and the total number of sample units classified in this category. Both are needed to assess the accuracy of the classification. Finally, Cohen's Kappa coefficient, eq. (2.2), is also often used when assessing the accuracy of a map. This coefficient compares the observed accuracy of the classification as previously defined, and the probability that agreement happened by chance.

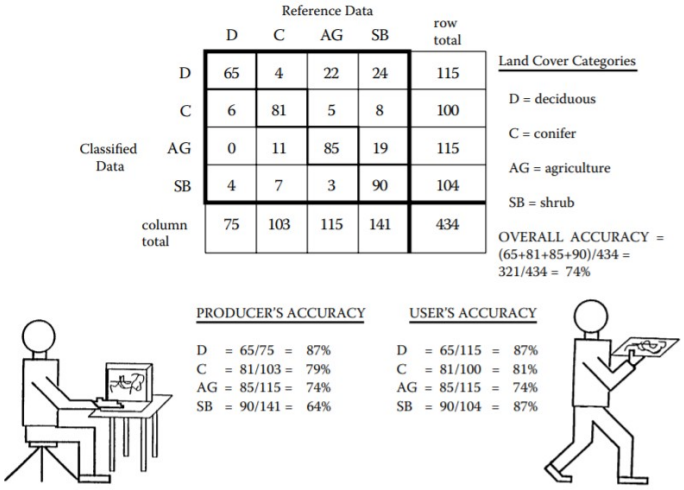

Figure 12: Example of a confusion matrix. Reprinted from Congalton and Green (2009).

$$\kappa = \frac{p_o - p_e}{1 - p_e} \tag{2.2}$$

where

p_o = the relative observed agreement between reference data and the classification;

p_e = the hypothetical probability of chance agreement (Congalton and Green, 2009).

2.4.1 Spectral indices

The discriminating variables used for land cover mapping are most often the sensor's spectral band values. Spectral indices are also useful for wetland monitoring and can

be used in classification algorithms. They are usually ratios between two or more spectral bands. Probably the most well-known spectral index is the normalized difference vegetation index (NDVI), eq. (2.3), which is sensitive to the vigor and quantity of vegetation. It is based on the red and near infrared (NIR) spectral bands. The NDVI varies from -1 to +1. Vegetation tends towards positive values, water takes low positive or negative NDVI values and soil has small positive values (Morell-Monzó et al., 2020). A shortcoming of NDVI is that dense vegetation can saturate it, as a result of saturation of the red band (W. et al., 2003). Enhanced vegetation index (EVI), eq. (2.4), was therefore developed to counter that flaw (Morell-Monzó et al., 2020). EVI usually varies between -1 and +1, although superior values are mathematically possible. Normalized difference water index is the name of two spectral indices, one related to water content of leaves ($NDWI_1$), eq. (2.5), and the other to water content in water bodies ($NDWI_2$), eq. (2.6). They are calculated using respectively the NIR and red bands and the NIR and shortwave infrared (SWIR) bands (Adam et al., 2008). Both indices range from -1 to +1 and higher values indicate a higher water content.

$$NDVI = \frac{NIR - Red}{NIR + Red} \tag{2.3}$$

$$EVI = 2.5 \cdot \frac{(NIR - Red}{(NIR + 6 \cdot Red - 7.5 \cdot Blue + 1} \tag{2.4}$$

$$NDWI\ 1 = \frac{NIR - SWIR}{NIR + SWIR} \tag{2.5}$$

$$NDWI\ 2 = \frac{Green - NIR}{Green + NIR} \tag{2.6}$$

2.4.2 Factors determining the spectral characteristics of the vegetation

When light interacts with vegetation, it is either reflected, absorbed or transmitted. As shown in figure 11 on page 15, plants have a high absorption in the visible spectrum (between 400 and 700 nm), with a reflectance spike in the wavelengths corresponding to the color green. Reflectance levels then rapidly increase in wavelengths greater than 700 nm. This region of the electromagnetic spectrum is called the red edge. It is this property that is commonly used to distinguish vegetation from other land covers, for which reflectance levels do not vary as dramatically in the red edge. Water for example has very low levels of reflectance in the near infrared and can therefore easily be differentiated from vegetation by classification algorithms or on false-color images, as illustrated on figure 13. In false color images, colors are assigned to wavelengths that humans cannot see. In the case of infrared false-color images, the blue, green and red

colors are respectively assigned to wavelengths corresponding to green, red and near infrared.

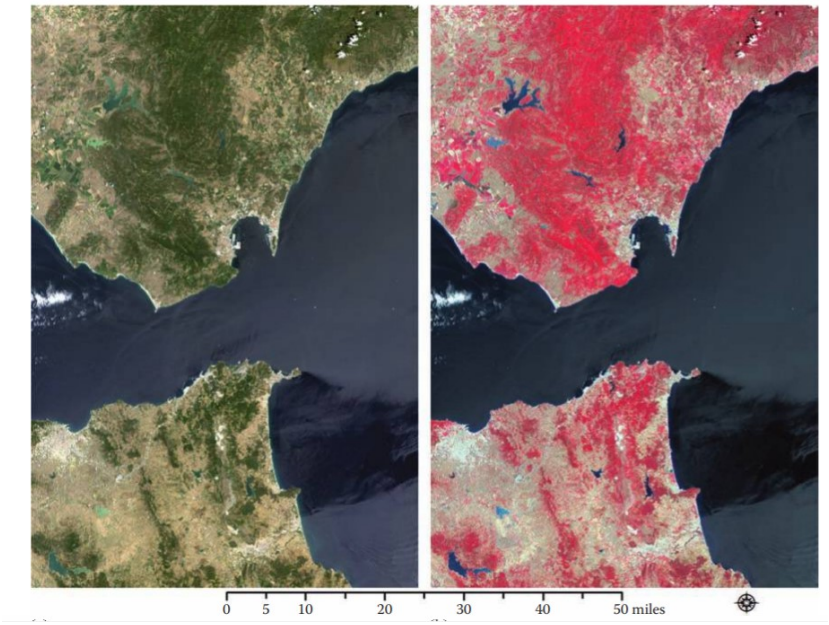

Figure 13: Illustration of an infrared false-color visualization and its ability to effectively highlight live vegetation. Reprinted from Thenkabail (2016).

The spectral signature of plants is quite similar between species because they contain the same components that influence light reflectance: "chlorophyll and other light-absorbing pigments, water, proteins, starches, waxes and structural biochemical molecules, such as lignin and cellulose" (Adam et al., 2008). The differences that do exist in spectral signature of different plant species usually come from differences in leaf optical properties and biochemical and biophysical status of the plants. Leaf optical properties depend on leaf surface, thickness and structure, water content and pigment concentration. Biochemical and biophysical status of plants depend, for example, on the time of year and possible water or nutrients stresses (Adam et al., 2008). The hydrologic regime of the wetland therefore has a great influence on the health and phenological status of the plants and thus on their spectral reflectance.

2.4.3 Challenges of wetland vegetation mapping

Vegetation mapping in wetland ecosystems presents challenges. First, plant phenology varies according to interactions with water. Because hydrological conditions are not uniform over large wetland areas, the phenology of a particular plant species might not be identical over the entire area. This phenomenon increases the variability of the spectral signature for the same species. It can therefore be difficult to identify clear demarcations between vegetation types or species. This is further complicated by the fact that different vegetation types in wetland ecosystems often have similar spectral

reflectance. The tendency of wetlands to have very mixed vegetation is an additional obstacle and can make the spatial resolution of satellite imagery a limiting factor. Second, the plants reflectance spectra are combined with those of the underlying soil or water and atmospheric vapour. This decreases spectral reflectance in the near and mid-infrared regions of the electromagnetic spectrum, rendering vegetation mapping more difficult (Adam et al., 2008).

Cloud cover is another problem that cannot be avoided. Satellite sensors will inevitably capture clouded areas on some images. Depending on the regional climate, there will be more or less usable images. For example, in the tropical regions, where Costa Rica and PVNP are located, very few images are almost or completely cloud-free during the rainy season. Monitoring a wetland in this type of climate must therefore be based almost entirely on images acquired during the dry season, when cloud cover is low. Clouds and cloud shadows masking is possible. Both Landsat and Sentinel products have per-pixel cloud information, which allows images to be selected based on cloud cover over a given area or to mask pixels that are likely cloudy.

2.5 Remote sensing of vegetation at PVNP

2.5.1 Previous vegetation classification of the Palo Verde sub-wetland

Studies on the distribution of vegetation types at PVNP have already been done in the past. Castillo and Guzmán (2004) studied the evolution of vegetation cover in the Palo Verde sub-wetland from 1975 to 2000 using orthophotos, as shown in figure 14. Solano (2004) classified the vegetation cover of the Palo Verde sub-wetland using MODIS-ASTER image from 2004, figure 15. Guzmán Álvarez (2007) classified Modis-Aster images of the Palo Verde sub-wetland from May 2003, January 2005 and March 2006, figure 16 However, no rigorous accuracy assessment of these maps was found, making it difficult to have complete confidence in these results. No other studies of vegetation cover distribution have been conducted using more recent satellite images. They are nevertheless a good indication of the type of plants that have been and are present in this sub-wetland.

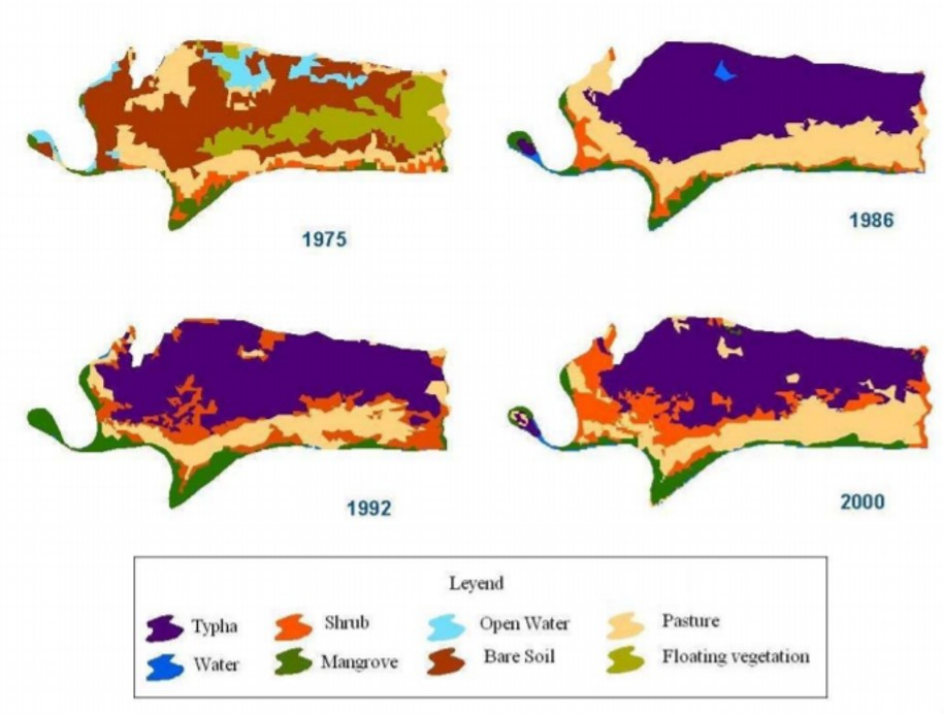

Figure 14: Evolution of the vegetation cover of the Palo Verde sub-wetland from 1975 to 2000 classified from orthophotos. Reprinted from Castillo and Guzmán (2004).

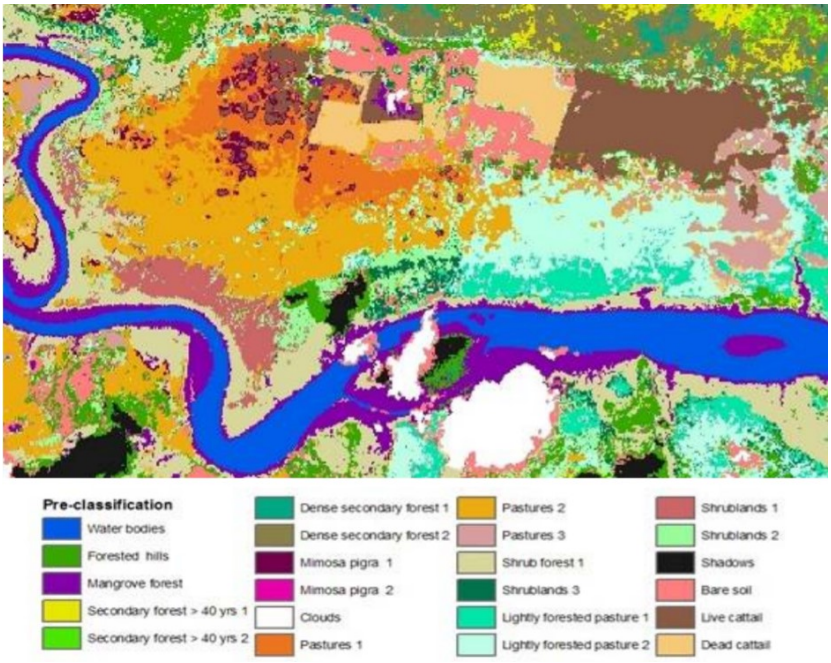

Figure 15: Vegetation cover of the Palo Verde sub-wetland in 2004 classified from a MODIS-ASTER image. Reprinted from Solano (2004).

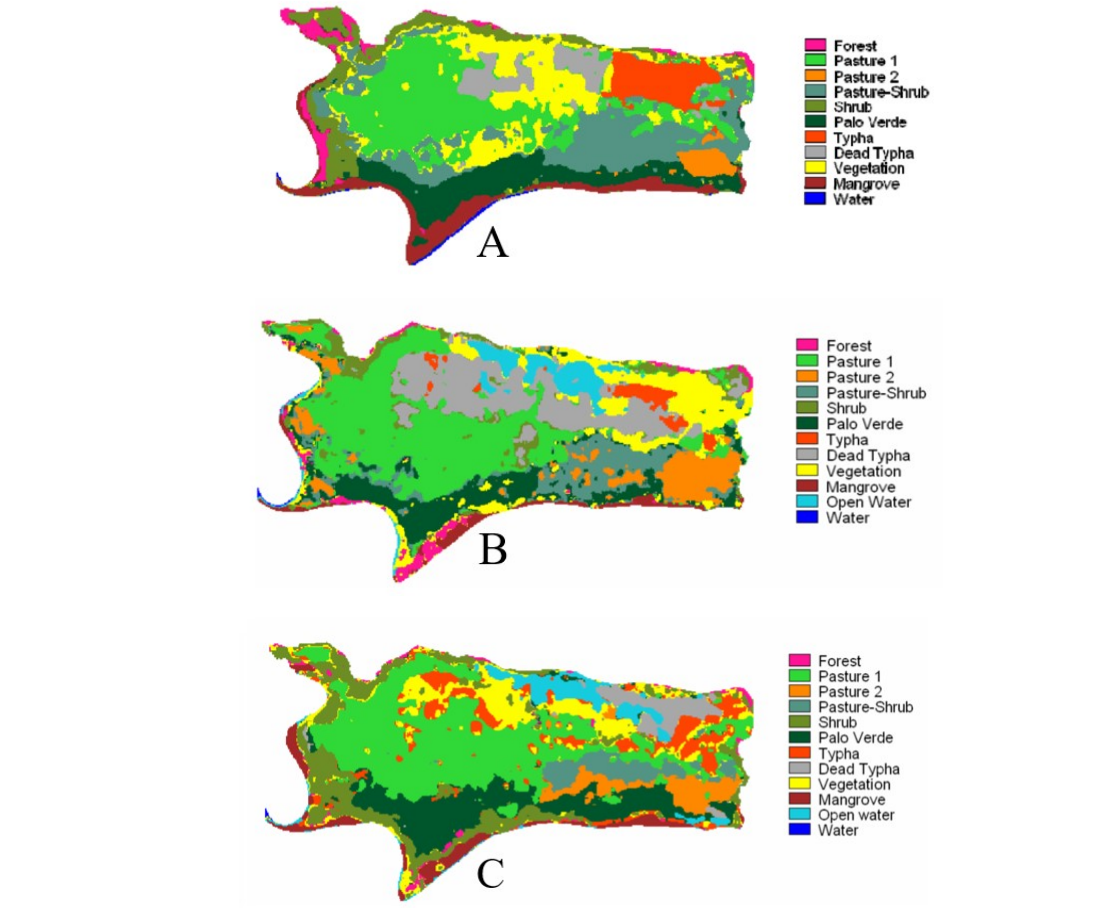

Figure 16: Landcover classifications from **A)** May 2003, **B)** January 2005, **C)** March 2006. Reprinted from Guzmán Álvarez (2007)

2.5.2 Hyperspectral remote sensing of the Palo Verde sub-wetland

Hyperspectral sensors acquire data over hundreds of narrow continuous spectral bands. They are usually handhell or airborne, fixed to drones for instance. The images obtained have a much better spectral resolution than, for example, the Landsat and Sentinel satellite images. In ecosystems where different vegetation types have similar spectral signatures, the use of hyperspectral sensors is particularly useful for discriminating between them.

Lørup Arildsen (2020) mapped the vegetation of an area of 66 hectares in the Palo Verde sub-wetland using hyperspectral data acquired during a drone flight in November 2018. After a principal component analysis was applied, a maximum likelihood classification algorithm was able to classify the vegetation cover in 8 classes with an accuracy of 95.8%.

Figure 17: RGB image of a 66 ha studied area in the Palo Verde sub-wetland and the corresponding vegetation map, classified with an accuracy of 95.82%. Reprinted from Lørup Arildsen (2020).

A vegetation classification was also done using simulated Landsat 8 and Sentinel-2 images obtained by reducing the spectral and spatial resolution of the hyperspectral images. The observed accuracy was respectively 64.3 and 73.6% for the simulated Landsat and Sentinel images.

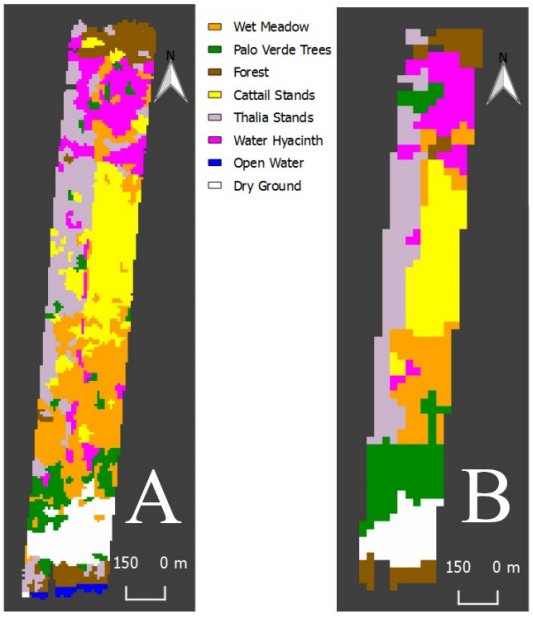

Figure 18: Vegetation classification of simulated Sentinel-2 (A) and Landsat 8 (B) images. Reprinted from Lørup Arildsen (2020).

2.6 Remote sensing of open water areas

As stated before, open water areas can be of particular interest. In the Palo Verde wetlands, open water areas which turn into exposed ground during the dry season are the two preferred land cover for waterbirds (Trama, 2009). Monitoring the temporal and spatial distribution of open water areas is therefore helpful in assessing the quantity of bird habitat at PVNP.

Water absorbs more energy than live vegetation in the near infrared and shortwave infrared regions of the electromagnetic spectrum. This property is therefore most often used to detect open water areas. Spectral indices have been developed, although not specifically for wetlands. $NDWI_2$, eq. (2.6) page 19, is a spectral index that is used to highlight water features. It uses the green and NIR bands. It takes positive values for water features while soil, and vegetation features have zero or negative values. This index however fails to efficiently discriminate between open water and built-up areas (McFeeters, 1996). Modified normalized vegetation index (MNDWI) was developed to get rid of this flaw. MNDWI can be expressed as follows :

$$MNDWI = \frac{Green - MIR}{Green + MIR} \tag{2.7}$$

where MIR is a middle infrared band. With MNDWI, water will have greater positive values than for NDWI, built-up land will take negative values as will vegetation and soil. MNDWI should work better than NDWI at enhancing water features (XU, 2006).

A single-band method also exists to extract open water information. It consists in choosing one band and applying a threshold to discriminate between water and other land covers. The band should be chosen in the near infrared or shortwave infrared regions of the electromagnetic spectrum, where water absorbs a lot of energy as opposed to live vegetation (Rundquist et al., 1987). This method requires the analyst to carefully choose a threshold as to not over- or underestimate open water areas.

The application of these methods to wetland environments might not be as straightforward as it could be in terrestrial ecosystems. In wetlands, it is necessary to be able to distinguish areas of open water from areas of closed water, where the water is under a layer of vegetation. In those areas, reflectance signals from water and vegetation are mixed and could therefore easily be wrongly interpreted as open water areas.

3 Objectives

This Master thesis is a descriptive eco-hydrological study of the Palo Verde National Park wetland areas in North-West Costa Rica. The objectives of this work are to improve our knowledge of water dynamics, the spatial distribution of a particular plant, and the water and vegetation response to human-induced disturbances to manage vegetation. 3 specific objectives have been developed and are presented below.

- **Study the spatial distribution of *Typha domingensis* in the Palo Verde National Park**

  Typha domingensis is a problematic plant at Palo Verde National Park because it is an invasive species. It reduces vegetation diversity and closes off open water areas. Such conditions tend to reduce migratory bird visits to PVNP. The spatial distribution of this plant in the area is not well documented. The first objective is therefore to map the spatial distribution of Typha.

- **Reconstruct and analyze historic open water areas at fine spatial resolution in the Palo Verde National Park and surrounding wetlands**

  Open water areas of PVNP are of particular interest because they form the preferred land cover for migratory and resident birds. The surface of open water areas was drastically reduced due to the Typha proliferation in the Park after 1980. This section aims to quantify open water areas, to study their long-term evolution and their annual dynamics.

- **Evaluate the long-term impact of the Fangueo vegetation management technique on open water and vegetation cover in the Palo Verde National Park**

  The Fangueo technique has been applied at PVNP during the past two decades to fight against *Typha domingensis* spread. Studies have shown it to be effective in reducing the Typha cover and opening water areas during the year following the intervention. This section aims to study the long-term impact of Fangueo on vegetation and open water areas.

4 Material and methods

4.1 Wetland vegetation mapping

4.1.1 Satellite imagery

In this work, Landsat 4, 5, 7 and 8 and Sentinel-2 images were used. All Landsat collections considered here are "Surface Reflectance Tier 1" collections. All Sentinel images are Bottom of Atmosphere reflectance images, also called Level-2A. Surface and bottom of the atmosphere means that the images were atmospherically corrected. These images are available for free. They were processed using the cloud-based Google Earth Engine (GEE) platform (Gorelick et al., 2017).The number of images covering PVNP, without cloud filtering, and available on GEE is as follows:

- Landsat 4 : 17 images from December 1987 to June 1993;
- Landsat 5 : 105 images from July 1984 to March 2011;
- Landsat 7 : 246 images from 1999 to date;
- Landsat 8 : 167 images from July 2013 to date;
- Sentinel 2 : 190 images from December 2018 to date[1].

Image filtering according to cloud cover and masking of clouds and cloud shadows is necessary to avoid data pollution. Clouds and cloud shadows masking can be a hard task, it was therefore decided to apply strict cloud filters to avoid masking errors. The Landsat data set contains pixel quality attributes which include per pixel cloud and cloud shadows information. To filter out cloudy images, these pixel quality attributes were first used to create a cloud and cloud shadows mask. This mask was used to count the number of cloudy pixels and calculate the percentage of clouded surface over the whole considered area. Images were then filtered by applying a clouded surface percentage threshold. An arbitrary threshold of 1 percent was chosen. Remaining clouds and shadows were masked using the aforementioned cloud and cloud shadows mask.

For Sentinel, a supplementary data set called "Sentinel-2: Cloud Probability" quantifies the probability that each pixel is cloudy. A cloud and cloud shadows mask was

[1] As of 30th July 2021.

created by selecting pixels with a cloud probability above an arbitrary threshold of 15 percent. This mask was used for calculating a clouded surface percentage which is used to filter images by applying a threshold of 3 percent cloudy area.

The two cloud image filtering methods for Landsat and Sentinel may seem arbitrary and strict, but the threshold values were carefully chosen to minimize the number of cloud-covered images, considering the fact that the cloud identification features of Landsat and Sentinel are not always consistent and effective.

4.1.2 Creation of Typha domingensis map

With an accuracy of more than 95 percent, the vegetation classification performed by Lørup Arildsen (2020) presented in section 2.5.2 can be considered as ground truth. This classification was performed using hyperspectral data acquired during a drone flight in November 2018. It covers an area of 66 hectares in the Palo Verde sub-wetland.

The EVI values of all pure Sentinel pixels, i.e. containing only one vegetation cover on Lorup's classification, were retrieved for each vegetation cover on 35 Sentinel images from December 15, 2018 to December 1, 2019. A map of the spatial distribution of Typha was created based on the differences in EVI evolution for different vegetation covers between these two images.

Besides the main objectives of this thesis, we also aimed at assessing the accuracy of Landsat-8 and Sentinel-2 images based vegetation classifications on the same area than Lorup's classification. Because they represent side results, the method and results are presented in Appendix 1.

4.2 Open water mapping

In this section, cloud filtering was applied on each of the 10 sub-wetlands to create 10 separate image collections, using Landsat 4, 5, 7 and 8 and Sentinel-2 imagery. Applying the cloud filters over smaller areas maximizes the amount of data. In order to differentiate between rain-fed and river-fed open water areas, the Nicaragua and Cipanci sub-wetlands were divided in two, by isolating the river-flooded areas in the South of the Nicaragua and the East of the Cipanci sub-wetlands.

The use of MNDWI, NIR and SWIR bands for open water detection in PVNP by applying a threshold value was then investigated. MNDWI was calculated using

the green and shortwave infrared bands of the Landsat and Sentinel images[2] as in eq. 2.7. The NIR or SWIR band threshold method is used to take advantage of the low reflectance of water compared to vegetation in these spectral regions. This method is applicable here because there is no or very little construction in the area of the Ramsar classified wetlands. Constructions can have a similar reflectance to open water in the NIR and SWIR spectral regions. Open water mask layers of each sub-wetland were generated for each available image by selecting all pixels with values higher than the chosen threshold for MNDWI or lower for the NIR and SWIR bands.

The threshold values were chosen through a trial and error process by calculating observed accuracy and Cohen's Kappa coefficient of open water masks for sequences of threshold values. These masks are binary, meaning that a pixel is either considered open water or other land cover. Hundreds of validation points were selected by hand for the class "Open water". For the class "Other land covers", 1000 validation points were randomly selected among the pixels with a MNDWI value lower than -0.5. This process was applied on a small sample of 20 images from the different satellite sensors.

Time series of total open water area for each sub-wetland were created. The location of the wetland subareas is shown in Figure 4. The Cipanci and Nicaragua wetland subareas were divided into two to isolate the areas frequently flooded by the Tempisque river. Their location are shown in figure 37 in Appendix 2

To document the spatial distribution of open water areas, a map of the frequency of occurrence of detection of open water for each pixel from 1984 to 2021 was made. Frequency of occurrence is defined as the ratio of the number of times a pixel is classified as open water to the total number of classifications performed on that pixel. The resulted map has a 30 m spatial resolution. Open water classifications made from Sentinel-2 images therefore had to be reprojected to the Landsat projection. The same map was also created for the months of January, February, March, April and December for which the most cloud-free images are available.

4.3 Evaluation of the long-term impact of Fangueo on open water and vegetation cover

The impact of the Fangueo vegetation management technique on open water and vegetation were evaluated using satellite imagery. Six zones where Fangueo was applied were

[2]B2-B7 for Landsat 4, 5 and 7, B3-B7 for Landsat 8 and B3-B12 for Sentinel-2

identified from park managers' documents, see table 2. Two of them underwent two vegetation management events a few years apart. These managed zones were delineated in GEE as well as adjacent control zones where no Fangueo was done. These control areas were placed right next to the managed zones and had similar spectral reflectance right before the Fangueo event. We can therefore assume that both had similar vegetation. As example, figure 19 shows Fangueo and control zones from 2019 in the Nicaragua sub-wetland. All images of Fangueo and control zones for each Fangueo event can be found in Appendix 3. Landsat 8 and Sentinel-2 images were selected based on cloud cover as in previous sections, calculated over the Fangueo and control zones.

Control areas were used to compare open water areas opened by Fangueo to those existing without vegetation management. EVI times series are also used to analyze revegetation of the managed areas and to compare long term vegetation dynamics in control and managed areas.

Table 2: Area of Fangueo and control zones and date of vegetation management

Zones ID	**Sub-wetland**	**Fangueo managed zone area (ha)**	**Control zone area (ha)**	**Fangueo date(s)**
PB	Piedra Blanca	7.1	8.5	December 2013
NIC1	Nicaragua	365.7	124.6	December 2013
NIC2	Nicaragua	23.8	27.5	December 2014
NIC3	Nicaragua	38.3	60.0	December 2015 - September 2019
PV1	Palo Verde	14.2	27.4	January 2014 - February 2020
PV2	Palo Verde	36.0	37.3	January 2014

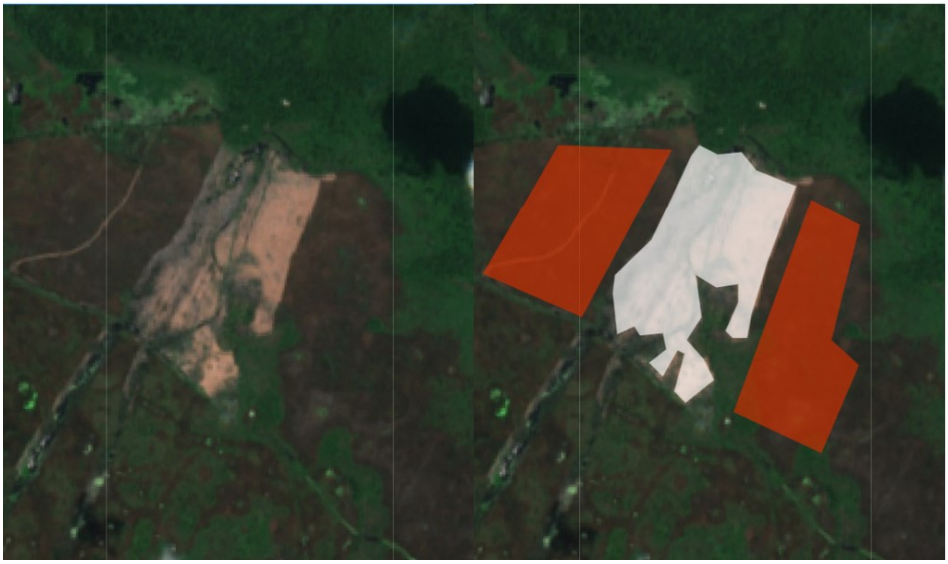

Figure 19: Fangueo event in the Nicaragua sub-wetland in 2019. The white zone corresponds to the Fangueo area, the red zone to the control areas

5 Results

5.1 Wetland vegetation mapping

The evolution of the EVI of the different vegetation covering a period of one year after November 2018 were plotted, as shown in figure 20. Data were collected in pure Sentinel-2 pixels in Lørup's classification area. 20 depicts an expected pattern for all vegetation types, except for Typha, with a decrease in EVI during the dry season and an increase during the wet season. Forest and particularly Dry Vegetation have more stable EVI values during the year. Typha on the other hand shows a different dynamic, with an increase in EVI from November to February before a decrease until June. This characteristic of Typha to become more vigorous after the end of the wet season unlike other vegetation covers can be used to detect it on satellite images. It is done by calculating the difference in EVI for pairs of images from the months of December 2018, January and February 2019. The pair of images, from which the median difference in EVI is most different for Typha compared to other vegetation covers, are the images from December 15, 2018 and January 28, 2019. As illustrated in figure 21, the difference in EVI between the two images seems clearly to be lower for Typha compared to other land covers.

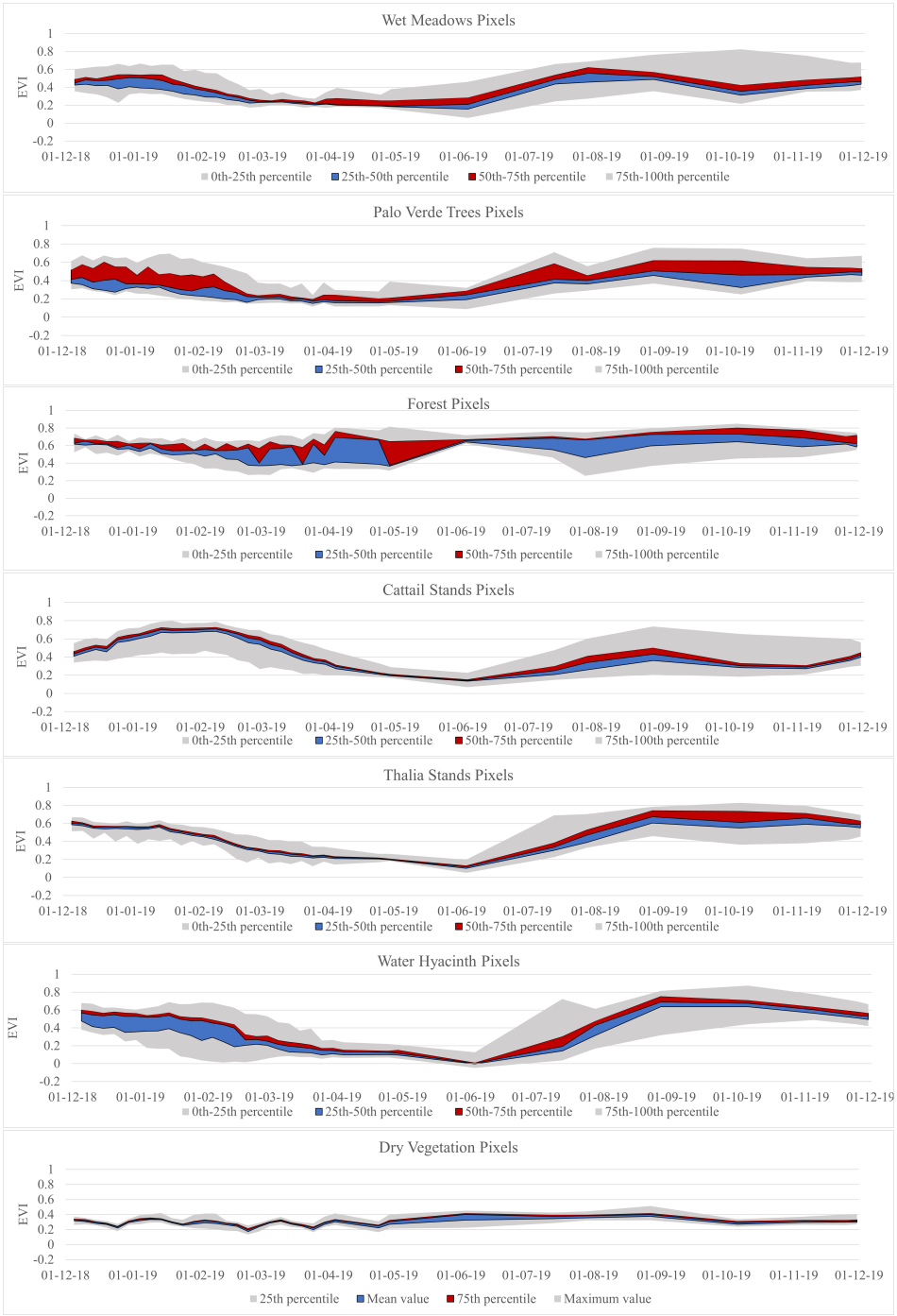

Figure 20: Year-long evolution of EVI of different PVNP land covers in Lørup's classification area.

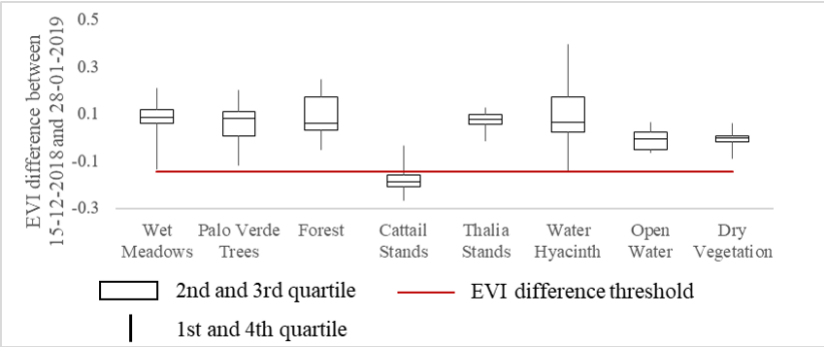

Figure 21: Differences of EVI for each vegetation cover between Sentinel images from December 15, 2018 and January 28, 2019 over Lørup's classification area and chosen EVI threshold for Typha discrimination.

Figures 22 and 23 show the EVI difference in the Palo Verde sub-wetland and in the entire PVNP for the period from December 15, 2018 to January 28, 2019. Negative values correspond to pixels for which the EVI was greater at the end of January than in December.

To create a binary map of Typha cover, a threshold of EVI difference was applied. A threshold value of -0.145 was chosen, corresponding to the minimum value of EVI difference measured in pure pixels of the other vegetation covers in Lørup's classified area, as seen on figure 21. Figure 24 shows a Typha map covering the entire PVNP produced with an EVI difference threshold of -0.145. Table 3 is the confusion matrix of the Typha map assessing its accuracy in Lørup's classified area. It was created by randomly selecting 15,000 pixels on the 37 cm spatial resolution Lørup classification and comparing their land cover. There are few commission errors for Typha, the user's accuracy is indeed very high at 90.6%. There are, however, a lot of omission errors, the producer's accuracy for Typha being only 44.3%.

Table 3: Confusion matrix of the Typha binary map on the Lørup's classified area.

		Reference, Lorup's classification		
		Not Typha	**Typha**	**User's accuracy**
EVI-difference-based classifier	**Not Typha**	12475	1060	92.2%
	Typha	137	1328	90.6%
	Producer's accuracy	98.9%	44.3%	

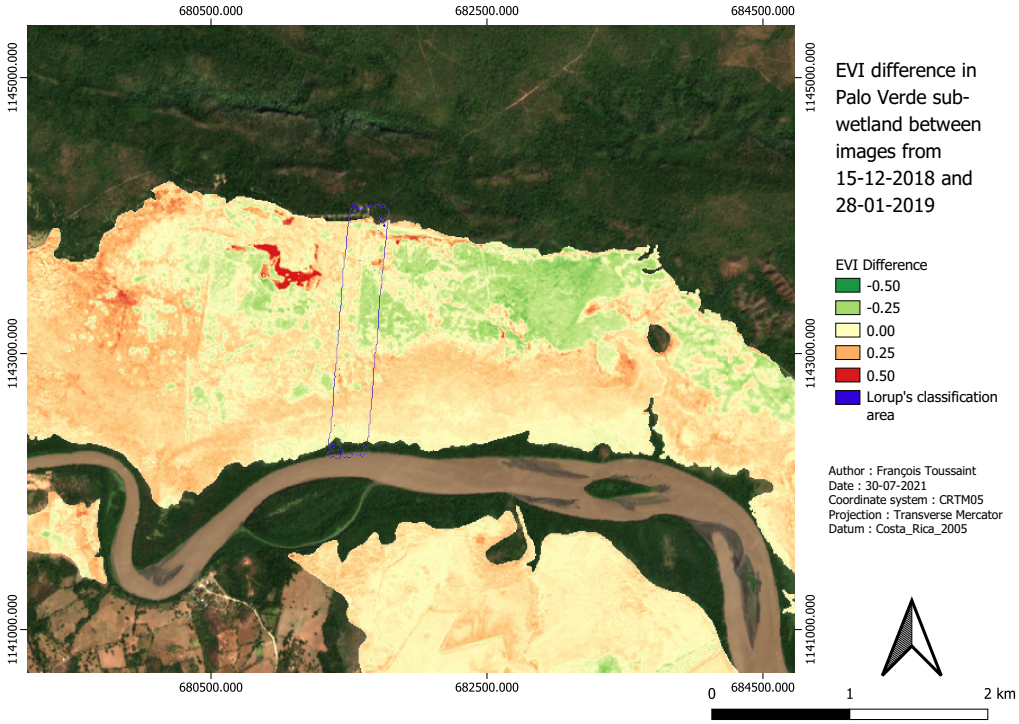

Figure 22: EVI difference between 15-12-2018 and 28-01-2019 in the Palo Verde sub-wetland.

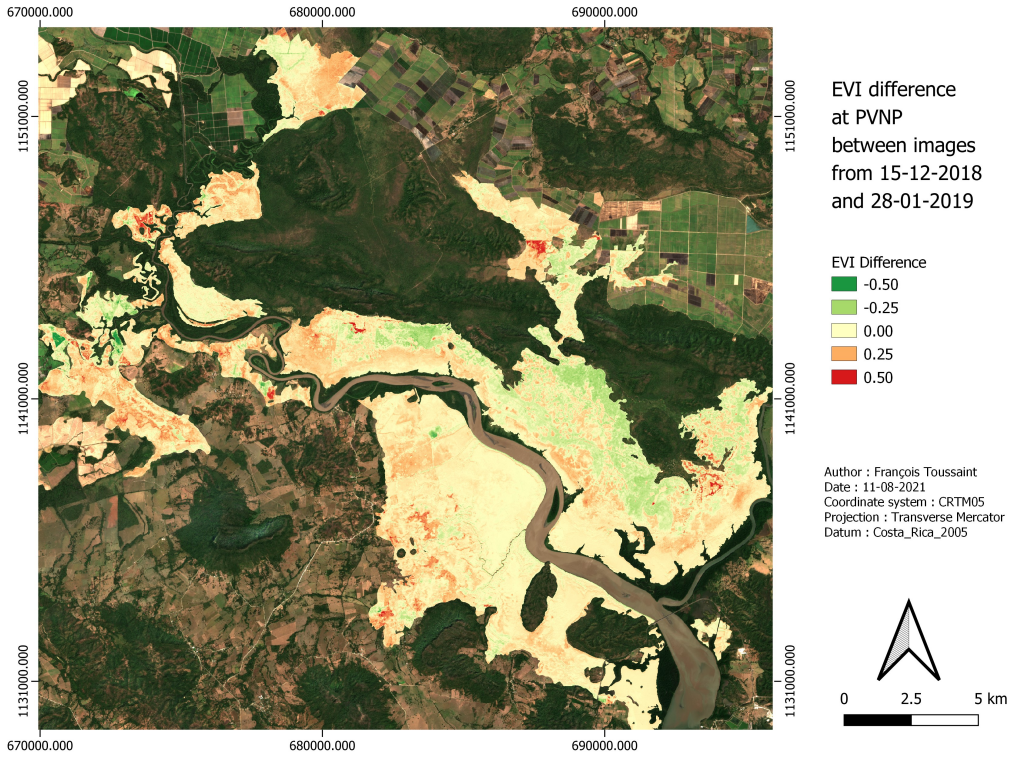

Figure 23: EVI difference between 15-12-2018 and 28-01-2019 in the Palo Verde National Park.

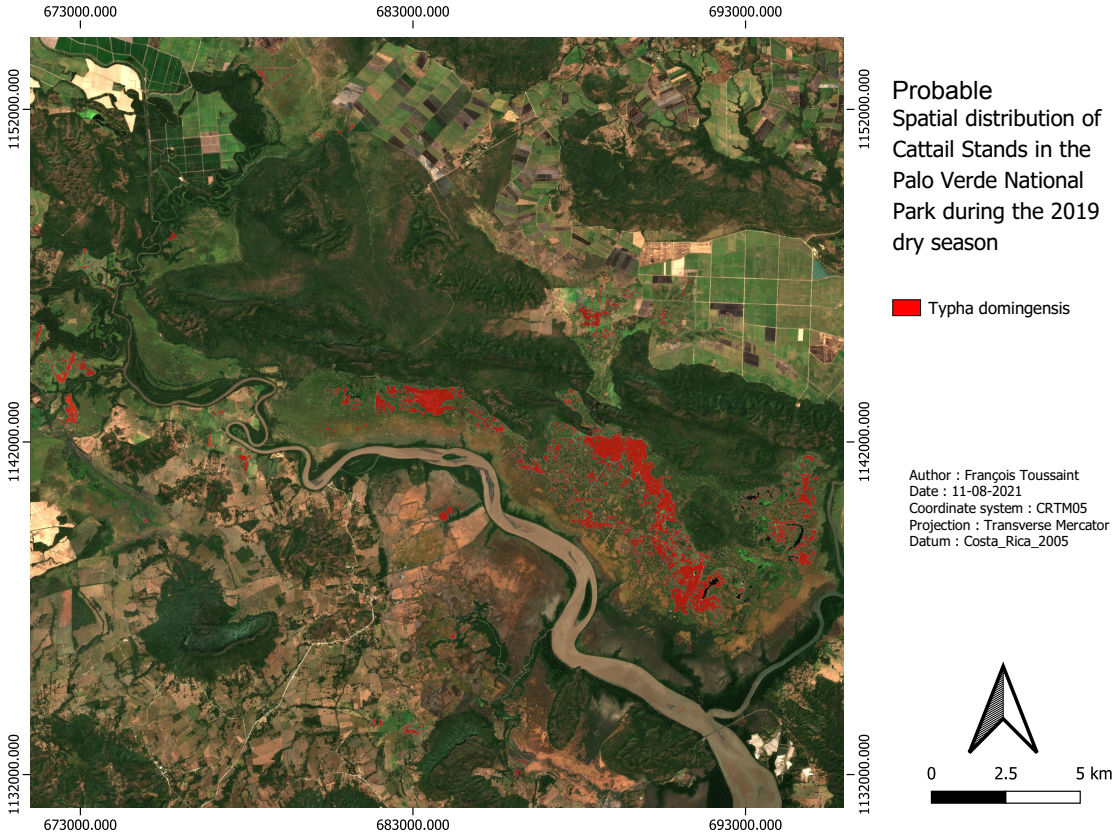

Figure 24: Map of *Typha domingensis* during the 2019 dry season at the Palo Verde National Park and surrounding wetlands based on the thresholded EVI difference.

5.2 Open water mapping

To create image collections from which open water information could be drawn, cloud filters were applied on the Landsat 4, 5, 7 and 8 and Sentinel-2 surface reflectance image collections. These filters were applied on each of the 10 sub-wetlands inside and around the Palo Verde National Park. The number of available cloud-free images ranged from 146 to 169 for the different sub-wetlands over the 1985-2021 period. About half of these images were acquired after December 2018 from the Sentinel-2 and Landsat-8 sensors. Between 1985 and 2003, between 1 and 8 cloud free images per year are available, with a data gap between 1993 and 1997. After Landsat-7's Scan Line Corrector failure in May 2003, no image from this sensor can be used for monitoring entire sub-wetlands. The GEE catalog also contains only 5 Landsat-5 cloud free images covering the PVNP area after 2003. There is therefore a data gap between 2003 and 2013, when the first Landsat-8 images are available. After December 2018, there are 25 to 30 cloud-free images available per year. Overall, 80% of these cloud-free images are from the months of December to April. This corresponds to the dry season at PVNP. Comprehensive information regarding the number of images per year and per month are given in Appendix 4.

Different methods were investigated to detect open water areas, using either the MNDWI, the NIR or SWIR bands. It was decided to use the NIR band by applying a threshold value based on an observational analysis of open water maps created with the three methods. More detail on this analysis can be found in Appendix 5. The threshold was chosen by calculating observed accuracy and Cohen's Kappa coefficient for sequences of values. It was found that, on average, the highest accuracy was performed with a reflectance threshold of 14%. The average observed accuracy and Cohen's Kappa coefficient were 96.8% and 0.82. The complete accuracy assessment is detailed in Appendix 6. Figure 25 shows an example of a sequence of images in the Nicaragua sub-wetland and their corresponding open water masks. This area was chosen because it presents large areas of open water in a relatively small area of the park. The correspondence between the open water bodies observed in the RGB map and those mapped by the classification rule is a good illustration of the satisfactory performance of the chosen method for open water detection.

Figure 25: QR code access to a sequence of Sentinel-2 RGB images (displayed as pseudo-true colors) of the Nicaragua sub-wetland and corresponding open water masks.

Times series of open water areas were created for each of the ten sub-wetlands from 1985 to 2021 as shown on figure figure 26 All open water area time series can be found in Appendix 7. Most open water areas can be found in the Cipanci, Corral de Piedra, Mata Redonda and Nicaragua sub-wetlands. Very few open water areas were detected in the the Piedra Blanca, Poza Verde and Varillal sub-wetlands. The location of the sub-wetland can be found in figure 2.

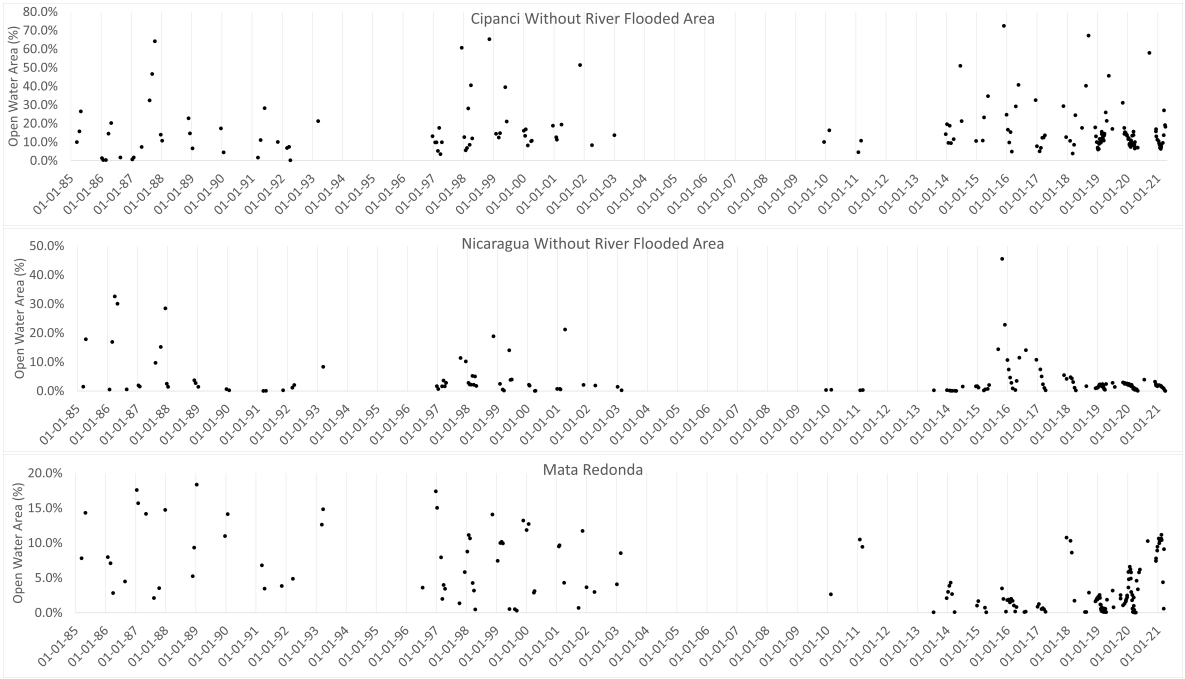

Figure 26: Times series from 1985 to 2021 of percentage of open water coverage in different sub-wetlands: Cipanci without the river flooded area (585 ha), Nicaragua without the river flooded area (696 ha) and Mata Redonda (1760 ha).

After 2014, more images were available due to the Landsat-8 and Sentinel-2 launch. Figure 27 shows the same time series zoomed in the 2014-2021 time span. It allows to better visualize the annual dynamic of open water areas in the different sub-wetlands. The few values measured during the wet season, between May and November, were generally higher. Open water areas were generally lower or declining at the end of the rainy season, but in some cases increased after the rains ended (e.g. in January 2020 in the Mata Redonda sub-wetland in figure 27.

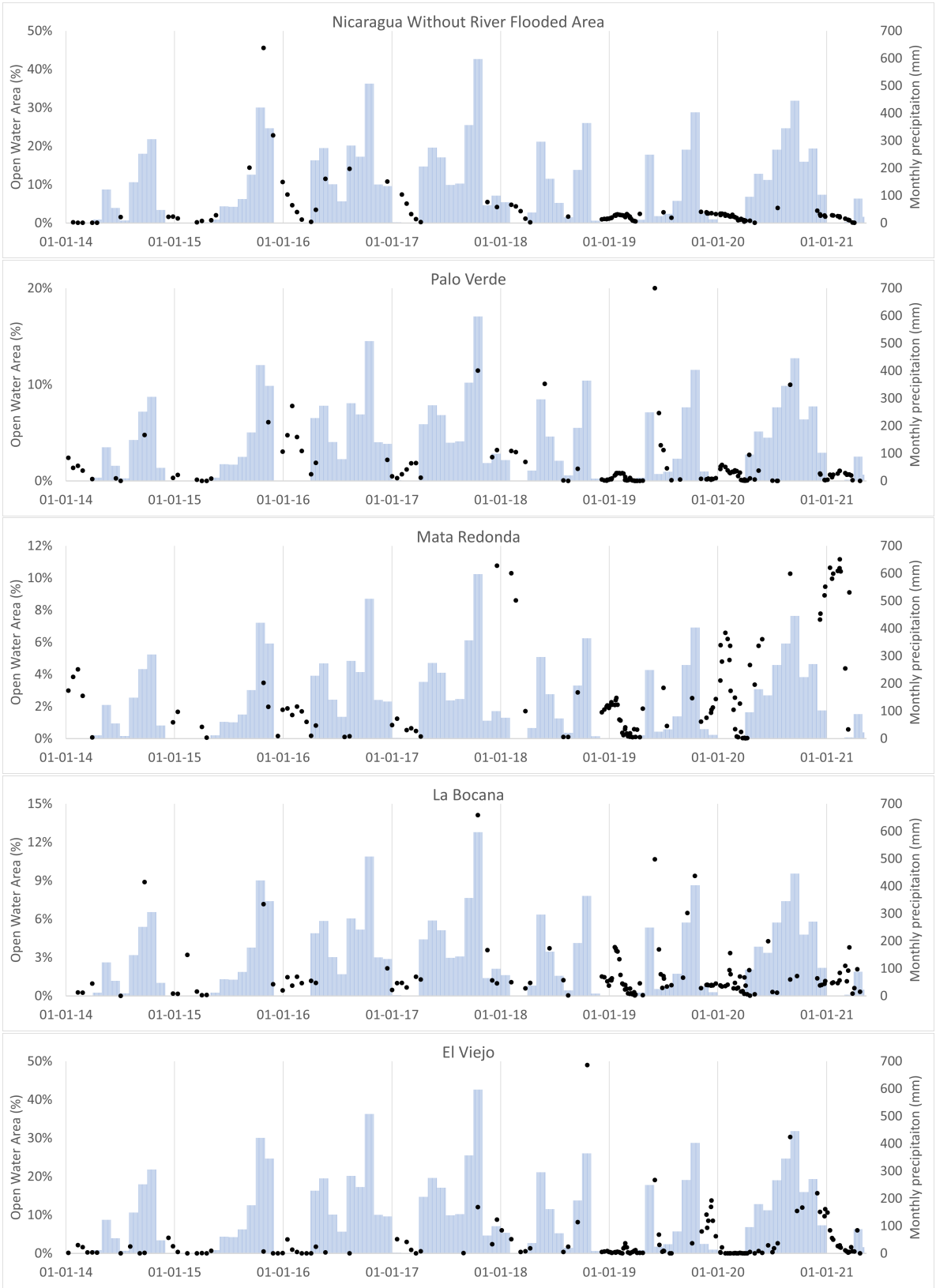

Figure 27: Times series from 2014 to 2021 of percentage of open water coverage in different sub-wetlands - Nicaragua, Palo Verde, Mata Redonda, La Bocana and El Viejo (black dots), and monthly precipitations (blue bars).

The spatial distribution of the open water areas at PVNP is illustrated by figure 28 showing the frequency of occurrence of open water for each 30 m-pixel of PVNP from 1985 to 2021. There are frequent open water areas in the Mata Redonda in the West, Nicaragua in the Est, and Corral de Piedra and Cipanci sub-wetlands in the South of the PVNP area. The areas in the South of the Nicaragua and the East of the Cipanci sub-wetlands are flooded by the Tempisque river. Figure 48 in Appendix 7 shows the monthly evolution of open water areas, averaged over the 1985-2021 period.

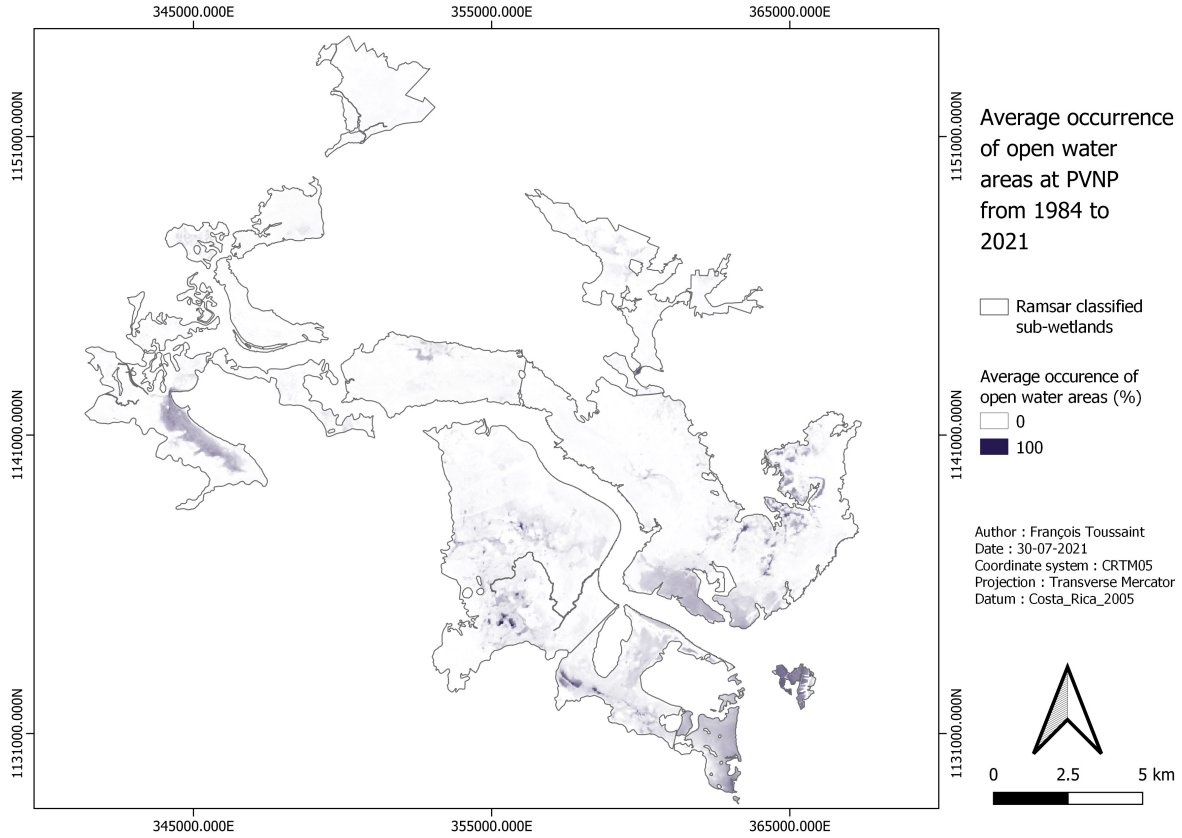

Figure 28: Frequency of occurrence of open water at PVNP from 1985 to 2021.

5.3 Evaluation of the long-term impact of Fangueo on open water and vegetation cover

5.3.1 Impact of Fangueo on open water

To monitor the impact of the Fangueo vegetation management technique, open water areas in Fangueo and control zones were measured. For some Fangueo events, open water areas were very low in control and Fangueo zones, so the effect of the technique could not be evaluated. For other areas such as the three Fangueo sites in the Nicaragua sub-wetland, open water area is distinctly higher in Fangueo than in control zones after

each Fangueo event, and during two to three years (figure 29). This effect becomes less apparent over time. In the NIC1, NIC3, PV1, PV2 and PV Fangueo zones, no significant differences in open water area between Fangueo and control zones were measured from two to three years after the intervention.

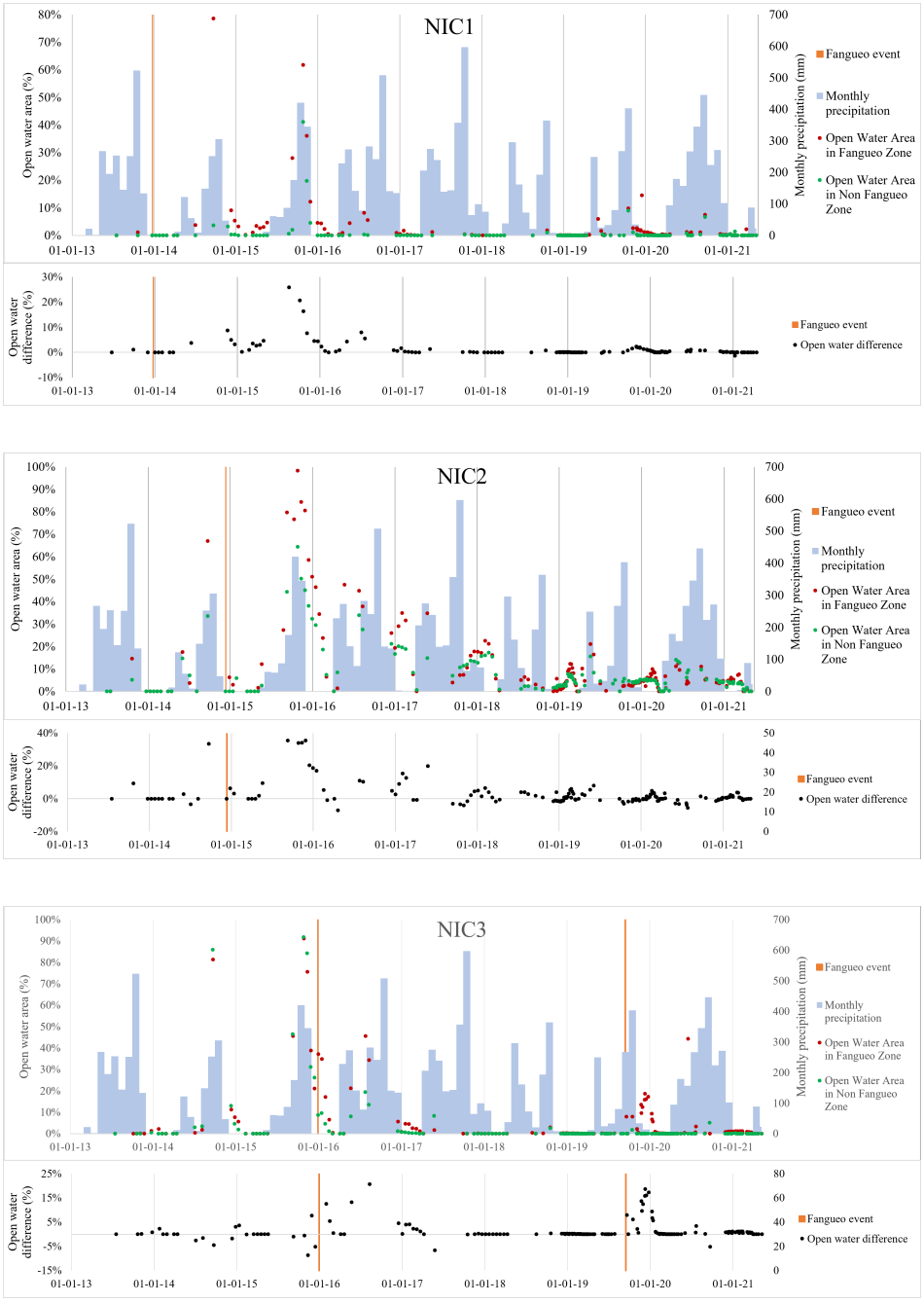

Figure 29: Evolution of open water areas in NIC1, NIC2 and NIC3 Fangueo and control zones. The time series graphs for the PB, PV1 and PV2 Fangueo zones can be found in Appendix 8.

5.3.2 Impact of Fangueo on vegetation

To monitor the impact of Fangueo on vegetation and more precisely on the presence of Typha in the intervention areas, times series of average EVI in Fangueo and control zones were created. They show a drop in EVI right after the Fangueo intervention which is not measured in the control zones (figures 30 and 31. The EVI Delta is the difference in EVI between the Fangueo and control areas. It is calculated from same-day EVI measurements in the two zones. In figure 30, EVI Delta decreases after each Fangueo event and approaches zero about one year after the intervention. This pattern is observed EVI Delta for a Fangueo area in the Nicaragua sub-wetland, shown on figure 31, does not stagnate around zero but has positive values in the first months of the year before decreasing to around zero around the half year. The EVI time series for the next 3 Fangueo areas are less representative. They can be found in Appendix 9.

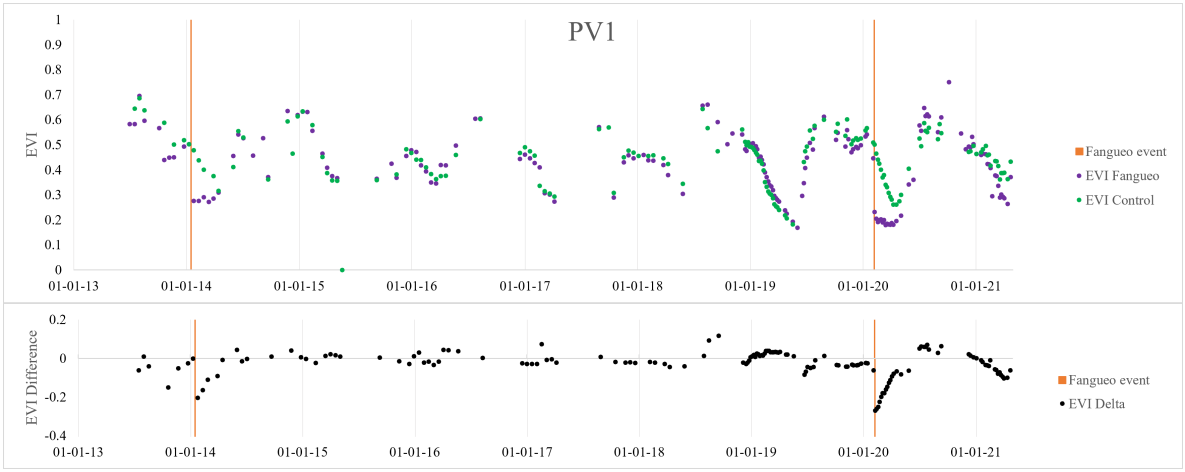

Figure 30: Evolution of average EVI and EVI Delta in PV1 Fangueo and control zones.

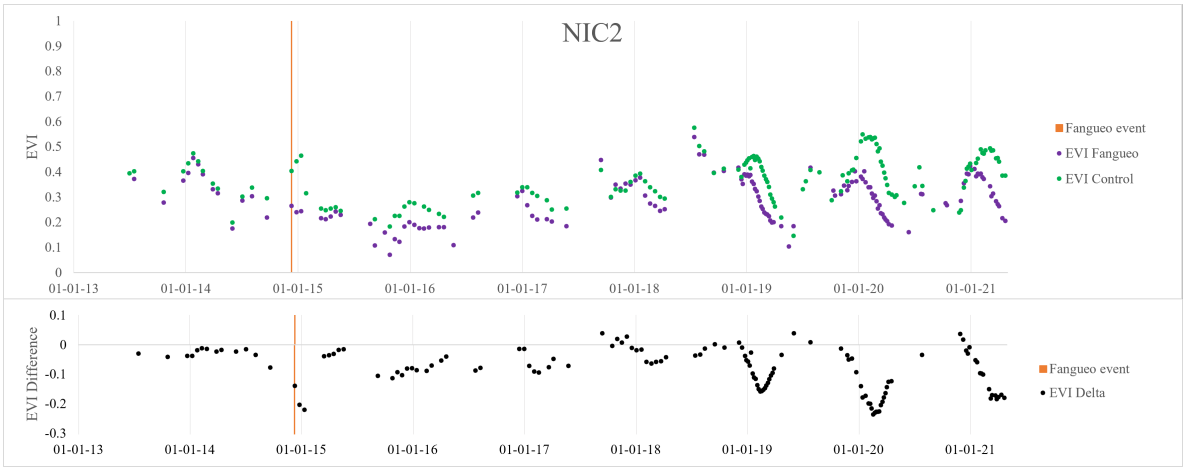

Figure 31: Evolution of average EVI in NIC2 Fangueo and control zones and of the EVI Delta between control and Fangueo zones.

6 Discussion

This explorative work aimed to improve the knowledge of vegetation and water dynamics and their interactions in the Palo Verde National Park and surrounding wetland. It was divided into three parts:

- Part 1 consisted in a descriptive analysis of the EVI dynamics of different vegetation covers and creation of a map of the spatial distribution of Typha domingensis;
- Part 2 consisted in the quantification of open water areas in each sub-wetland and the descriptive analysis of their temporal dynamics;
- Part 3 consisted in the evaluation of the impact of the Fangueo vegetation management technique on open water areas and vegetation.

The discussion is structured according to the 3 parts of this thesis.

6.1 Wetland vegetation mapping

The first part of this thesis The spatial distribution of Typha in the PVNP area has been mapped. Typha showed a different phenological dynamic at the end of the wet season than the other vegetation covers. The EVI of Typha increased at the beginning of the dry season in 2019 while the EVI of other plants remained stable or decreased, as shown in figure 20. The difference in EVI from images from December 15, 2018 and January 28, 2019 was used to highlight the spatial distribution of Typha and map it in PVNP. The map was created by applying a threshold on the EVI difference between the two images. This threshold was chosen to minimize commission errors.

First, EVI values were collected only on pure Sentinel pixels, i.e. containing only one vegetation cover on Lørup's classification. This method drastically reduced the amount of pixels from which EVI values were retrieved. Pixels with a predominant vegetation type covering a majority of the pixel's area could have been used. However, using mixed pixels would have resulted in a less accurate evaluation of the EVI trends of each vegetation types. EVI was used in this section to avoid the saturation effect of NDVI. NDVI could, however, have given similar results.

Second, EVI values were plotted over a one-year period for each group of pixels belonging to a vegetation group in December 2018. It is possible that the vegetation

types of these pixels changed during this one-year period. For example, the aquatic vegetation, such as water hyacinths, might not have survived during the dry season. It could have been replaced by bare ground or other types of vegetation. It is likely that the pixels that contained Typha in November still did later, as this species thrives during the dry season, as shown in figure 7.

An increase in EVI between December 2018 and February was measured for the Typha pixels. This trend was not measured for other vegetation covers, for which EVI stayed stable or decreases over the same period. The difference in EVI trends between different vegetation covers at PVNP during the start of the dry season is not reported in the literature. Trama (2009) reports that the soil under Typha plants would retain moisture during the dry season, but without elaborating on the mechanisms involved. There is no clear evidence explaining the increase in Typha greenness between December 2018 and February 2019.

Assuming that the pixels of all the vegetation covers other than Typha did not become completely covered by Typha by February 2019, which seems unlikely over a 2 month-period, it can be considered that the EVI increase between December and February is characteristic of Typha. This particular feature was therefore used to detect it using the difference in EVI between two images. The images used were captured on December 15, 2018 and January 28, 2019. This pair of images had the largest gap between the median Typha EVI difference and the median EVI difference of all the other vegetation types.

A map of Typha was created by applying a EVI difference threshold. Its value was chosen to minimize commission errors on sampled pure pixels in the Lørup classification area. The chosen threshold was -0.145, which is the minimum EVI difference value of the other vegetation types than Typha. The commission error for Typha on pure pixels is therefore zero. The omission value is around 25% for pure pixels.

When measured on the entire Lørup classification area, considering non-pure and pure pixels, the commission and omission errors for Typha are not as low. The confusion matrix, table 3, created from 15,000 randomly selected pixels over Lørup's classification area, shows that the commission and omission errors for Typha are respectively 9.4 and 55.7%. This means that there is a very high confidence level that pixels identified as Typha were correctly assigned in this category. However, this map misses out on a lot of Typha pixels.

It should be noted that the confusion matrix compares Lørup's 37 cm spatial reso-

lution classification with a 10 m spatial resolution Typha map. There is no doubt that a part of the above-mentioned errors are caused by the difference in spatial resolution. The confusion matrix just described is therefore a good assessment of the actual accuracy of the map but it certainly underestimates the actual performance of the method used to map Typha.

The method to detect Typha was applied out of Lørup's classification area, in the entire PVNP as depicted on figure 24. No ground truth data is available and no accuracy assessment could be made in these areas. This map is therefore only indicative of the areas in which we could expect to find Typha between December 15, 2018 and January 28, 2019. In no way should this map be considered as the correct spatial distribution of Typha during this period.

A flaw of this method to map Typha is linked to the vegetation response to variable water conditions in wetlands. The temporal and spatial dynamics of water levels in PVNP are highly dynamic. The vegetation responds to these varying water and soil humidity levels. The same type of vegetation could therefore experience different phenological stages in different areas of the park and during different periods. EVI varies with vegetation abundance and vigour and could therefore greatly differ for the same vegetation type in areas with different soil humidity and water levels. The assumption that the evolution of EVI for a certain type of vegetation in a certain area will be the same in other zones is therefore not valid. Great care should therefore be taken to only use this method in areas with similar water or soil humidity levels, which was not done for the production of the Typha map in figure 24.

The EVI difference method could however show promise to precisely map Typha in small areas. The difference in EVI trends for different vegetation types at the end of the wet season should systematically be proven. Extensive ground data should be used to assess the accuracy of the map created over the entire classified area. An EVI threshold could then be chosen to either minimize commission errors or maximize overall accuracy, for example, depending on the intended use of the map. Further work could combine the EVI difference method with other data, such as absolute EVI values or other spectral band or band indices values, to improve the classification. It could also be integrated into a more "classic" classification, using different spectral bands and the EVI difference value between two or more images for each pixel.

6.2 Open water areas

The second part of this thesis allowed us to reconstruct times series of open water in PVNP from 1985 to 2021. Open water area was largest in the Cipanci, Corral de Piedra, La Bocana, Mata Redonda and Nicaragua sub-wetlands, in terms of absolute surface. Open water area was generally highest during the wet season and there were measured instances of increasing open water area in the early dry season. No long-term trend analysis of open water area could be conducted due to limited data before 2013.

As stated in the result section, there are few cloud-free available images before 2013, when the first Landsat-8 images covering PVNP were available. This is due to the strict cloud filters applied on the Landsat and Sentinel image collections. These cloud filters were applied to individual sub-wetlands to create separate image collections for each of them. The allowed cloud coverage for an image to be considered cloud-free was very low. This reduced data noise caused by confusing clouds with open water by the detection methods used in this section. Due to high cloud cover during the wet season in PVNP's tropical region, only 20% percent of the images were captures during the months of May to November.

Three methods were considered for the detection of open water areas on satellite images : the uses of the MNDWI, the NIR and the SWIR bands. MNDWI is a standard spectral index usually used to detect large open water bodies. The uses of the NIR and the SWIR bands to detect open water rely on the difference in reflectance in this spectral region between vegetation and water. Each method was visually assessed on a great number of images from different sub-wetland areas and different periods of the year. Two illustrations are presented in Appendix 5 in figure 43 and 44. MNDWI was fairly successful in detecting humid areas but struggled to differentiate between open and closed water areas. MNDWI usually quite easily differentiates between vegetation and water, because they have very distinct reflectance in the middle infrared (MIR) band, which is used to calculate this index. But in the case of aquatic vegetation, for which pixel reflectance consists of mixed reflectance from both vegetation and water, MNDWI values are similar to open water pixels. The NIR and SWIR bands, on the contrary, showed good result in discriminating between aquatic and open water areas and to detect open water areas in general. Because the Sentinel band has a spatial resolution of 10 m compared to the 20 m SWIR band, it allows for a more accurate measurement of open water area. The detection of water was therefore done using only the NIR band.

Figure 43 shows that the Tempisque river in the bottom of the image has a different NIR reflectance than inland open water. This could be due to the fact that the river

water has more sediments which affects light reflectance.

Open water was detected by considering that all pixels with NIR reflectance values below a certain threshold are open water. This threshold was chosen by calculating the overall accuracy and Cohen's Kappa coefficient for open water classifications performed from different threshold values on 20 images. 20 images are a small subset of the 146 to 169 cloud-free images available for all wetlands. However, this process of evaluating the accuracy of open water detection is time consuming. The accuracy was assessed by comparing actual and predicted land cover for a validation dataset of 1000 randomly selected "not open water" pixels and hundreds of manually selected "open water" pixels. The 1000 "not open water" pixels were randomly selected among pixels with an MNDWI value less than -0.5, for which there should be complete certainty that they are indeed no open water. A NIR reflectance threshold value of 14% achieved the best overall accuracy and Kappa coefficient with respective values of 96.8% and 0.82. While these high numbers do indicate that this method did a better job at detecting open water than a random classification of pixels, they don't give a clear indication on the performance of open water detection, particularly in disputed pixels, i.e. pixels of aquatic vegetation, isolated open water pixels or pixels at the land-water border. This would require a much more detailed accuracy assessment, requiring the operator to manually select thousands of points in disputed area. Figure 25 shows a sequence of images in the Nicaragua sub-wetland, an small area with a lot of relatively small open water areas and their corresponding classification by the NIR threshold method. Although no numerical precision in the disputed areas is available, a visual inspection of this sequence of images gave us confidence that the method was quite accurate.

Figures 26 and 45 in Appendix 7 show the time series of open water area in each sub-wetland. As stated before, there are data gaps from 1993 to 1997 and from 2003 to 2013. Due to these data gaps and the low number of available images before 2013, no long-term trend of open water area could be analyzed. Most open water area was measured in the Cipanci, Corral de Piedra, Mata Redonda, Nicaragua and La Bocana sub-wetlands. Few open water areas were detected in the Piedra Blanca, Poza Verde and Varillal sub-wetlands.

More cloud-free images of PVNP have been available since 2014. The annual dynamic of open water in each wetland can therefore better be observed, as depicted in figure 27 and figure 47 in Appendix 7. We observe that the evolution of open water area tends to be consistent with the precipitation curve, with higher open water area during the wet season and lower during the dry season. This is well illustrated by the Nicaragua graph in figure 27. Unfortunately, cloud cover during the wet season

does not allow for the measurement of year-round open water curve. Data from the Nicaragua sub-wetland graph in figure 27 was measured on areas of the sub-wetland which are not flooded by the Tempisque river. Open water area in the river flooded area of the Nicaragua and Cipanci sub-wetlands does not follow seasonal patterns, as shown in figure 47, because overbank flooding, possibly resulting in open water in the wetland, can occur anytime during the year.

As we have established, the open water curves tend to exhibit a seasonal pattern, with higher open water area values during the wet season. Another pattern can be observed in different sub-wetlands. The area of open water often increases at the end of the wet season, when precipitations decrease or after they have completely stopped. This can for example be observed during the month of January 2020 in the Mata Redonda sub-wetland (figure 27). An increase in open water is either linked to an increase in surface water elevation caused in an input of water into the wetland, or by a decrease in vegetation cover. Since the observed pattern during the late wet season is not in phase with precipitations and surface water levels trends shown in figure 5, it can only be explained by a decrease in aquatic vegetation cover, opening up water areas.

Although few data are available for the wet season and no year-round open water curve could be measured, we can speculate on the shape of this curve. The overall open water curve in the PVNP could have two peaks, one during the wet season and one at the beginning of the dry season. We can also speculate on the drivers of this hypothetical curve. Starting at the end of the dry season, there are few areas of open water because the wetland is dry. As the wet season advances, the area of open water increases. The park vegetation in the wetlands changes from a dominance of emergent species to a dominance of floating and submerged vegetation. There is a peak in open water during the wet season followed by a decrease due to thriving aquatic vegetation covering the open water areas. As the dry season begins, these plants die, opening up areas of water, resulting in a second peak in open water area. As the dry season continues, the open water areas dry up. This is of course hypothetical and every assumptions made here should be tested. However, this is a logical explanation consistent with the observed data.

The spatial distribution of detected open water, figure 28, was mapped by calculating the average occurrence of open water for each pixel on every available image. As more cloud-free images are available during the dry season, this map is certainly an underestimation of the actual average occurrence of open water. It is nonetheless a good indications of where open water areas are located. As previously mentioned, most

open water areas are located in the Cipanci, Corral de Piedra, Mata Redonda, Nicaragua and La Bocana sub-wetlands. The areas in the South of the Nicaragua sub-wetland and the East of the Cipanci sub-wetland are regularly flooded with river water.

The year-round pattern and spatial distribution and quantification of open water in the different sub-wetlands could be of interest for the calculation of the water balance, to quantify evaporation from the total open water area. It could also be used in correlation with avian populations, which appear to be more numerous in open water areas, as established by previous studies.

6.3 Evaluation of the long-term impact of Fangueo on open water and vegetation cover

6.3.1 Impact of Fangueo on open water

This descriptive analysis of the impact of Fangueo on open water confirmed the results and hypotheses stated by previous studies (Trama, 2009; Osland et al., 2011). Both concluded that there was an increase in open water area in Fangueo zones during the year following the intervention. They did not study the long term impact of Fangueo, although (Osland et al., 2011) assumed that this effect would only last for 2 to 4 years. The results presented here confirm that the impact of Fangueo on open water is not sustained over time, with the area of open water decreasing to levels comparable to those in areas where no intervention was applied.

The method in the previous section for detecting open water was applied in 6 areas where Fangueo interventions were performed and in adjacent control areas. Open water was measured in Fangueo and control zones before the Fangueo event and until 2021 on available cloud-free images. In 3 of the 6 Fangueo sites, shown in figure 29, superior open water area was measured in Fangueo than in control zones. For the NIC1 and NIC3 Fangueo sites, the difference in open water between Fangueo and control zones went back down to zero after 3 and 2 years, respectively. At the Fangueo NIC2 site where the intervention was made in December 2013, a difference in open water area between the Fangueo and control areas was still measured in 2021, but not at the same level as just after the intervention. At the PV1, PV2 and PB Fangueo sites, a majority of measurements showed no difference in open water between Fangueo and control zones. But, unlike for NIC1, NIC2 and NIC3, open water measurements in the PV1, PV2 and PB control zones during the period after the Fangueo intervention were very low or zero.

The ability of the Fangueo vegetation management technique to increase the prevalence of open water areas is judged by comparing with control areas. It is the preferred method for two reasons. First, most of the Fangueo events studied occurred in 2013 and 2014. Studying the impact of Fangueo on open water by comparing with the period before Fangueo would therefore not have been possible as there are few cloud-free images available in the years before 2014. Second, even if it had been possible to systematically compare open water area before and after Fangueo, this method could be misleading. Indeed, by only observing open water area in Fangueo zones in figure 29, we could conclude that the considerable increase open water area observed at the end of 2015 was the consequence of Fangueo. However, open water area in control zones does also increase in that period, although less than in Fangueo zones. The comparison with the control areas requires that they achieve comparable levels of open water surface if they have the same vegetation. This should be the case since these areas are very close and have the same topography.

6.3.2 Impact of Fangueo on vegetation

The impact of Fangueo on vegetation was assessed by creating average EVI time series in Fangueo and control zones. It was found that EVI dropped in Fangueo zones after the intervention, which was expected as it consists in crushing vegetation. The long-term impact of Fangueo on EVI was found to be different at the different Fangueo sites. For some, such as the PV1 and NIC3 sites, EVI of Fangueo and control areas was very similar after 1 and 2 years, respectively. At the NIC1 and PV2 sites, the EVI difference between Fangueo and control sites is nearly identical before slightly increasing during the early dry season. The EVI level becomes nearly identical again around mid-year. At the PB and NIC2 sites, the contrary is observed, with a decrease in EVI difference between Fangueo and control zones during the early dry season.

Overall, these results show that vegetation recolonized the Fangueo areas quite quickly as seen by the similar EVI between Fangueo and control areas. EVI varies with vegetation abundance, its phenological state and potential stresses. Based on EVI measurements but Without ground information, it is therefore difficult to make assumptions on the types of vegetation present in the Fangueo area after the intervention. Similar EVI values in Fangueo and control zones measured years after the intervention could be a sign that the vegetation type is similar in these two zones. On the contrary, differences in EVI between control and Fangueo areas measured years after the intervention could be a sign that the vegetation types are different in these two zones. This was however not proven. Furthermore, no information on Typha presence in Fangueo or control zones could be drawn from these EVI measurements. This method can therefore

be considered unsuccessful at assessing whether Fangueo leads to a long-term decrease or not of Typha cover in intervention areas.

7 Conclusions

This Master thesis was a descriptive eco-hydrological study of the Palo Verde National Park wetland areas in North-West Costa Rica. The objectives of this work were to improve our knowledge of water dynamics, the spatial distribution of a particular plant, and the water and vegetation response to human-induced disturbances to manage vegetation.

The first objective is to study the spatial distribution of Typha. This plant showed a different phenological dynamic at the end of the wet season than the other vegetation covers. The measured difference in EVI dynamic during that period was used to highlight the spatial distribution of Typha and map it in PVNP. No accuracy assessment could be made and this map is therefore only indicative of the areas in which we could expect to find Typha during the early dry season in 2019. This map should not be considered a correct spatial distribution of Typha during that period. The method used should only be applied in areas with similar water or soil humidity levels and could show promise to precisely map Typha in small areas.

The second objective of this thesis was to analyze open water dynamics at PVNP. Times series of open water in PVNP from 1985 to 2021 were reconstructed. Open water area was largest in the Cipanci, Corral de Piedra, La Bocana, Mata Redonda and Nicaragua sub-wetlands, in terms of absolute surface. Open water area was generally highest during the wet season and there were measured instances of increasing open water area in the early dry season. Since the observed pattern during the late wet season is not in phase with precipitations and surface water levels trends, it can only be explained by a decrease in aquatic vegetation cover, opening up water areas. No long-term trend analysis of open water area could be conducted due to limited data before 2013. These analyses could be of interest for the calculation of the water balance, to quantify evaporation from the total open water area. It could also be analyzed in correlation with avian populations.

The third and final objective was to study the long-term effects of the Fangueo vegetation management technique on open water and vegetation cover in the Palo Verde National Park. The descriptive analysis of the impact of Fangueo on open water confirmed that the increase in open water area after the intervention was not sustained over time. Open water area indeed decreased to levels comparable to those in areas where

no intervention was applied. This method employed to study the vegetation cover after a Fangueo event was unsuccessful at assessing whether Fangueo leads to a decrease or not of Typha cover in intervention areas. It could only show that the intervention areas were rapidely revegetated, only around a year after the intervention.

8 Bibliography

Adam, E., Mutanga, O., and Rugege, D. (2008). Multispectral and hyperspectral remote sensing for identification and mapping of wetland vegetation: a review. *Wetlands ecology and management*, 18:281–296.

Alonso, A. (2017). *Novel quantification of long-term hydrological and landscape spatiotemporal dynamics of coupled natural human systems: the case study of the Tempisque-Palo Verde National Park coastal wetland, Costa Rica*. PhD thesis, University of Florida.

Alonso, A., Estornell, J., and Sebastiá-Frasquet, M. (2020). Coupling high-resolution field monitoring and MODIS for reconstructing wetland historical hydroperiod at a high temporal frequency. *Remote sensing of environment*, 247:111807.

Alonso, A., Muñoz-Carpena, R., Kennedy, R., and Murcia, C. (2016). Wetland landscape spatio-temporal degradation dynamics using the new Google Earth Engine cloud-based platform: opportunities for non-specialists in remote sensing. *American Society of Agricultural and Biological Engineers*, 59(5):1333–1344.

Andrews, N. and Pratt, D. (1978). Energy potential of cattails (Typha spp.) and productivity in managed stands. *Journal of the Minnesota Academy of Science*, 44.

Bansal, S. e. a. (2019). Typha (Cattail) invasion in North American wetlands: biology, regional problems, impacts, ecosystem services, and management. *Wetlands*, 39:645–684.

Castillo, M. and Guzmán, J. (2004). Cambios en la cobertura vegetal en el Humedal Palo Verde segun SIG. *Ambientico*, 129:4–6.

Colwell, R. (1983). *Theory, instruments, and techniques*, volume 1 of *Manual of Remote Sensing*. American Society of Photogrammetry.

Congalton, S. and Green, K. (2009). *Assessing the accuracy of remotely sensed date : principles and practices*. CRC Press.

Coops, N. and Tooke, T. R. (2017). Introduction to remote sensing. In *Learning landscape ecology*. Springer-Verlag.

Crombé, B. (2019). *Estimation de la variabilité spatiotemporelle de l'évapotranspiration dans une zone humide en stress hydroécologique*. Master's thesis, Université Catholique de Louvain.

Davis, R. and Hirji, R. (2005). Water resources and environment. Technical note, The World Bank.

European Space Agency (n.d.). Sentinel-2 msi technical guide. [Online; accessed July 26, 2021].

Foody, G. and Arora, M. (1997). An evaluation of some factors affecting the accuracy of classification by an artificial neural network. *International journal of remote sensing*, 18(4):799–810.

Gorelick, N., Hancher, M., Dixon, M., Ilyushchenko, S., Thau, D., and Moore, R. (2017). Google Earth Engine: Planetary-scale geospatial analysis for everyone. *Remote sensing of environment*, 202:18–27.

Guzmán Álvarez, J. A. (2007). Effects of land cover changes on the water balance of the Palo Verde Wetland, Costa Rica. Master's thesis, International Institute for Geo-information Science and Earth Observation, Enschede, The Netherlands.

Jiménez-Rodríguez, C., Esquivel-Vargas, C., Coenders-Gerrits, M., and Sasa-Marín, M. (2019). Quantification of the evaporation rates from six types of wetland Cover in Palo Verde National Park, Costa Rica. *Water*, 11(4):674.

Ledeganck, G. (2019). *Combinaison d'analyses chimiques et isotopiques pour déterminer les origines de l'eau à Palo Verde (Costa Rica)*. Master's thesis, Université Catholique de Louvain.

Lørup Arildsen, R. (2020). *Hyperspectral remote sensing of functional biodiversity using UAV in Palo Verde National Park*. Bachelor Thesis, Danmarks Tekniske Universitet.

Mahdavi, S., Bahram, S., Granger, J., Amani, M., Brisco, B., and Huang, W. (2018). Remote sensing for wetland classification: a comprehensive review. *GIScience and remote sensing*, 55(5):623–658.

McCoy, M. B. (1996). The importance of grazing for the seasonal, freshwater marsh at palo verde national park, costa rica. In *Workshop Proceedings*, Latin America regional livestock assessment.

McFeeters, S. (1996). The use of the Normalized Difference Water Index (NDWI) in the delineation of open water features. *International journal of remote sensing*, 17(7):1425–1432.

Millard, K. and Richardson, M. (2015). On the importance of training data sample selection in random forest image classification: a case study in peatland ecosystem mapping. *Remote sensing*, 7:8489–8515.

Mitsch, W. J. and Gosselink, J. G. (2015). *Wetlands*. John Wiley Sons, Inc., Hoboken, New Jersey.

Morell-Monzó, S., Estornell, J., and Sebastiá-Frasquet, M. (2020). Comparison of Sentinel-2 and high-resolution imagery for mapping land abandonment in fragmented areas. *Remote sensing*, 12:2062.

NASA (n.d.). Landsat science. [Online; accessed July 26, 2021].

Osland, M. J., González, E., and Richardson, C. J. (2011). Restoring diversity after cattail expansion: disturbance, resilience, and seasonality in a tropical dry wetland. *Ecological Applications*, 21(3):715–728.

Osland, M. J. and Richardson, C. J. (2011). Coastal freshwater wetland plant community response to seasonal drought and flooding in Northwestern Costa Rica. *Wetlands*, 31:614–652.

Ozesmi, S. L. and Bauer, M. E. (2002). Satellite remote sensing of wetlands. *Wetlands ecology and management*, 10:381–402.

Rundquist, D., Lawson, M., Queen, L., and Cerveny, R. (1987). The Relationship between the Timing of Summer-Season Rainfall Events and Lake-Surface Area. *Water resources bulletin*, 23:493–508.

Society for ecological restoration (2014). Costa rica: Restauración del humedal palo verde en la guanacaste. [Online; accessed July 25, 2021].

Solano, J. (2004). *Estudio de la distribucion y abundacia de Parkinsonia aculata y Typha dominguensis en el Humdela Palo Verde.*

Thenkabail, P. S. (2016). *Remote sensing handbook*, volume 1 of *Remotely sensed data characterization, classification, and accuracies*. CRC Press.

Trama, F. A. (2009). Wetland cover types and plant community changes in response to cattail-control activities in the Palo Verde marsh, Costa Rica. *Ecological Restoration*, 27(3):278–289.

Trama, F. A., Rizo Patron Viale, F. L., Kumar, A. S., Stynoski, J. L., McCoy Colton, M. B., and Springer, M. C. (2017). The Management of Typha domingensis (Typhaceae) affects macroinvertebrate assemblages in the Palo Verde wetland, Guanacaste, Costa Rica. *Ecological Restoration*, 35(2):1522–4740.

United States Geological Survey (n.d.). Landsat missions. [Online; accessed July 26, 2021].

W., Z., C., L., and W.N., H. (2003). From AVHRR-NDVI to MODIS-EVI: Advances in vegetation index research. *Acta Ecologica Sinica*, 23(5):979–987.

Waylen, P. and Laporte, M. S. (1999). Flooding and the El Niño-Southern oscillation phenomenon along the Pacific coast of Costa Rica. *Hydrological Processes*, 13(16):2623–2638.

XU, H. (2006). Modification of normalised difference water index (NDWI) to enhance open water features in remotely sensed imagery. *International journal of remote sensing*, 27(14):3025–3033.

Zedler, J. and Kercher, S. (2004). Causes and consequences of invasive plants in wetlands: opportunities, opportunists, and outcomes. *Critical reviews in plant sciences*, 23(5):431–452.

9 Appendix

1. Vegetation classification of 66 ha area in the Palo Verde sub-wetland using satellite imagery

1.1. Material and Method

A classification on the area classified by (Lørup Arildsen, 2020) was done using Sentinel-2 and Landsat-8 images. The land cover classes remained the same than the ones Lorup defined: Wet Meadows, Palo Verde Trees, Forest, Cattail Stands, Thalia Stands, Water Hyacinth, Open Water and Dry Vegetation. Pure pixels were sampled for each land cover on Sentinel and Landsat images respectively captured on December 5 and 6, 2018. These images are the two closest cloud-free images from November 2018 and the vegetation cover can be considered identical. In order to recreate the results of a realistic classification done using data sampled on the ground, not all pure pixels were sampled.

For a supervised classification algorithm to distinguish between different land covers, the spectral signatures should be statistically different. A Mann-Whitney U-test was performed for pairs of land covers reflectance for each Sentinel and Landsat band. The hypothesis tested is that there is no significant difference between the median reflectance of each individual waveband for each pair of land covers. Stated formally, the null hypothesis is as follows:

$$H_0 = \eta_n(i) = \eta_{n+1}(i) \tag{1}$$

with η_n the median reflectance for land cover number n=1, 2, 3, ..., and i=1, 2, 3, ..., are the wavebands considered. The null hypothesis was tested at a significance level of α=0.01. If the null hypothesis was rejected, the alternative hypothesis was that the reflectance medians of two land covers are not equal:

$$H_1 = \eta_n(i) \neq \eta_{n+1}(i) \tag{2}$$

All the available classification algorithms on GEE [1] were tested to find the most

[1]Maximum Entropy, Support Vector Machine, Minimum distance, CART, Gradient Tree Boost,

accurate, which was the Random Forest classifier. The classification was performed in a loop using a sequence of number of decision trees to find the optimal value. For Sentinel, all bands from B2 to B12 and the NDVI and MNDWI indices were used in the classification algorithm. For Landsat, bands between B2 and B7 and NDVI and MNDWI indices were used.

The accuracy of both Landsat and Sentinel classifications were assessed in two ways. First, the accuracy compared to the 30 cm resolution classification from Lørup Arildsen (2020) was evaluated. To do this, 15000 points were randomly selected on the classified area and their predicted and actual land cover classes were compared in a confusion matrix. It was then used to calculate observed classification accuracy and Cohen's Kappa coefficient. This method gives a good assessment of the real accuracy of the map created. However, it does not consider the fact that the Landsat and Sentinel have different spatial resolutions than the Lorup's classification. To account for this, the map's accuracy are evaluated by comparing them to ground truth maps of the same spatial resolution.

1.2. Results

To classify vegetation on Sentinel-2 and Landsat-8 images, 461 and 116 training points were sampled, which represent 6.3 and 14.4 percent of Lørup's classified area. Detail on the number of training points per class can be found in table 4. The reflectance of each land cover class for all Landsat and Sentinel bands as well as NDVI and MNDWI values were retrieved from the satellite images and can be compared in figures 32 and 33. The spectral signatures follow expected patterns with vegetation reflectance increasing in near-infrared and shortwave infrared spectral regions. The different types of vegetation cover have very similar spectral reflectance in all bands. The open water reflectance has distinctive lower values in the NIR and SWIR spectral regions. It also logically has lower NDVI and higher MNDWI values.

Naive Bayes and Random Forest classifiers.

Table 4: Vegetation classification training data set.

		Landsat		Sentinel	
Land cover classes	**Part of total area**	**Number of training points**	**Part of total number of training points**	**Number of training points**	**Part of total number of training points**
Wet Meadows	25.7%	17	14.7%	73	15.8%
Palo Verde Trees	15.4%	13	11.2%	49	10.6%
Forest	10.3%	13	11.2%	51	11.1%
Cattail Stands	16.1%	18	15.5%	96	20.8%
Thalia Stands	16.7%	10	8.6%	52	11.3%
Water Hyacinth	8.4%	12	10.3%	46	10.0%
Open Water	1.2%	23	19.8%	62	13.4%
Dry Vegetation	6.3%	10	8.6%	32	6.9%

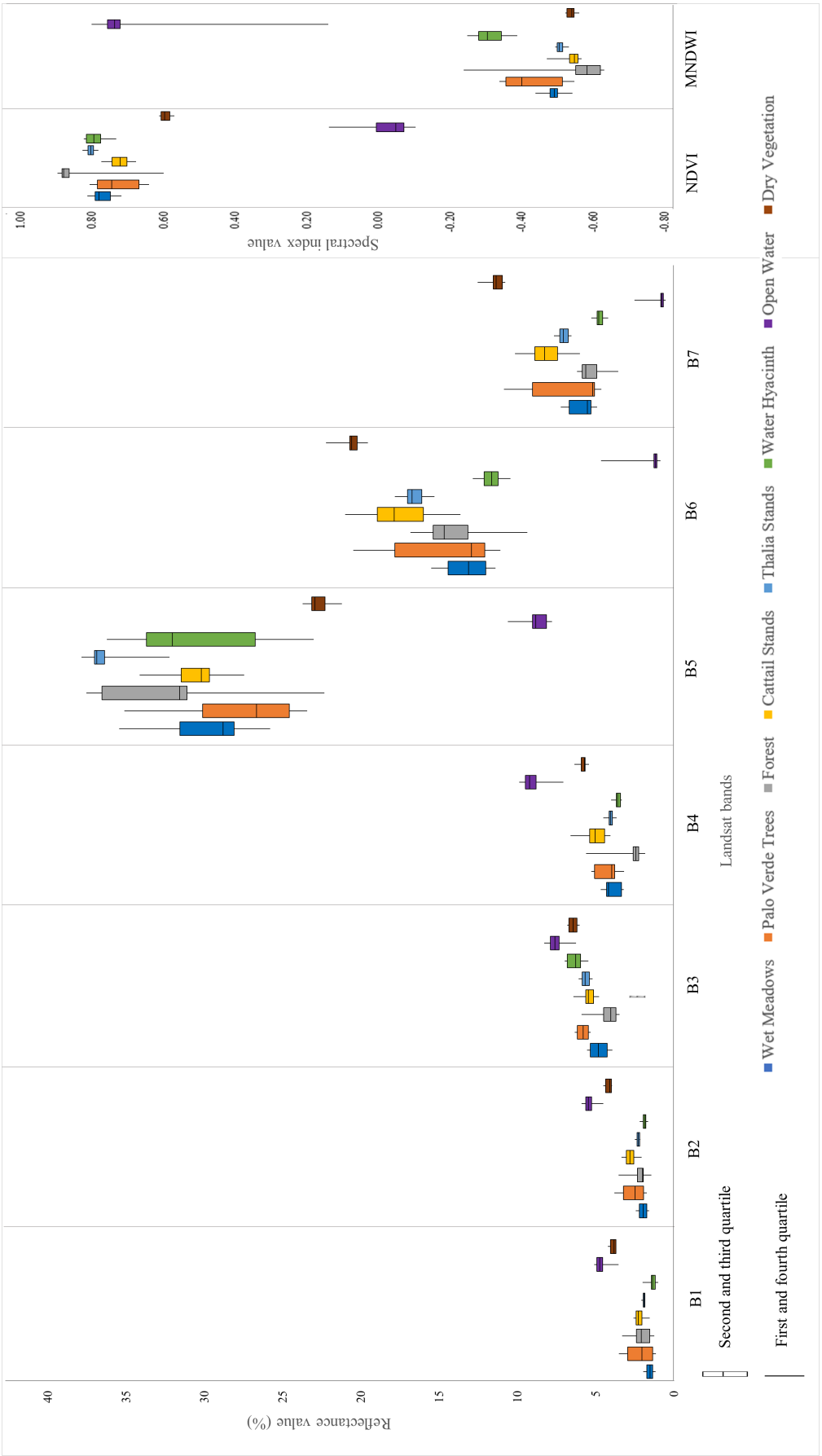

Figure 32: Landsat reflectance, NDVI and MNDWI values of sample points from 8 PVNP land cover classes.

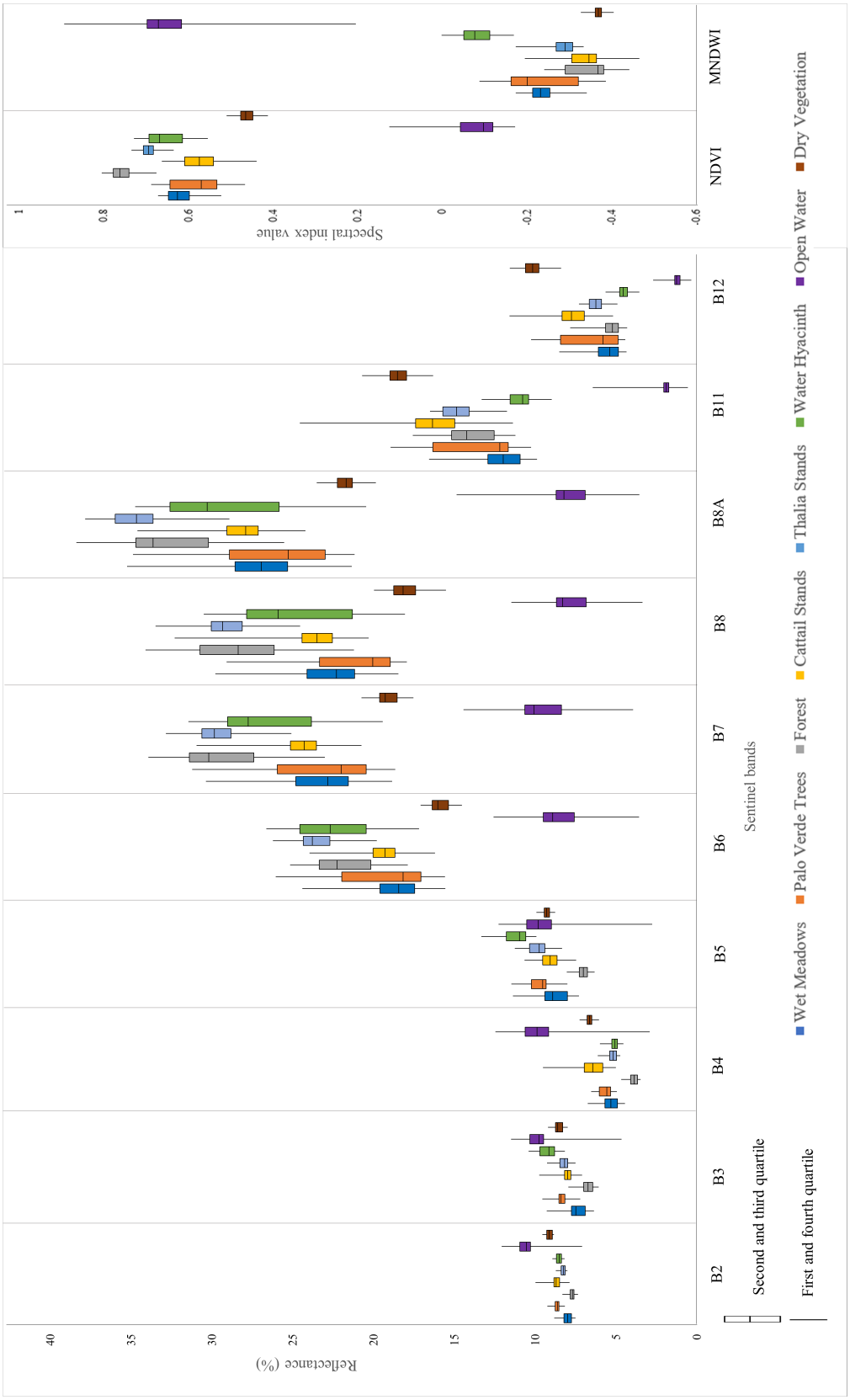

Figure 33: Sentinel reflectance, NDVI and MNDWI values of sample points from 8 PVNP land cover classes.

A Mann-Whitney U-test was performed in the software R which tested the null hypothesis that the medians of two land covers were equal in a particular waveband, with a signifance level of α=0.01. For the Landsat training points, it was found that it is difficult to distinguish between some land cover pairs, as shown in table 5. Wet Meadows and Palo Verde Trees in particular have similar reflectance to other land covers in most bands. In contrast, dry vegetation and open water should be easier to distinguish from other land covers by the classification algorithm. All land cover pairs have statistically different medians in at least two bands.

The training points of different land covers have less similar reflectance in the Sentinel bands, as shown in table 6. In this case, all land covers can be distinguished by at least 8 bands.

Table 5: Lansdat bands for which median reflectance of land cover pairs are not statistically different.

	Wet Meadows	**Palo Verde Trees**	**Forest**	**Cattail Stands**	**Thalia Stands**	**Water Hyacinth**	**Open Water**
Palo Verde Trees	B1, B2, B4, B5, B6, B7, NDVI						
Forest	B1, B2, B3, B5, B6, B7	B1, B2, B6, B7					
Cattail Stands	B5	B1, B2, B3, B6, B7, NDVI	B1, B5				
Thalia Stands	B2, B4, MNDWI	B1, B2, B3, B4, B6, B7	B1, B2, B5	B3, B6			
Water Hyacinth	B1, B2, B4, B5, NDVI	B1, B3, B5, B6, NDVI, MNDWI	B2, B5, B7	B5, MNDWI	NDVI		
Open Water	/	/	/	/	/	/	
Dry Vegetation	/	/	/	/	/	B3	/

Table 6: Sentinel bands for which median reflectance of land cover pairs are not statistically different.

	Wet Meadows	**Palo Verde Trees**	**Forest**	**Cattail Stands**	**Thalia Stands**	**Water Hyacinth**	**Open Water**
Palo Verde Trees	B6, B7, B8A,B12						
Forest	B12, MNDWI	B11					
Cattail Stands	B5	B2, B6, NDVI, MNDWI	/				
Thalia Stands	B4, MNDWI	B5,B11, B12	B7, B8, B8A, MNDWI	/			
Water Hyacinth	B4	/	B6	B8, B8A	B4, B6		
Open Water	/	B5	/	/	B5	/	
Dry Vegetation	/	B3	/	B4, B5	/	/	/

The land cover classifications of a Landsat-8 and a Sentinel-2 images were performed

on the GEE online platform. All available classification algorithms were tested and the best accuracy was achieved by using a Random Forest classifier with 100 decision trees. The Landsat and Sentinel classifications are presented on figure 34 alongside Lørup's vegetation map. They have spatial resolutions of 30 m, 10 m and 37 cm respectively.

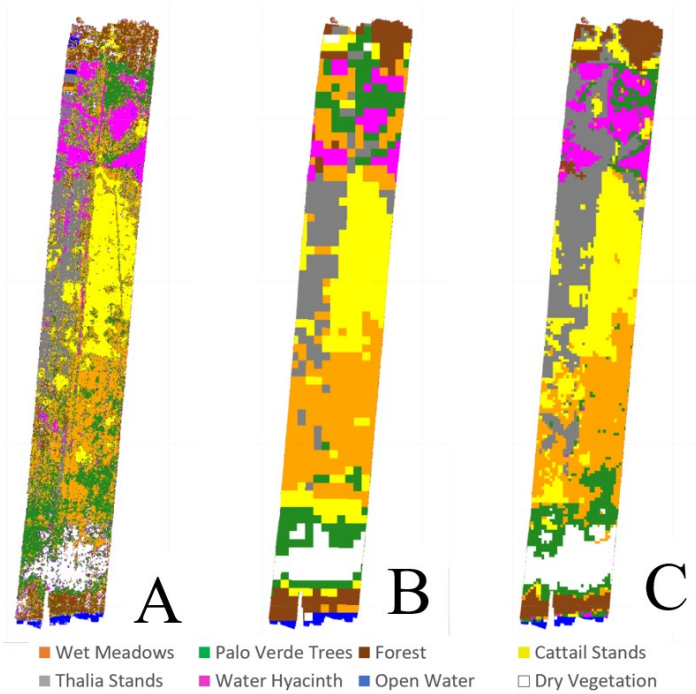

Figure 34: Land cover classifications performed from **A)** hyperspectral images (reprinted from Lørup Arildsen (2020)), **B)** Landsat-8 and **C)** Sentinel-2 imagery.

The accuracy of both classifications were assessed by creating confusion matrices from 15,000 randomly selected points. Table 7 shows the confusion matrix for the Landsat classification. The producer's accuracies show that Forest, Water Hyacinth and Open Water were the land covers that were best identified by the algorithm with values from 68 to 74%. It struggled most to identify Wet Meadows and Palo Verde Trees as expected from the abovementioned statistical analysis. The user's accuracies show that commission errors, committed when an area is included in an incorrect category, were most frequent for Palo Verde Trees and Forest. The observed classification accuracy and Cohen's Kappa coefficient are 58.4% and 0.48 respectively.

Table 8 is the confusion matrix for the Sentinel-2 image classification. Overall, it shows better results than the Landsat classification, with higher producer's accuracy for all land covers except Thalia Stands and Water Hyacinth and user's accuracy expect for Open Water. The observed classification accuracy and Cohen's Kappa coefficient are 64.0% and 0.55 respectively.

Table 7: Confusion matrix of the Landsat-8 image land cover classification.

		Ground truth								
		Wet Meadows	**Palo Verde Trees**	**Forest**	**Cattail Stands**	**Thalia Stands**	**Water Hyacinth**	**Open Water**	**Dry Vegetation**	**User's accuracy**
Classifier	**Wet Meadows**	2199	319	53	761	392	25	9	91	57%
	Palo Verde Trees	696	892	39	274	80	169	1	237	37%
	Forest	323	103	484	153	152	24	10	26	38%
	Cattail Stands	344	31	0	1848	152	0	0	13	77%
	Thalia Stands	636	172	84	277	1320	39	0	7	52%
	Water Hyacinth	259	231	44	47	116	601	0	1	46%
	Open Water	6	11	1	5	0	2	70	8	68%
	Dry Vegetation	10	246	7	46	7	2	5	628	66%
	Producer's accuracy	49%	44%	68%	54%	59%	70%	74%	62%	

Table 8: Confusion matrix of the Sentinel-2 image land cover classification.

		Ground truth								
		Wet Meadows	**Palo Verde Trees**	**Forest**	**Cattail Stands**	**Thalia Stands**	**Water Hyacinth**	**Open Water**	**Dry Vegetation**	**User's accuracy**
Classifier	**Wet Meadows**	1807	366	63	643	767	76	0	127	47%
	Palo Verde Trees	503	1007	4	245	144	190	0	295	42%
	Forest	173	71	542	142	323	24	0	0	43%
	Cattail Stands	219	12	1	1983	163	8	0	2	83%
	Thalia Stands	214	56	47	267	1789	157	0	5	71%
	Water Hyacinth	35	93	30	48	290	802	0	1	62%
	Open Water	0	38	2	10	14	6	33	0	32%
	Dry Vegetation	26	101	3	57	13	3	0	748	79%
	Producer's accuracy	60.7%	57.7%	78.3%	58.4%	51.1%	63.3%	100.0%	63.5%	

The classifications accuracies assessments mentioned above don't take into account the fact that Lørup's classification has a very fine spatial resolution. This has an obvious negative effect on the calculated accuracies in an environment with such a mixed vegetation. Even a perfect 10 or 30 m spatial resolution classification would indeed not have an accuracy close to 100%.

To better assess the quality of the classification maps created, they were compared with Lørup's classification at a reduced spatial resolution, as shown in figures 35 and 36. Landsat and Sentinel's classifications were as expected more accurate, with an observed accuracy of 72.4 and 71.3% and a Cohen's Kappa coefficient of 0.66 and 0.65 respectively. This shows that, when taking the differences in spatial resolution

into account, both sensor's classifications have very similar and fairly good accuracies. Tables 9 and 10 show the confusion matrices for both classifications.

Figure 35: **A)** Lørup's vegetation map with a reduced 30 m spatial resolution, **B)** Landsat-8 vegetation map.

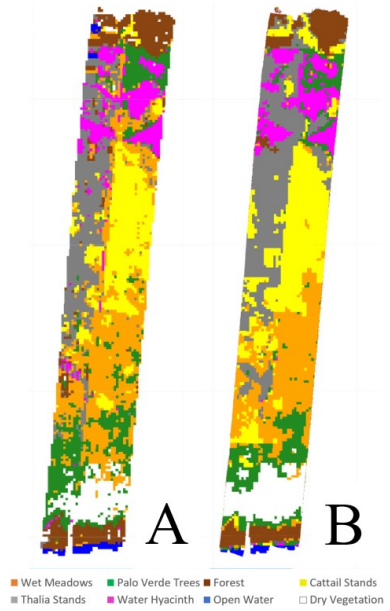

Figure 36: **A)** Lørup's vegetation map with a reduced 10 m spatial resolution, **B)** Sentinel-2 vegetation map.

Table 9: Confusion matrix of the Landsat-8 image land cover classification compared to Lørup's 30 m spatial resolution classification.

		Ground truth								
		Wet Meadows	**Palo Verde Trees**	**Forest**	**Cattail Stands**	**Thalia Stands**	**Water Hyacinth**	**Open Water**	**Dry Vegetation**	**User's accuracy**
Classifier	**Wet Meadows**	141	9	0	35	18	0	0	0	69%
	Palo Verde Trees	25	57	3	11	0	6	0	8	52%
	Forest	9	10	46	10	3	0	0	1	58%
	Cattail Stands	14	1	0	114	3	0	0	1	86%
	Thalia Stands	31	4	4	13	84	1	0	0	61%
	Water Hyacinth	9	9	1	0	2	38	0	0	64%
	Open Water	0	1	0	0	0	0	8	1	80%
	Dry Vegetation	0	11	0	0	0	0	0	41	79%
	Producer's accuracy	62%	56%	85%	62%	76%	84%	100%	79%	

Table 10: Confusion matrix of the Sentinel-2 image land cover classification compared to Lørup's 10 m spatial resolution classification.

		Ground truth								
		Wet Meadows	**Palo Verde Trees**	**Forest**	**Cattail Stands**	**Thalia Stands**	**Water Hyacinth**	**Open Water**	**Dry Vegetation**	**User's accuracy**
Classifier	**Wet Meadows**	976	156	15	283	375	28	0	44	52%
	Palo Verde Trees	207	544	1	96	44	68	0	124	50%
	Forest	59	28	446	63	121	4	0	2	62%
	Cattail Stands	99	5	0	1015	66	1	0	1	86%
	Thalia Stands	56	19	28	105	913	69	0	0	77%
	Water Hyacinth	13	39	16	19	96	388	0	1	68%
	Open Water	0	27	3	6	9	3	42	0	47%
	Dry Vegetation	6	38	0	16	1	0	0	389	86%
	Producer's accuracy	68.9%	63.6%	87.6%	63.3%	56.2%	69.2%	100.0%	69.3%	

1.3. Discussion

The results presented here confirm the results acquired by Lørup Arildsen (2020). Based on simulated Landsat-8 and Sentinel-2 images, they calculated an observed accuracy of 71 and 72%, respectively. The observed calculated here based on real Landsat-8 and Sentinel-2 images are 72 and 71% respectively when comparing with Lorup's classification at reduced spatial resolution.

A statistical test was performed to determine if the spectral reflectance of different land covers was significantly different, which is needed for the classification algorithm to work properly. It tested the differences between median reflectance in each band. Even if this test was reported in the literature, it seems a little basic for such assessment, because it does not consider the distribution around the median reflectance.

The classification was done based on training data collected in pure pixels. The number of training pixels was limited to try and replicate a real vegetation classification process, with the needed ground observations. Using more training data could have improved the accuracy of the classification but was considered less realistic.

The validation was performed using the maximum amount of data that GEE's computing power allowed. The best accuracy was achieved for the classes with most singular spectral reflectance, open water and dry vegetation, as predicted by the statistical test above. The observed accuracies for both Landsat and Sentinel classifications were poor, with respective values of 58.4 and 64%. To account for the spatial differences between

Lorup's classification and the Landsat and Sentinel images, the accuracy assessment was then performed on Lorup's classification with a reduced spatial resolution. In this case, the observed accuracy was better with values of 72.4 and 71.3 % for the Landsat and Sentinel classifications respectively, very close to what Lorup predicted based on simulated Landsat and Sentinel images. Still, these observed accuracy numbers are quite low. The classifications give a good insight of the location of each vegetation type but are not accurate enough for land cover change detection.

There is however room for improvement. The classification process used here to obtain was very straightforward, using all spectral bands and vegetation indices in the algorithm and only one image. Multi-temporal classification could definitely improve the classification accuracy. It could not be done in this work due to lack of ground data.

2. Location of the river flooded areas of the Nicaragua and Cipanci sub-wetlands

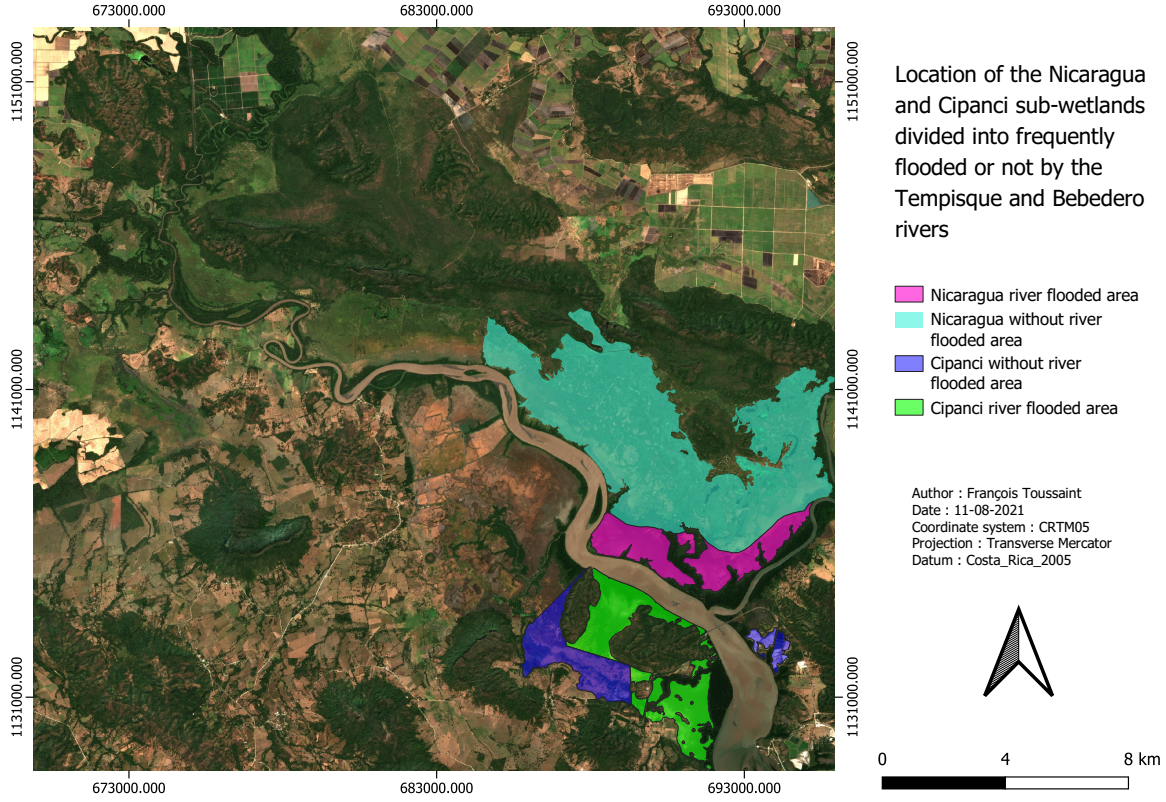

Figure 37: Location of the river flooded areas of the Nicaragua and Cipanci sub-wetlands

3. Satellite images of Fangueo events at PVNP

Figure 38: Fangueo (white) and control zones (red) in the Piedra Blanca sub-wetland in 2013. Zones ID : PB.

Figure 39: Fangueo (white) and control zones (red) in the Nicaragua sub-wetland in 2013. Zones ID : NIC1.

Figure 40: Fangueo (white) and control zones (red) in the Nicaragua sub-wetland in 2014. Zones ID : NIC2

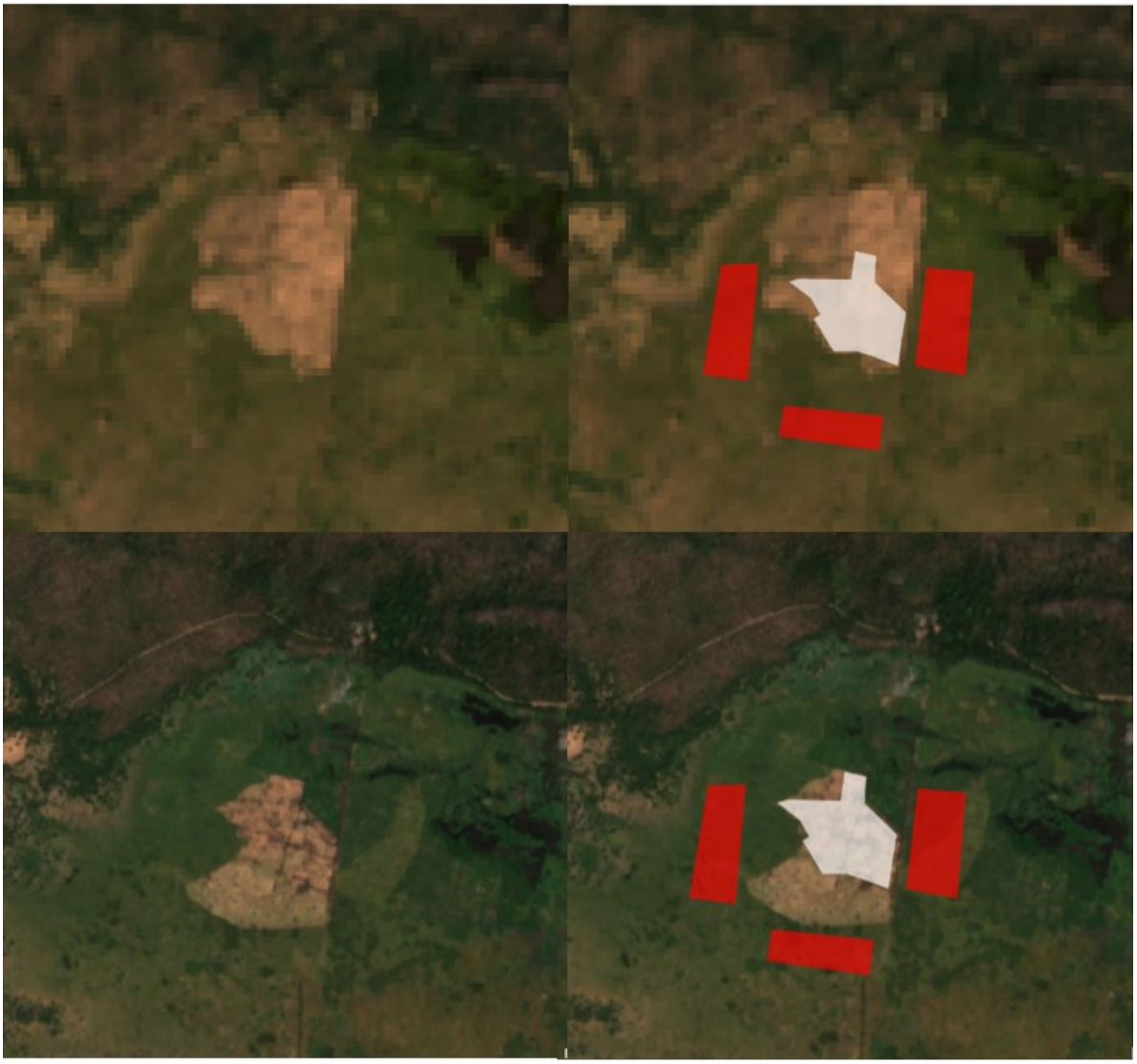

Figure 41: Fangueo (white) and control zones (red) in the Palo Verde sub-wetland in 2014 and 2020. Zones ID : PV1.

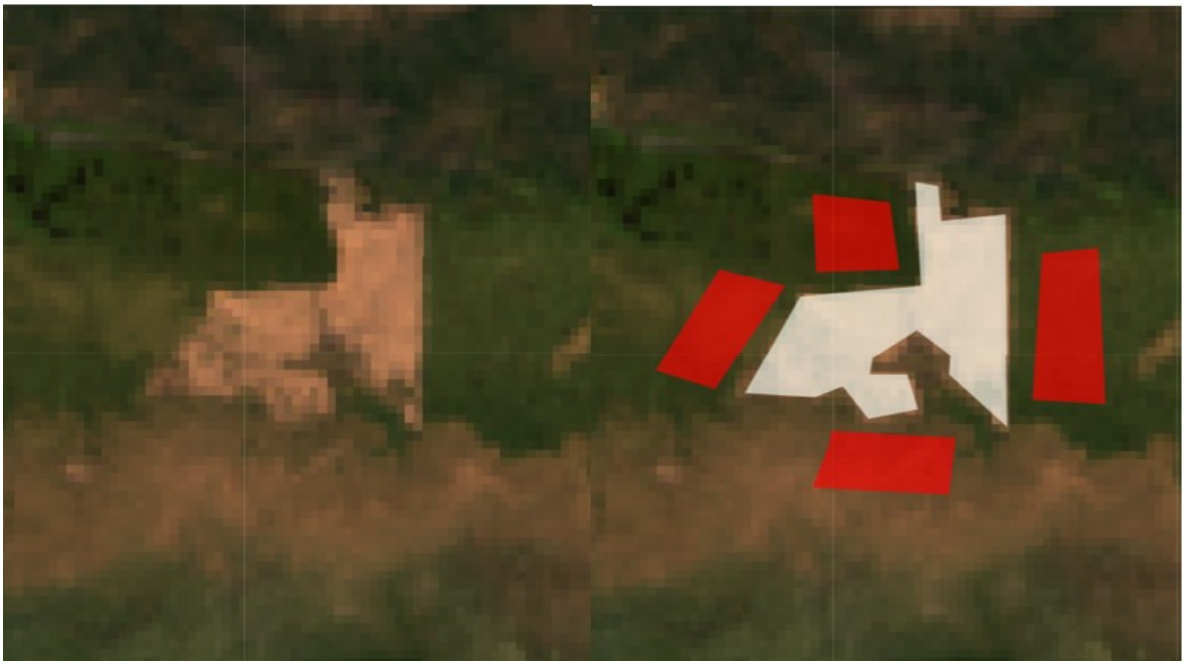

Figure 42: Fangueo (white) and control zones (red) in the Palo Verde sub-wetland in 2014. Zones ID : PV2.

4. Number of available cloud-free images of PVNP sub-wetlands

Table 11: Total number of available cloud-free images from 1984 to 2021 for the different sub-wetlands inside and aroud PVNP.

	Cipanci	Corral de Piedra	El Viejo	La Bocana	Mata Redonda	Nicaragua	Palo Verde	Piedra Blanca	Poza Verde	Varillal
1985	2	2	2	2	1	2	2	2	2	1
1986	4	4	3	4	3	3	3	3	3	3
1987	2	3	2	3	2	2	2	2	2	2
1988	2	3	2	2	1	3	2	2	2	1
1989	2	2	3	1	2	2	2	2	1	1
1990	2	2	2	2	2	2	2	2	2	2
1991	2	2	3	3	2	2	2	2	3	2
1992	3	2	2	2	1	2	2	2	2	2
1993	1	2	2	2	2	1	3	2	1	2
1994	0	0	0	0	0	0	0	0	0	0
1995	0	0	0	0	0	0	0	0	0	0
1996	0	0	0	0	0	0	0	0	0	0
1997	7	6	7	7	6	6	6	6	7	6
1998	8	8	8	8	7	8	8	8	7	8
1999	3	3	4	3	4	3	3	4	5	4
2000	6	3	6	4	4	4	5	5	4	6
2001	4	3	5	3	3	4	6	6	3	3
2002	1	1	1	1	2	1	1	2	0	2
2003	1	2	2	2	2	2	2	2	1	2
2004	0	0	0	0	0	0	0	0	0	0
2005	0	0	0	0	0	0	0	0	0	0
2006	0	0	0	0	0	0	0	0	0	0
2007	0	0	0	0	0	0	0	0	0	0
2008	0	0	0	0	0	0	0	0	0	0
2009	0	0	0	0	0	0	0	0	0	0
2010	2	2	1	2	1	2	2	1	2	1
2011	2	2	2	2	2	2	2	2	2	2
2012	0	0	0	0	0	0	0	0	0	0
2013	0	0	0	0	0	0	0	0	0	0
2014	6	5	7	4	6	6	6	6	6	6
2015	3	5	7	6	4	5	5	7	4	6
2016	6	7	9	7	9	7	7	9	9	9
2017	7	7	5	7	6	6	8	5	6	5
2018	5	6	7	5	4	6	5	7	5	5
2019	27	30	30	29	30	29	31	30	29	29
2020	23	27	27	27	27	26	29	26	25	26
2021	18	17	20	18	14	15	18	17	13	20

Table 12: Total number of available cloud-free images per month for the different sub-wetland inside and around PVNP.

	Cipanci	Corral de Piedra	El Viejo	La Bocana	Mata Redonda	Nicaragua	Palo Verde	Piedra Blanca	Poza Verde	Varillal
January	36	33	35	33	34	32	36	34	28	32
February	33	32	34	30	32	33	32	35	36	34
March	39	43	45	42	37	41	43	40	37	44
April	18	20	26	26	19	19	23	25	22	24
May	9	4	9	4	6	6	8	7	7	9
June	4	2	8	9	1	2	7	5	7	3
July	2	7	12	9	7	5	9	10	6	10
August	3	6	10	4	6	4	5	8	7	10
September	3	2	8	5	3	1	3	7	4	4
October	1	3	9	6	5	3	5	4	6	9
November	10	11	9	12	8	11	10	6	9	12
December	23	28	29	25	25	26	30	28	23	22

5. Open water detection methods

Different methods were investigated to detect open water areas. The uses of the MNDWI, the NIR and SWIR bands were considered. MNDWI is a standard, well-documented method for the remote sensing of open water areas. It was found that the MNDWI does allow for detection of humid areas, however it struggles to differentiate between open water areas and aquatic vegetation. The RGB visualization on Figure 43 shows dark areas corresponding to open water and bright green areas that are aquatic vegetation. Both have similar MNDWI values. The NIR and SWIR visualizations show more promise as there are clear differences in reflectance values between open water and other vegetation covers. The Sentinel SWIR band only has a spatial resolution of 20 m, so quantification of open water areas would be somewhat less accurate.

Figure 44 is an other example, located in the Mata Redonda sub-wetland, of the ability of the MNDWI, NIR and SWIR bands to detect open water. It shows that the NIR band does a good job at only isolating the open water pixels, while the MNDWI and the SWIR band have similar values for open water and other vegetation covers.

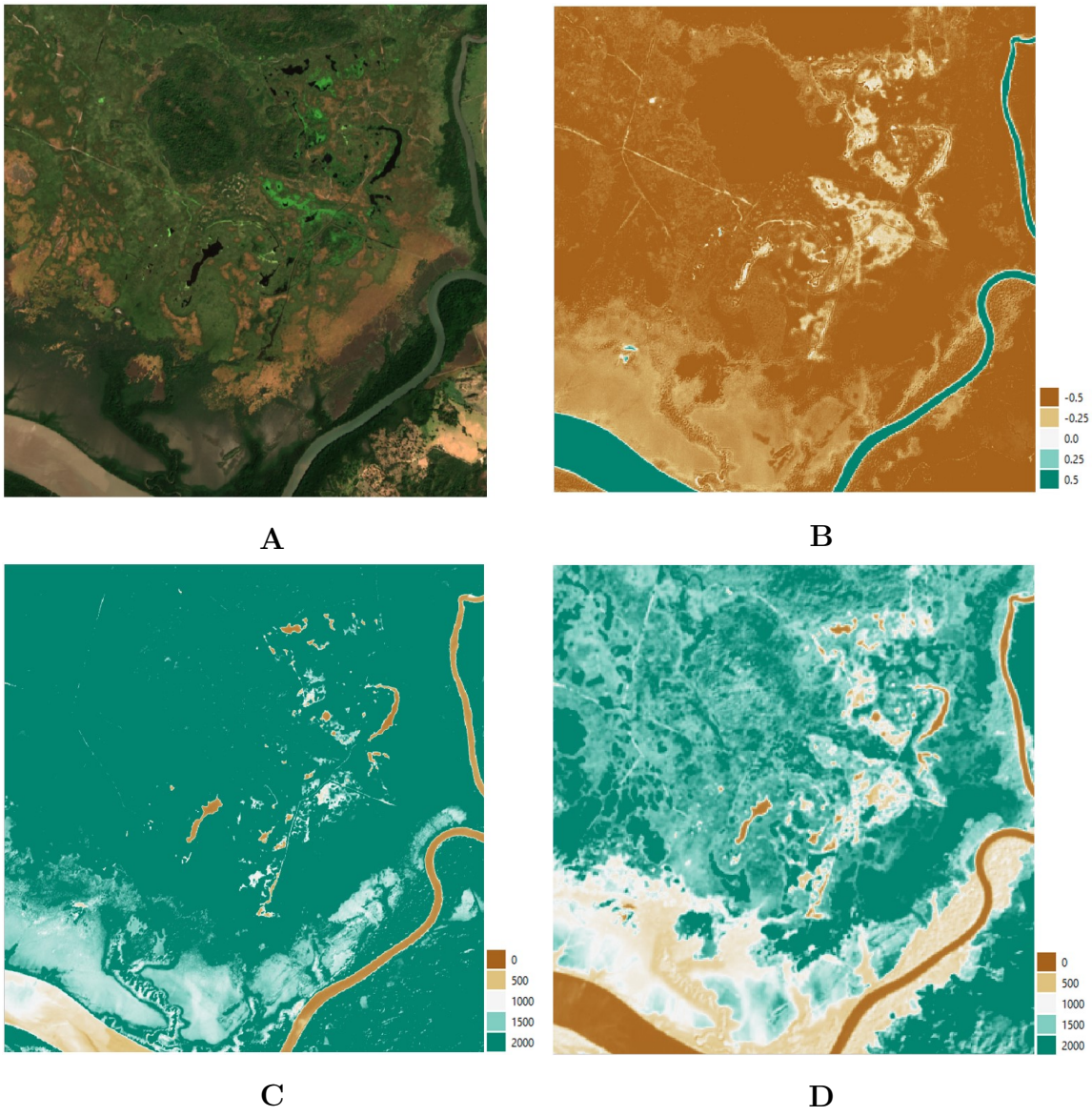

Figure 43: Visualizations of a Sentinel-2 image from 04-01-2019 over an area of the Nicaragua sub-wetland, illustrating their ability to detect open water areas. **A)** RGB, **B)** MNDWI, **C)** NIR band (B8) and **D)** SWIR band (B11) visualizations.

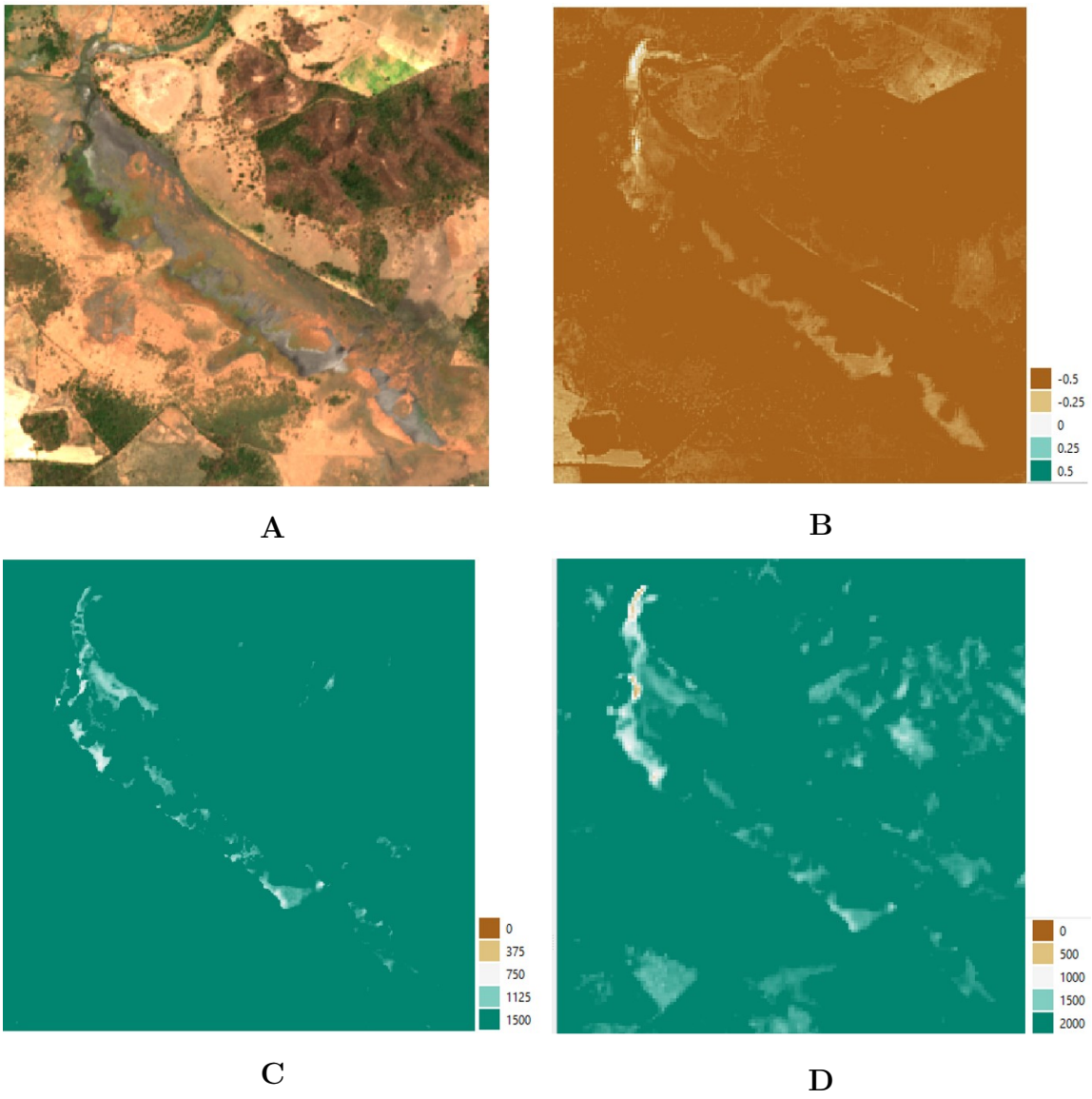

Figure 44: Visualizations of a Sentinel-2 image from 28-02-2019 over an area of the Mata Redonda sub-wetland, illustrating their ability to detect open water areas. **A)** RGB, **B)** MNDWI, **C)** NIR band (B8) and **D)** SWIR band (B11) visualizations.

Based on the observation of many other examples similar to the two presented here above, it was decided to detect open water on satellite images using the NIR band by applying a threshold value. Pixels with a value below this threshold are considered as open water.

6. Accuracy assessment of open water detection

Table 13: Observed accuracy and Cohen's Kappa coefficient of open water detection by applying a NIR band threshold of 14% reflectance.

Sensor	Date	Observed accuracy	Cohen's Kappa coefficient
Sentinel-2	15-12-18	99.7%	0.86
	28-02-19	94.4%	0.77
	20-03-19	94.0%	0.54
	25-12-19	92.9%	0.87
	14-01-20	98.8%	0.90
	13-02-20	98.6%	0.92
	24-03-20	91.3%	0.87
	09-12-20	97.7%	0.89
	07-02-21	98.2%	0.91
Landsat 8	10-02-14	99.5%	0.79
	02-04-15	96.7%	0.73
	30-12-15	98.0%	0.74
	16-02-16	98.5%	0.80
	23-01-19	99.8%	0.88
Landsat 7	27-01-00	98.2%	0.84
	13-11-01	98.4%	0.86
Landsat 5	14-03-85	92.9%	0.70
	10-11-91	99.3%	0.90
	16-04-97	94.0%	0.80
Landsat 4	25-03-92	95.4%	0.90

7. Times series of open water area in PVNP sub-wetlands

Table 14: Area of PVNP and surrounding sub-wetlands.

Sub-wetland	**Area (ha)**
Cipanci river flooded area	786.82
Cipanci without river flooded area	585.17
Corral de Piedra	3542.56
El Viejo	157.48
La Bocana	1055.07
Mata Redonda	1760.72
Nicaragua river flooded area	696.17
Nicaragua without river flooded area	3756.33
Palo Verde	1164.67
Piedra Blanca	389.97
Poza Verde	738.93
Varillal	402.18

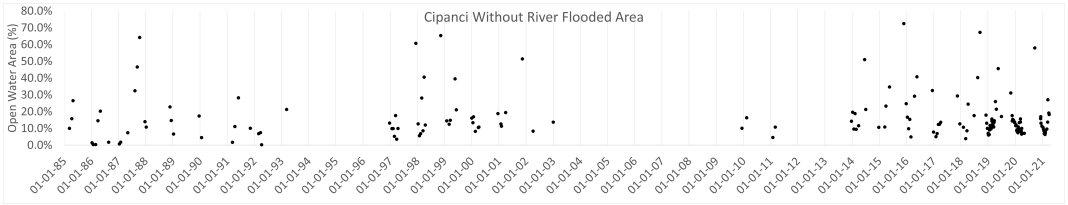
Cipanci Without River Flooded Area
Open Water Area (%)
80.0%
70.0%
60.0%
50.0%
40.0%
30.0%
20.0%
10.0%
0.0%
01-01-85
01-01-86
01-01-87
01-01-88
01-01-89
01-01-90
01-01-91
01-01-92
01-01-93
01-01-94
01-01-95
01-01-96
01-01-97
01-01-98
01-01-99
01-01-00
01-01-01
01-01-02
01-01-03
01-01-04
01-01-05
01-01-06
01-01-07
01-01-08
01-01-09
01-01-10
01-01-11
01-01-12
01-01-13
01-01-14
01-01-15
01-01-16
01-01-17
01-01-18
01-01-19
01-01-20
01-01-21

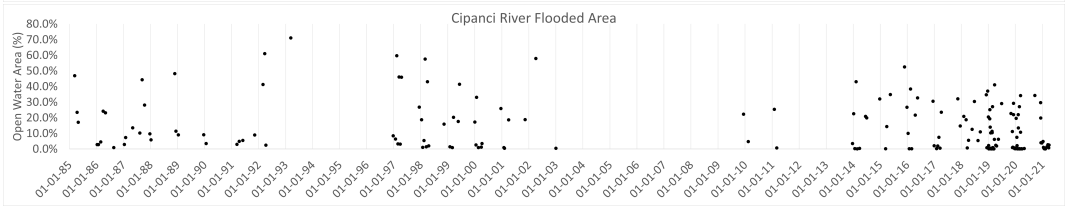
Cipanci River Flooded Area
Open Water Area (%)
80.0%
70.0%
60.0%
50.0%
40.0%
30.0%
20.0%
10.0%
0.0%
01-01-85
01-01-86
01-01-87
01-01-88
01-01-89
01-01-90
01-01-91
01-01-92
01-01-93
01-01-94
01-01-95
01-01-96
01-01-97
01-01-98
01-01-99
01-01-00
01-01-01
01-01-02
01-01-03
01-01-04
01-01-05
01-01-06
01-01-07
01-01-08
01-01-09
01-01-10
01-01-11
01-01-12
01-01-13
01-01-14
01-01-15
01-01-16
01-01-17
01-01-18
01-01-19
01-01-20
01-01-21

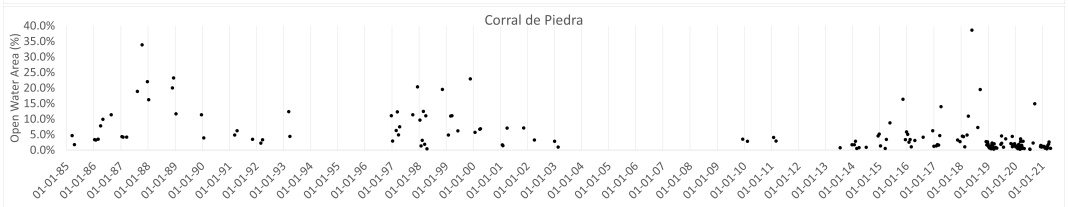
Corral de Piedra
Open Water Area (%)
40.0%
35.0%
30.0%
25.0%
20.0%
15.0%
10.0%
5.0%
0.0%
01-01-85
01-01-86
01-01-87
01-01-88
01-01-89
01-01-90
01-01-91
01-01-92
01-01-93
01-01-94
01-01-95
01-01-96
01-01-97
01-01-98
01-01-99
01-01-00
01-01-01
01-01-02
01-01-03
01-01-04
01-01-05
01-01-06
01-01-07
01-01-08
01-01-09
01-01-10
01-01-11
01-01-12
01-01-13
01-01-14
01-01-15
01-01-16
01-01-17
01-01-18
01-01-19
01-01-20
01-01-21

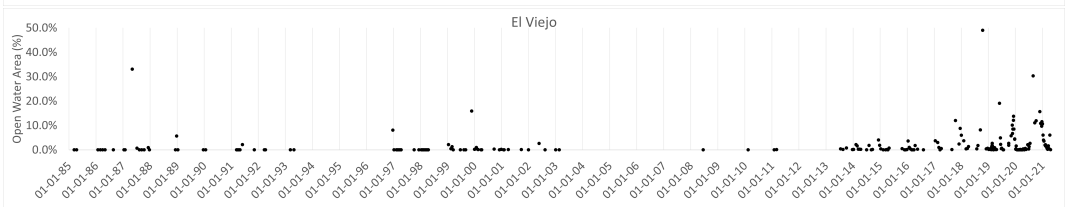
El Viejo
Open Water Area (%)
50.0%
40.0%
30.0%
20.0%
10.0%
0.0%
01-01-85
01-01-86
01-01-87
01-01-88
01-01-89
01-01-90
01-01-91
01-01-92
01-01-93
01-01-94
01-01-95
01-01-96
01-01-97
01-01-98
01-01-99
01-01-00
01-01-01
01-01-02
01-01-03
01-01-04
01-01-05
01-01-06
01-01-07
01-01-08
01-01-09
01-01-10
01-01-11
01-01-12
01-01-13
01-01-14
01-01-15
01-01-16
01-01-17
01-01-18
01-01-19
01-01-20
01-01-21

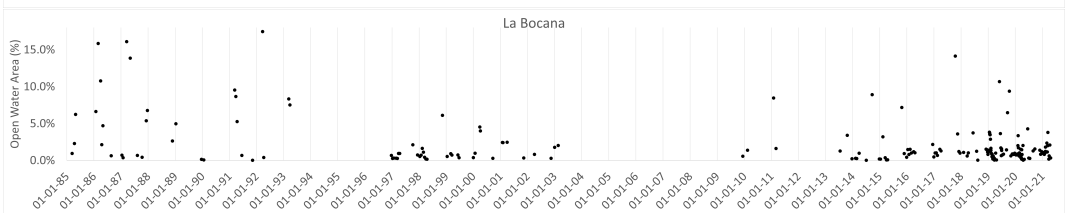
La Bocana
Open Water Area (%)
15.0%
10.0%
5.0%
0.0%
01-01-85
01-01-86
01-01-87
01-01-88
01-01-89
01-01-90
01-01-91
01-01-92
01-01-93
01-01-94
01-01-95
01-01-96
01-01-97
01-01-98
01-01-99
01-01-00
01-01-01
01-01-02
01-01-03
01-01-04
01-01-05
01-01-06
01-01-07
01-01-08
01-01-09
01-01-10
01-01-11
01-01-12
01-01-13
01-01-14
01-01-15
01-01-16
01-01-17
01-01-18
01-01-19
01-01-20
01-01-21

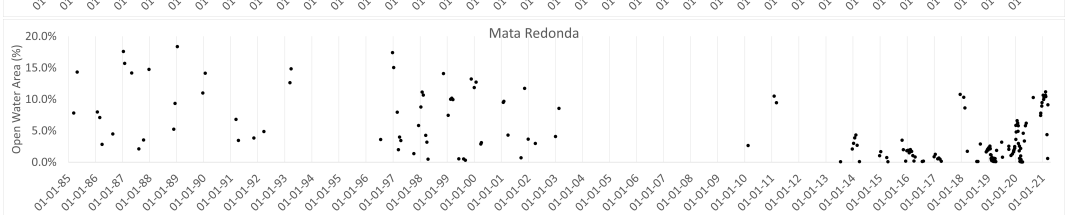
Mata Redonda
Open Water Area (%)
20.0%
15.0%
10.0%
5.0%
0.0%
01-01-85
01-01-86
01-01-87
01-01-88
01-01-89
01-01-90
01-01-91
01-01-92
01-01-93
01-01-94
01-01-95
01-01-96
01-01-97
01-01-98
01-01-99
01-01-00
01-01-01
01-01-02
01-01-03
01-01-04
01-01-05
01-01-06
01-01-07
01-01-08
01-01-09
01-01-10
01-01-11
01-01-12
01-01-13
01-01-14
01-01-15
01-01-16
01-01-17
01-01-18
01-01-19
01-01-20
01-01-21

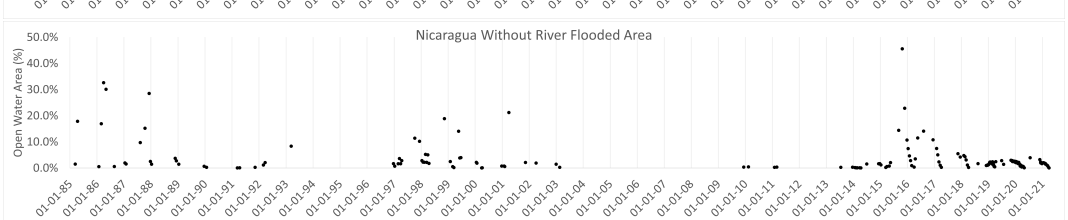
Nicaragua Without River Flooded Area
Open Water Area (%)
50.0%
40.0%
30.0%
20.0%
10.0%
0.0%
01-01-85
01-01-86
01-01-87
01-01-88
01-01-89
01-01-90
01-01-91
01-01-92
01-01-93
01-01-94
01-01-95
01-01-96
01-01-97
01-01-98
01-01-99
01-01-00
01-01-01
01-01-02
01-01-03
01-01-04
01-01-05
01-01-06
01-01-07
01-01-08
01-01-09
01-01-10
01-01-11
01-01-12
01-01-13
01-01-14
01-01-15
01-01-16
01-01-17
01-01-18
01-01-19
01-01-20
01-01-21

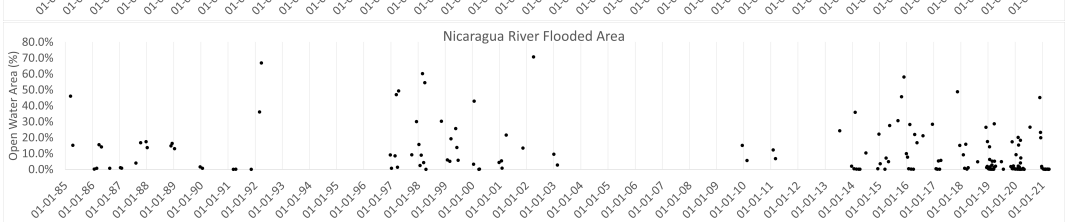
Nicaragua River Flooded Area
Open Water Area (%)
80.0%
70.0%
60.0%
50.0%
40.0%
30.0%
20.0%
10.0%
0.0%
01-01-85
01-01-86
01-01-87
01-01-88
01-01-89
01-01-90
01-01-91
01-01-92
01-01-93
01-01-94
01-01-95
01-01-96
01-01-97
01-01-98
01-01-99
01-01-00
01-01-01
01-01-02
01-01-03
01-01-04
01-01-05
01-01-06
01-01-07
01-01-08
01-01-09
01-01-10
01-01-11
01-01-12
01-01-13
01-01-14
01-01-15
01-01-16
01-01-17
01-01-18
01-01-19
01-01-20
01-01-21

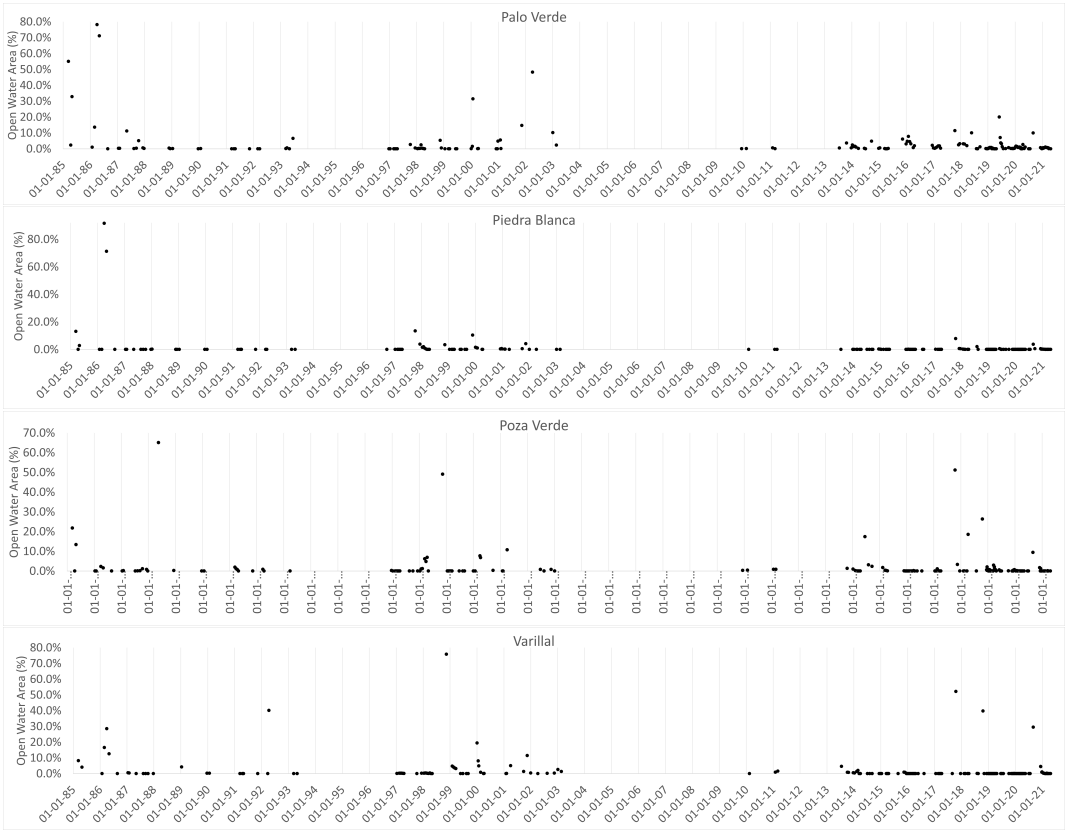

Figure 45: Times series from 1984 to 2021 of percentage of open water coverage in different sub-wetlands inside and around PVNP.

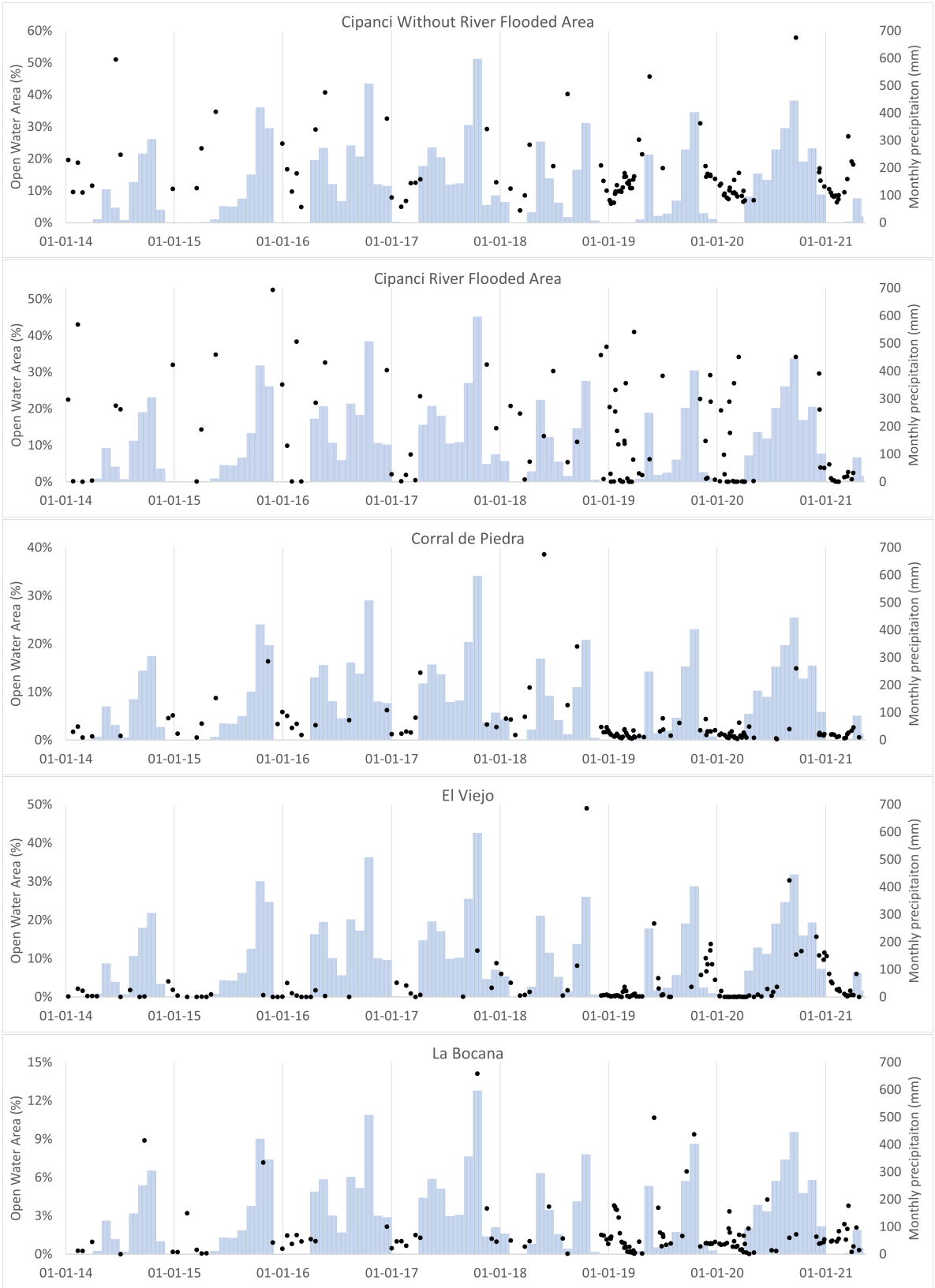
Cipanci Without River Flooded Area
Open Water Area (%)
60%
50%
40%
30%
20%
10%
0%
Monthly precipitaiton (mm)
700
600
500
400
300
200
100
0
01-01-14
01-01-15
01-01-16
01-01-17
01-01-18
01-01-19
01-01-20
01-01-21
Cipanci River Flooded Area
Open Water Area (%)
50%
40%
30%
20%
10%
0%
Monthly precipitaiton (mm)
700
600
500
400
300
200
100
0
01-01-14
01-01-15
01-01-16
01-01-17
01-01-18
01-01-19
01-01-20
01-01-21
Corral de Piedra
Open Water Area (%)
40%
30%
20%
10%
0%
Monthly precipitaiton (mm)
700
600
500
400
300
200
100
0
01-01-14
01-01-15
01-01-16
01-01-17
01-01-18
01-01-19
01-01-20
01-01-21
El Viejo
Open Water Area (%)
50%
40%
30%
20%
10%
0%
Monthly precipitaiton (mm)
700
600
500
400
300
200
100
0
01-01-14
01-01-15
01-01-16
01-01-17
01-01-18
01-01-19
01-01-20
01-01-21
La Bocana
Open Water Area (%)
15%
12%
9%
6%
3%
0%
Monthly precipitaiton (mm)
700
600
500
400
300
200
100
0
01-01-14
01-01-15
01-01-16
01-01-17
01-01-18
01-01-19
01-01-20
01-01-21

Figure 46

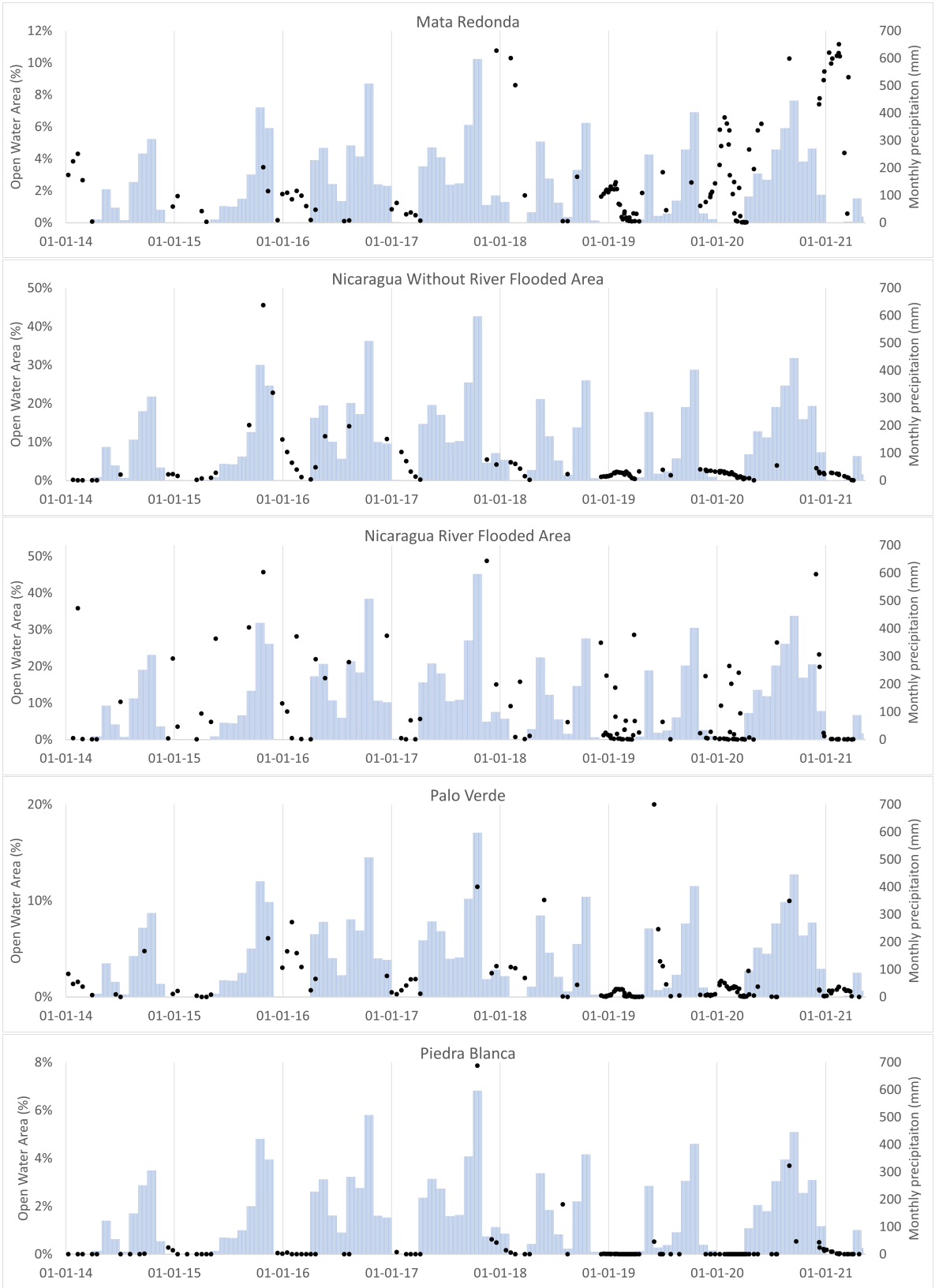
Mata Redonda
Open Water Area (%)
Monthly precipitaiton (mm)
12%
10%
8%
6%
4%
2%
0%
700
600
500
400
300
200
100
0
01-01-14
01-01-15
01-01-16
01-01-17
01-01-18
01-01-19
01-01-20
01-01-21
Nicaragua Without River Flooded Area
Open Water Area (%)
Monthly precipitaiton (mm)
50%
40%
30%
20%
10%
0%
700
600
500
400
300
200
100
0
01-01-14
01-01-15
01-01-16
01-01-17
01-01-18
01-01-19
01-01-20
01-01-21
Nicaragua River Flooded Area
Open Water Area (%)
Monthly precipitaiton (mm)
50%
40%
30%
20%
10%
0%
700
600
500
400
300
200
100
0
01-01-14
01-01-15
01-01-16
01-01-17
01-01-18
01-01-19
01-01-20
01-01-21
Palo Verde
Open Water Area (%)
Monthly precipitaiton (mm)
20%
10%
0%
700
600
500
400
300
200
100
0
01-01-14
01-01-15
01-01-16
01-01-17
01-01-18
01-01-19
01-01-20
01-01-21
Piedra Blanca
Open Water Area (%)
Monthly precipitaiton (mm)
8%
6%
4%
2%
0%
700
600
500
400
300
200
100
0
01-01-14
01-01-15
01-01-16
01-01-17
01-01-18
01-01-19
01-01-20
01-01-21

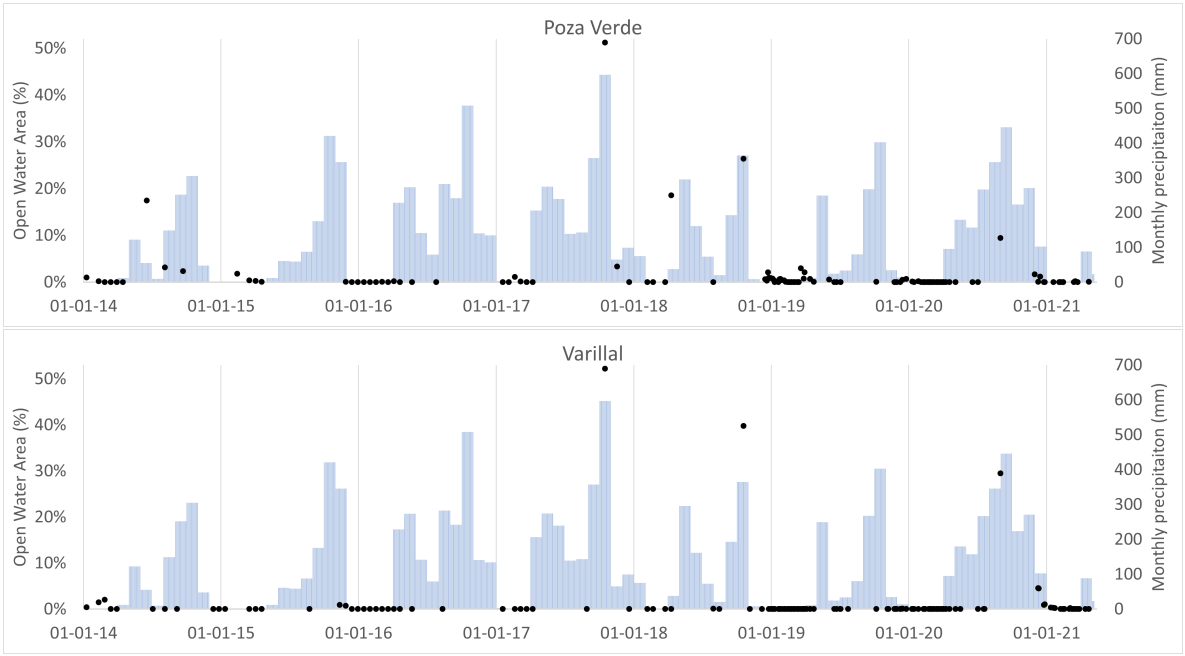

Figure 47: ime series from 2014 to 2021 of percentage of open water coverage in different sub-wetlands inside and around PVNP.

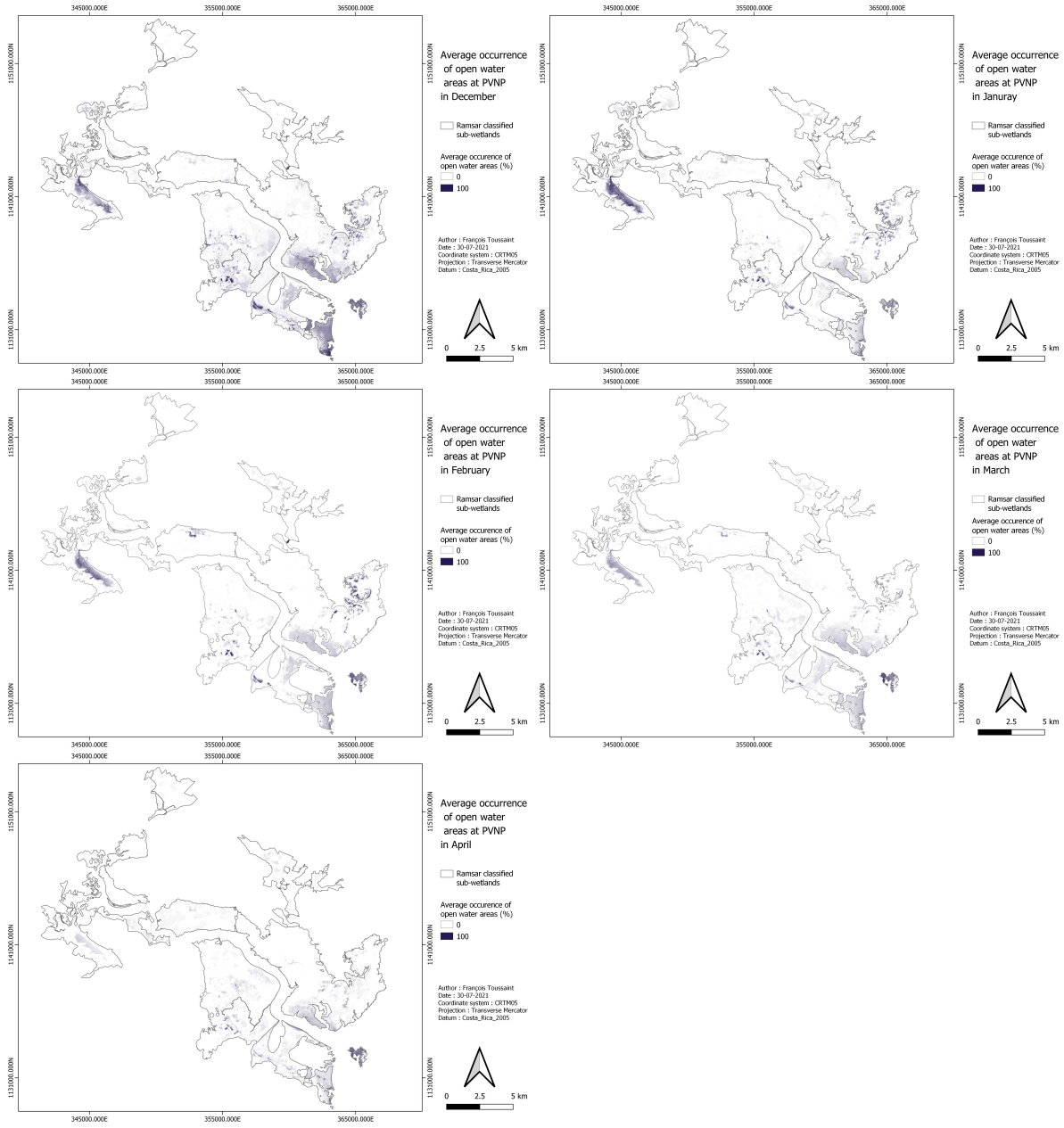

Figure 48: Frequency of occurrence of open water at PVNP for the months December to April, averaged based on images from 1985 to 2021.

8. Open water areas evolution at Fangueo and control zones

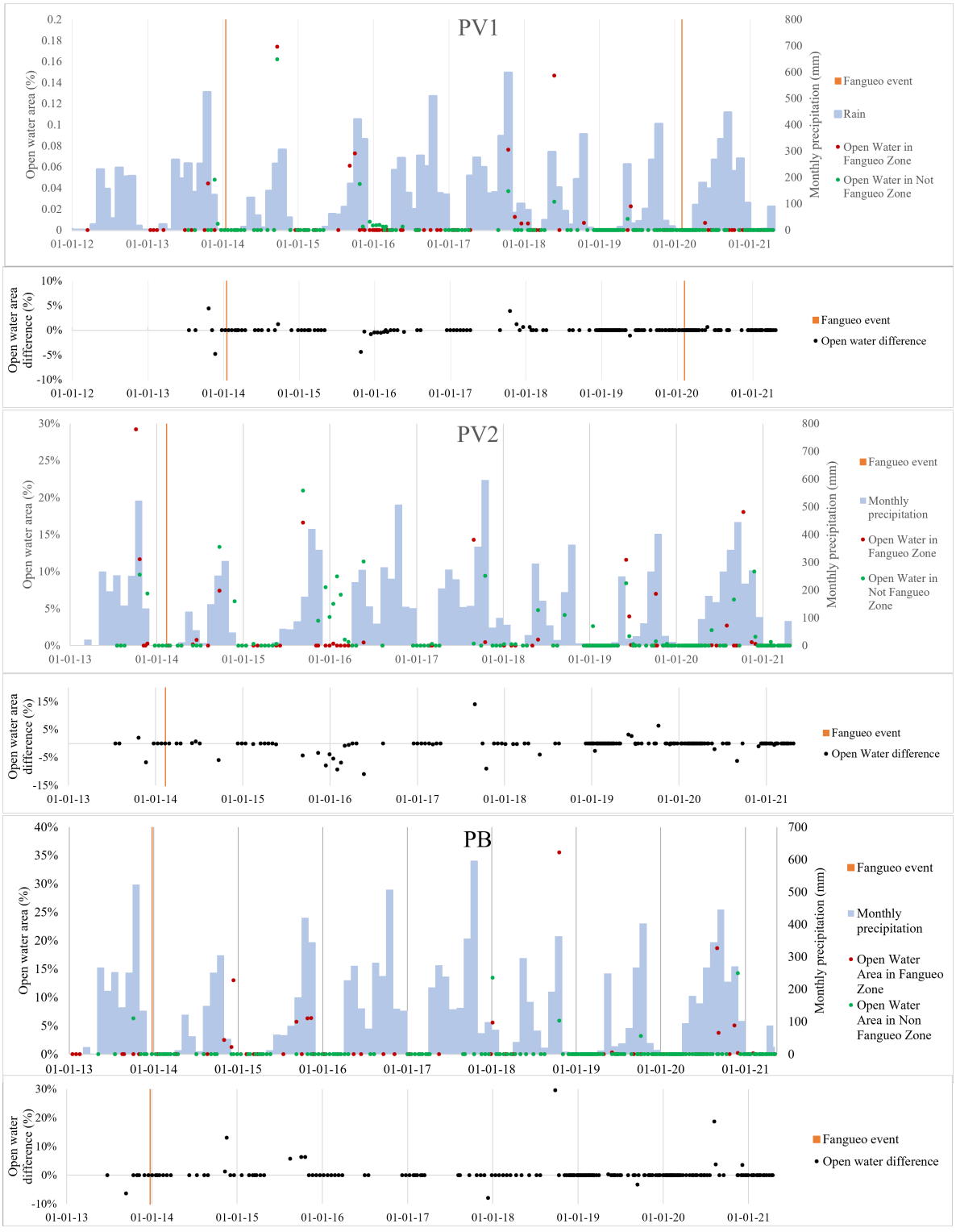

Figure 49: Evolution of open water areas in PV1, PV2 and PB Fangueo and control zones.

9. EVI evolution in Fangueo and control zones

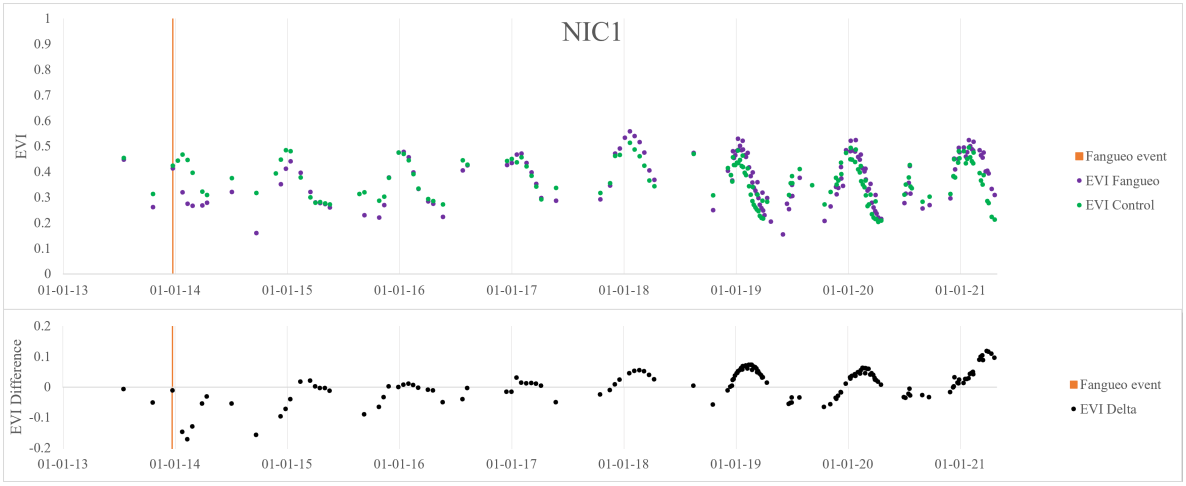

Figure 50: Evolution of average EVI in NIC1 Fangueo and control zones and of the EVI Delta between control and Fangueo zones.

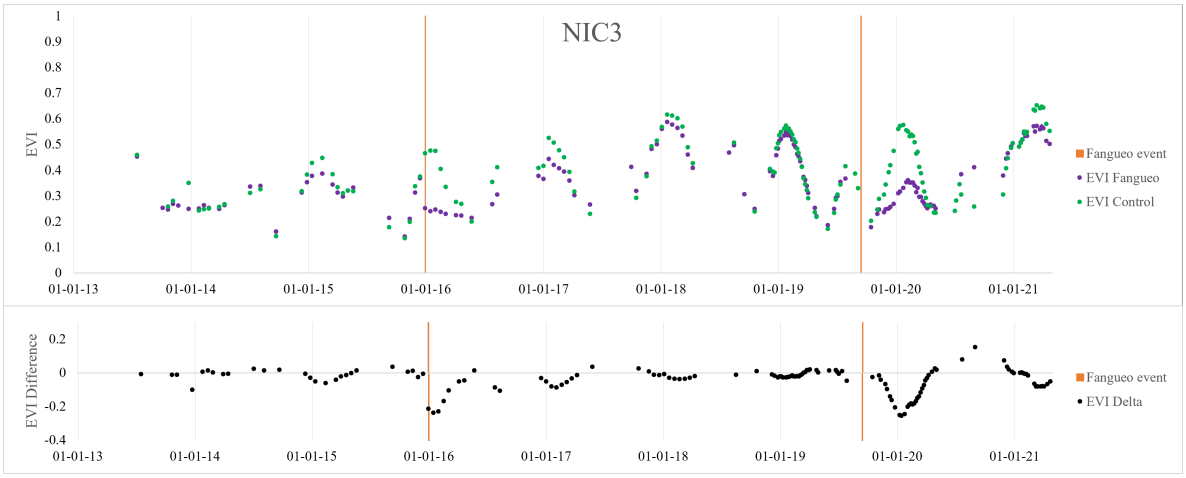

Figure 51: Evolution of average EVI and EVI Delta in NIC3 Fangueo and control zones.

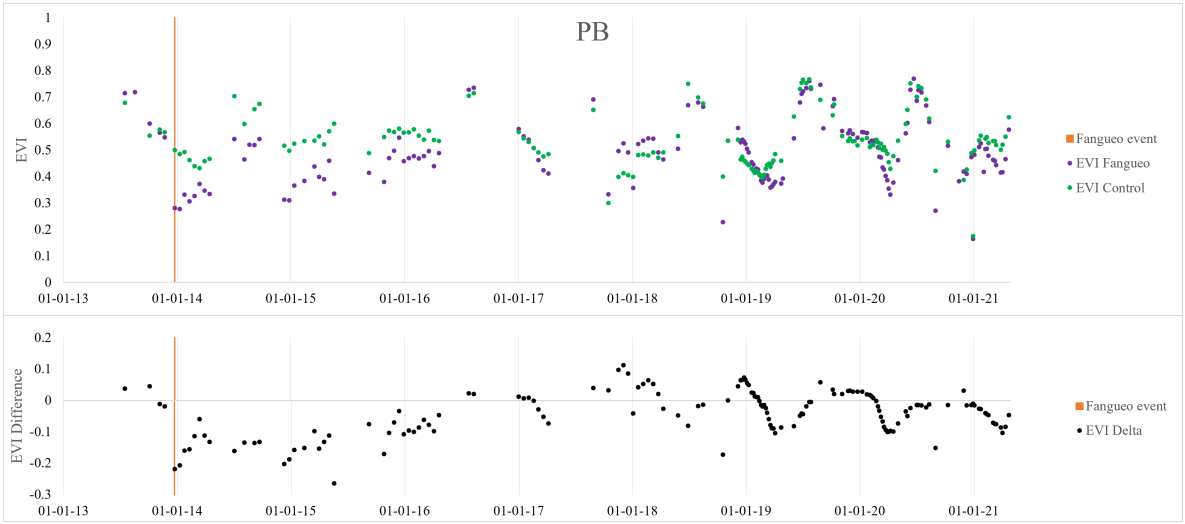

Figure 52: Evolution of average EVI and EVI Delta in PB Fangueo and control zones.

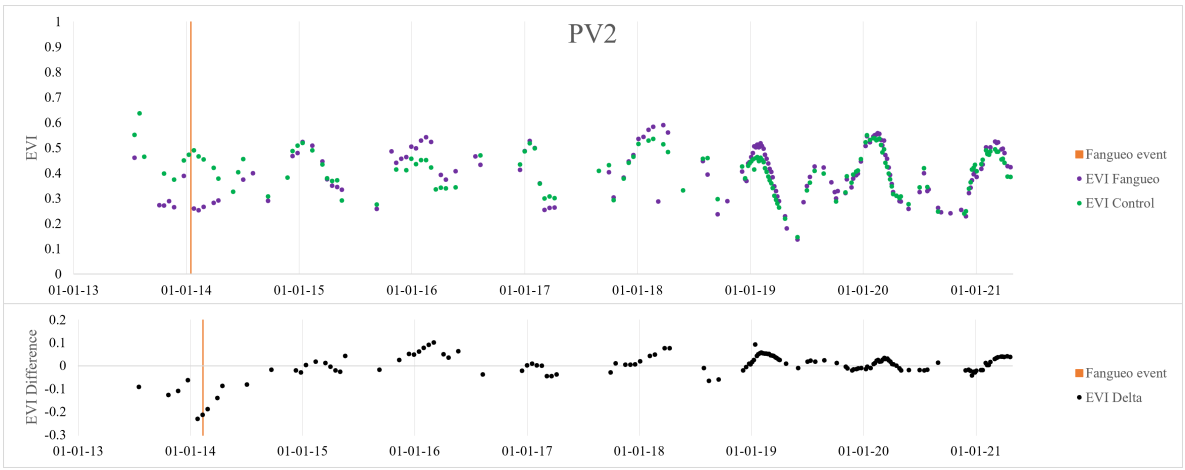

Figure 53: Evolution of average EVI in PV2 Fangueo and control zones and of the EVI Delta between control and Fangueo zones.

Mapping vegetation and open water in Palo Verde National Park, and impact of Fangueo technique : a descriptive study

François Toussaint

The Palo Verde National Park (PVNP), in Costa Rica, is an ecologically important wetland in Central America. After 1980, the wetland landscape changed from diverse vegetation and large open water areas to a monotypic stand of cattail, Typha domingensis. Programs to reduce Typha invasion were initiated and the Fangueo technique was adopted to reduce Typha spread. Studying Typha spatial distribution in the area, quantifying and mapping open water, and evaluating the long-term impact of the Fangueo technique on open water and vegetation cover is desirable to improve our knowledge of the eco-hydrology of PVNP.

Thresholded enhanced vegetation index (EVI) was used to create an indicative map of Typha distribution in PVNP. This method could be effective to map Typha in areas with similar hydrological situations. Open water areas were quantified and mapped by thresholding the near-infrared spectral band (NIR). The year-round dynamic indicated that there could be two peaks of open water area, one during the wet season and the other during the early dry season induced by aquatic vegetation retreat. Comparison of areas with versus without Fangueo was used to evaluate the impacts of the Fangueo technique. It was found that the initial increase in open water induced by Fangueo was not sustained over time. The method employed to monitor vegetation using EVI time series was found unsuccessful at assessing whether Fangueo leads to a long-term decrease of Typha cover in intervention areas.

Université catholique de Louvain

Faculty of bioscience engineering

Croix du Sud, 2 bte L7.05.01, 1348 Louvain-La-Neuve, Belgium | www.uclouvain.be/agro